University of Alberta

Development of Catalytic Stamp Lithography for
Nanoscale Patterning of Organic Monolayers

by

Hidenori Mizuno

A thesis submitted to the Faculty of Graduate Studies and Research
in partial fulfillment of the requirements for the degree of

Doctor of Philosophy

Department of Chemistry

Examining Committee

Jillian M. Buriak, Chemistry

Steven H. Bergens, Chemistry

D. Jed Harrison, Chemistry

Jonathan G. C. Veinot, Chemistry

Ken Cadien, Chemical and Materials Engineering

Byron D. Gates, Chemistry, Simon Fraser University

Abstract

Nanoscale patterning of organic molecules has received considerable attention in current nanoscience for a broad range of technological applications. In order to provide a viable approach, this thesis describes catalytic stamp lithography, a novel soft-lithographic process that can easily produce sub-100 nm patterns of organic monolayers on surfaces.

Catalytic stamps were fabricated through a two-step procedure in which the nanoscale patterns of transition metal catalysts are first produced on SiO_x/Si surfaces via the use of self-assembled block-copolymers, followed by the production of the poly(dimethylsiloxane) (PDMS) stamps on top of the as-patterned metals. Simply peeling off the as-formed PDMS stamps removes the metallic nanostructures, leading to the functional stamps. A number of different patterns with various metals were produced from a commercially available family of block copolymers, polystyrene-*block*-poly-2-vinylpyridine, by controlling the morphology of thin-film templates through the modulation of molecular weights of polymer blocks or solvent vapor annealing.

Using these catalytic stamps, hydrosilylation-based catalytic stamp lithography was first demonstrated. When terminal alkenes, alkynes, or aldehydes were utilized as molecular inks, the metallic (Pt or Pd) nanopatterns on catalytic stamps were translated into corresponding molecular arrays on H-terminated Si(111) or Si(100) surfaces. Since localized catalytic hydrosilylations

took place exclusively underneath the patterned metallic nanostructures, the pattern formations were not affected by ink diffusion and stamp deformation even at the sub-20 nm scale, while maintaining the advantages of the stamp-based patterning (i.e., large-area, high-throughput capabilities, and low-cost). The concept of catalytic stamp lithography was further extended with other catalytic reactions, and successful nanoscale patterning was performed using hydrogenation (on azide-terminated SiO_x surfaces) and the Heck reaction (on alkene- or bromphenyl-terminated SiO_x surfaces).

A range of nanopatterned surfaces with different chemical functionalities, including thiol, amine, and acid, were created, and they were further modified through appropriate chemical reactions. The potential utility of this simple approach for the construction of a higher degree of nanoarchitectures was suggested.

Acknowledgements

I am truly grateful to the following people who enriched my academic life at the University of Alberta. Without their assistance and understanding, this thesis would never have been completed.

First and foremost, I would like to express my deepest gratitude to my supervisor, Professor Jillian Buriak. Her continuous guidance, suggestions, and hearty encouragement provided me with an ideal environment for doing research. What I learned from her was more than Chemistry – it would become a core of my future career as an independent researcher.

I also would like to thank my supervisor committee members, Prof. Steven Bergens, Prof. Jed Harrison, Prof. Jonathan Veinot, and Prof. Ken Cadien, for their thoughtful and helpful comments into my research. Special thanks must go to Prof. Byron Gates from Simon Fraser University who made an effort to participate in my final defense despite his many other commitments.

I was fortunate to be surrounded by many excellent colleagues and collaborators. I would like to acknowledge the support and friendship from the current and past members of the Buriak group: Dr. Masato Aizawa (a true mentor for so many); Jennifer Bruce, Dr. Kenneth Harris, Sean McClure, Dr. David Rider (my English teachers); and Dr. Steven Chai, Anne Cooper, Dr. Brian Daly, Nicole Dehm, Dr. Anastasia Elias, Yuan Gao, Dr. Yunhui Li, Sayed Nagy, Greg Nilsson, Dr. Yinghong Qiao, Xiao Xing, Dr. Lina Xu, Dr. Dong Wang, Brian Worfolk, Dr.

Table of Contents

Abstract

Acknowledgement

Table of Contents

List of Figures

List of Tables

List of Abbreviations

List of Figures

silicon. (d) Cartoon schematic of metals on PDMS and cross-sectional SEM image of Pd nanostructures on PDMS obtained from (b).

Figure 3.19   AFM height images and section analyses of H-terminated Si(100) surfaces stamped with (a) phenylacetylene and (b) benzaldehyde, followed by etching with 4 M KOH (aq) containing 15% 2-propanol for 30 s.

Figure 3.20   (a) Outline for catalytic stamp lithography on an alkene-terminated surface. A Pt catalytic stamp was inked with phenylsilane (5 mM in 1,4-dioxane) for 1 min and stamped on an alkene-terminated SiO_x/Si surface for 20 min. In this case, however, no pattern formation was observed, as shown in the resulting AFM height image (b).

Figure 3.21   An AFM height image of a Pt catalytic stamp inked with phenylsilane (5 mM in 1,4-dioxane) for 1 min. Large unidentified "blobs" of material (possibly oligomerized/ polymerized phenylsilane) were observed.

Figure 3.22   Schematic representation of an AFM tip convolution effect. For instance, when an organic monolayer domain with 1 nm height and 10 nm lateral size is scanned with an AFM probe with ~15 nm tip diameter and 20° cone angle, the image is in fact convoluted, leading to an observed lateral size of ~20 nm.

Figure 3.23   Photographs of a wrench-based homemade stamping apparatus. An inked catalytic stamp was applied on a H-terminated Si sample until a slight resistance was felt by slowly rotating the screw of the wrench.

Figure 4.1   Schematic outline for the silane SAM formation on SiO_x/Si. The native oxide layer on bulk Si is usually hydroxyl-terminated either by acid/peroxide or UV-ozone treatment. When this activated surface is treated with a silane, the silane is first hydrolyzed by the surface-absorbed water molecules. The hydrolyzed silanes can form siloxane bonds with surface silanol groups and neighboring silanes, yielding an organosiloxane monolayer.

Figure 4.2   Chemical equation for transition metal-catalyzed hydrogenation of azide.

Figure 4.3   (a) Pd-catalyzed transfer hydrogenation of azide groups on a surface. (b) Confocal microscopy image (3 μm $\times$ 3 μm) of a TAMRA labeled-amine/azide patterned surface created via the reaction (a).

Figure 4.4   (a) Chemical equation for the Heck reaction. (b) Reaction mechanism for the Heck reaction. (1) Oxidative addition. (2) Alkene coordination. (3,4) *Syn*-insertion. (5) Bond rotation. (6,7,8) Reductive (*β*-hydride) elimination. (9) Pd^0 regeneration.

Figure 4.5   (a) Schematic of a PVP-stabilized Pd nanoparticle-coated AFM probe and the use of it for the Heck reaction between alkene (styrene)-terminated surface and 4-iodobenzoic acid. (b) AFM friction image of a patterned surface via the process (a). Each line is ~25 nm wide.

Figure 4.6   Outline for the fabrication of an azide-terminated siloxane monolayer on a native oxide-capped Si(100) surface. An activated oxide surface was treated with vaporized 11-bromoundecyltrichlorosilane under vacuum and high temperature (140 ^{o}C). After the formation of a corresponding bromine-terminated siloxane monolayer, nucleophilic substitution reaction was carried out with sodium azide to afford azide terminations.

Figure 5.5   Catalytic stamp lithography-based fabrication of biomolecular nanoarrays. Relatively small biomolecules, such as carbohydrates, might be attached to H-terminated Si surface via hydrosilylation. The remaining space can be filled with other functional terminations, such as PEG.

List of Tables

List of Abbreviations

AFM	Atomic force microscope
aq	Aqueous
DPN	Dip-pen nanolithography
μCP	Microcontact printing
MIMIC	Micromolding in capillaries
μTM	Microtransfer molding
NEMS	Nanoelectromecahnical systems
NP	Nanoparticle
PDMS	Poly(dimethylsiloxane)
PS-*b*-P2VP	Polystyrene-*block*-poly-2-vinylpyridine
PS-*b*-PB	Polystyrene-*block*-polybutadiene
PS-*b*-PMMA	Polystyrene-*block*-polymethylmethacrylate
REM	Replica molding
RIE	Reactive ion etching
SAM	Self-assembled monolayer
SAMIM	Solvent-assisted micromolding
SEM	Scanning electron microscope
STM	Scanning tunneling microscope
SPL	Scanning probe lithography
TBDMS	*Tert*-butyldimethylsilyl
TMS	Trimethylsilyl
TOAB	Tetraoctylammonium bromide
UV	Ultraviolet
XPS	X-ray photoelectron spectroscopy

Chapter 1
General Introduction

This thesis proposes the use of catalytically active flexible stamps to provide a new approach towards patterning organic monolayers on a sub-100 nm scale. We will present the design, strategy, and fabrication of hybrid transition metal catalyst/soft material architectures for the catalytic stamps and the proof-of-concept demonstrations of high resolution molecular patterning (catalytic stamp lithography), to expand the opportunities for the growing fields of nanoscience and nanotechnology.

As an overview of the entire story, this chapter first discusses the background behind this thesis work. We will then show some of the existing techniques that deal with patterning of small organic molecules, including their limitations, and examples from the literature that, in particular, harnesses catalysis in patterning. Finally, we will address how a catalytic stamping system can potentially overcome the limitations of existing patterning techniques.

1.1. Background

At present, there is a general consensus in the scientific and engineering communities that "nanoscale" refers to the length scale between 1-100 nm.[1] Fabrication of structures on this scale is already critical in the semiconductor industry as a result of the continuing miniaturization trend, commonly known as

Moore's Law.[2] The motivation for this trend is *the smaller, the better*; i.e., lower energy consumption, higher operational speed, lower materials use, and less expensive. Similarly, the demand for the creation of smaller structures has been a major driving force for the development of other important technologies, including optics,[3] fluidics,[4] and mechanics.[5] Research on the nanoscale has significant impact on biology and biotechnology as well,[6] since most of the fundamental biological units or systems, such as the DNA double helix and protein-protein interactions, are on the order of the nanoscale.

The tremendous interest in the nanoscale is also derived from a number of unexpected scientific discoveries that are specific to this dimension. These include, for example, the quantum size effect,[7] where the electronic properties of a material are altered due to the confinement of electrons into an extremely tiny space. The mechanical,[8] thermal,[9] magnetic[10] and catalytic[11] properties as well as the reactivity[12] of the material can be also tailored because of the great increase of the surface area to volume ratio. Some of the remarkable examples are carbon-based nanomaterials (fullerenes,[13] carbon nanotubes,[14] and graphene[15]), metallic nano-objects (particles, rods, wires, etc.),[16] and semiconductor quantum dots.[17] Thus, materials reduced to nanoscale dimensions can show different behaviors compared to what they exhibit on the macroscopic scale. It is likely that *there's (still) plenty of room at the bottom*[18] (on the nanoscale) in the foreseeable future, with continuous efforts towards nanostructuring materials.

Some of the key steps towards potential applications of these nanostructures and nanostructured materials involve their surface functionalization, assembly, and patterning, with defined orientation and alignment into functional networks. Integration of a wide variety of organic, inorganic, and biological materials with existing technologies is of interest to construct novel architectures with unique or improved functionalities. While there are many strategies, the use of organic monolayers provides a promising route to construct higher levels of complex systems in a flexible fashion, in terms of building blocks and resulting properties.[19] Organic monolayers are ultrathin films of (small) organic molecules covalently attached to solid surfaces, and have been utilized to control surface properties of a number of materials.[19] The design of constituent molecules plays an important role: the "head" group binds to a surface with specific affinity, while the "tail" group determines the physical and chemical properties of the resulting surface (Figure 1.1). The most extensively studied class of organic monolayers is self-assembled monolayers (SAMs) of alkanethiolates on gold,[19c] but other systems are also known as summarized in Table 1.1.
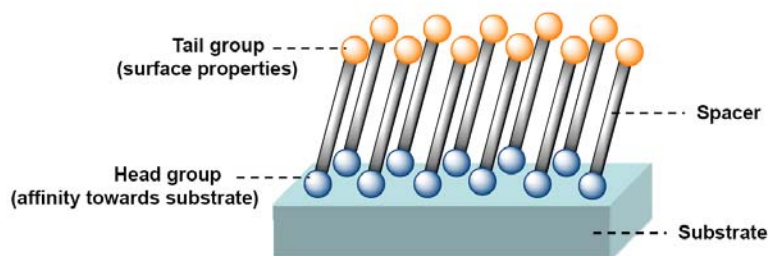
Figure 1.1. Representation of an ideal organic monolayer.

Molecules (Head group)	Substrate	Molecules (Head group)	Substrate
R⌒═	Si-H[20]	R−N≡N$^+$(BF$_4$)$^-$	Si-H[24]
R—≡	Si-H[20]	R−C(=O)OH (R−C(=O)O$^-$)	Al$_2$O$_3$[25]
R−OH	Si-H[21]	R−SiX$_3$ (X = Cl, Alkoxy)	SiO$_x$, glass, etc.[26]
R−SH	Noble metals (Au, Ag, Cu, etc.)[22]	R−NH$_2$	Mica[27]
R⌒═O	Si-H[23]	R−P(=O)(OH)OH, RO−P(=O)(OH)OH	Metal oxides (TiO$_2$, etc.)[28]

Table 1.1. Various molecular (head group)/substrate systems of organic monolayers.

Many unique and potentially significant applications are envisioned through the use of organic monolayers, including hybrid organic/biological-semiconductor devices,[29] molecular electronics,[30] organic nonlinear optics,[31] micro- and nanofluidics,[32] bio-NEMS (nanoelectromechanical systems),[33] ultrasensitive chemical and bioassays,[34] and photovoltaics.[35] Patterning of organic monolayers with desired sizes, shapes, compositions, and spatial location is thus increasingly important in the diverse fields of nanoscience and nanotechnology.

1.2.   Methods for Patterning Organic Monolayers

In general, patterning or shaping of structures is often characterized as "bottom-up (constructive)" or "top-down (destructive)".[36]   Methods from both perspectives have been developed for patterning of organic monolayers, through the use of specific tools that are capable of selective positioning of constituent molecules (for bottom-up) or changing/damaging preformed organic monolayers (for top-down). Although a number of techniques are currently available,[37] only four representatives (photolithography, scanning beam lithography, scanning probe lithography, and soft lithography) are highlighted in this section and evaluated in terms of resolution, operational speed, accessibility, and cost.

Photolithography

Photolithography, a central technique for the top-down fabrication of semiconductor devices (where inorganic materials are primary targets),[38] has been utilized in the patterning of many materials, including organic monolayers.[39] Irradiation of photons on organic monolayers through a patterned mask induces either photochemical reactions, such as photooxidation,[39a] or thermal desorption[39b] of the organic monolayers within the exposed area (Figure 1.2a). UV is a commonly used light source, and pattern sizes at the microscale are routinely produced.   For example, Takakusagi *et al.* demonstrated photo-decomposition ($\lambda = 254 + 185$ nm) of octadecyl monolayer covalently attached to Si(111) using a Cu grid as a photomask (Figure 1.2b).[39c] The resulting patterned

surface could be utilized for selective electroless deposition of a Cu thin film. Using an excimer laser (λ = 193 nm) with a phase mask technique, features as small as 100 nm have been also generated by Friebel and co-workers.[39d]
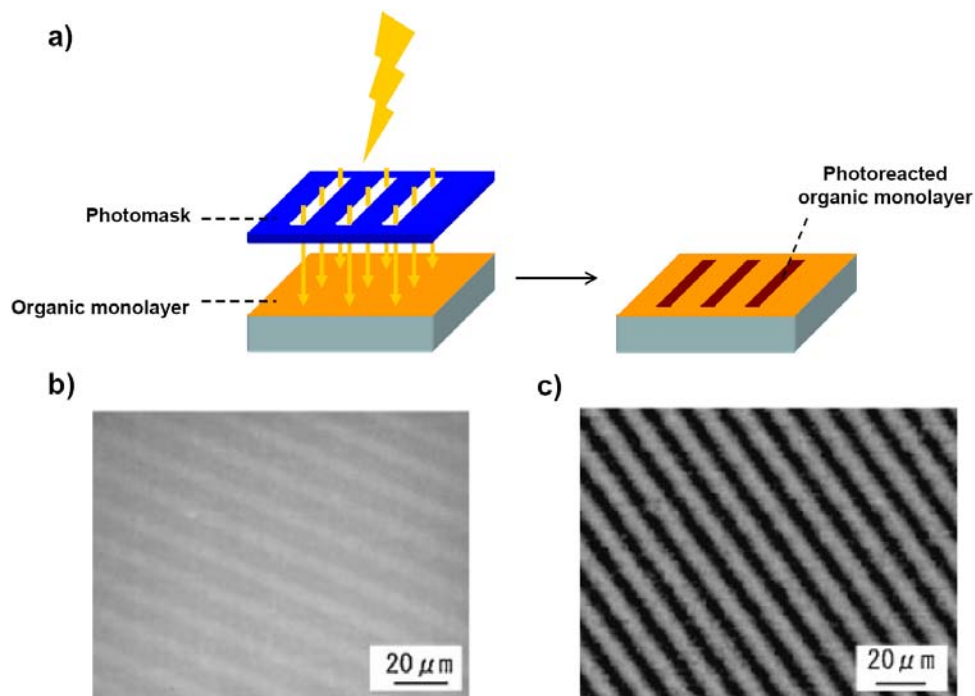
Figure 1.2. (a) Schematic representation of destructive photolithographic patterning. (b) An SEM image of a patterned octadecyl monolayer on Si(111) by UV irradiation. (c) An SEM image of a Cu-deposited Si(111) after UV-mediated patterning shown in (b). Reprinted with permission from ref. 39c. Copyright © 2006 Japan Society of Applied Physics.

Significant challenges remain, however, to create sub-100 nm patterns of organic monolayers by photolithography. The resolution of photolithography is diffraction-limited, and therefore it is necessary to shorten the wavelength of the light to achieve smaller structures.[38a] The shift to a shorter wavelength light

source is not, however, straightforward both technically and economically since a novel design is required for the entire system, including machines, lenses, and masks. The exponentially increasing capital cost is a primary drawback of this technique.[2c] While development of state-of-the-art photolithography has enabled sub-100 nm patterning using liquid immersion technology,[38a] material compatibility will always be an additional consideration in this case.

Scanning Beam Lithography

Scanning beam lithography as outlined here includes electron and focused ion beam lithography, which use energetically activated electrons or ions to create structures in a top-down fashion.[36] The resolution of scanning beam lithography can be very high (down to several nm), but the writing speed is usually very slow because of the serial nature of operation (patterning of 1 cm^2 requires ~24 h).[36] For this reason, scanning beam lithography is not suitable for large-area patterning; instead, it is used where ultrafine structures are necessary, such as production of masks for photolithography.

In the case of patterning organic monolayers, the scanning beam radiation can induce a number of chemical changes, such as bond cleavage, cross linking, and conformational disorder (Figure 1.3a).[40] Gold nanostructures as small as 10 nm have been generated based on the patterning of an alkanethiolate SAM by electron beam lithography followed by selective etching (Figure 1.3b).[40b] Comparable resolution is achievable with focused ion beam lithography.[41] While

scanning probe lithography enables patterning with ultra high resolution, the high operational cost, slow patterning speed, and the need of the ultrahigh vacuum system can limit the accessibility of this technology.
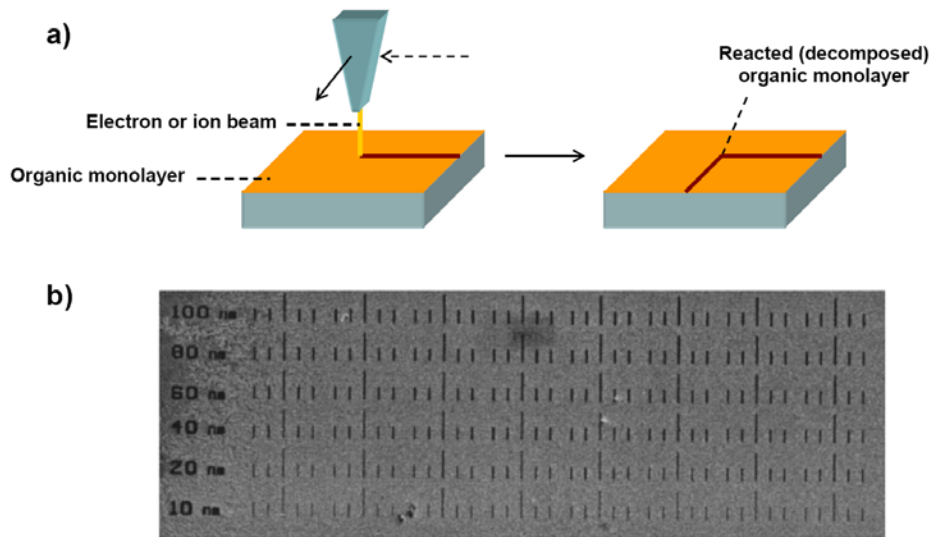
Figure 1.3. (a) Schematic representation of electron/ion beam lithography. (b) An SEM image of patterned gold films created via electron beam patterning of hexadecanethiol SAM followed by etching of the exposed regions of gold. Reprinted with permission from ref. 40b. Copyright © 2000 American Institute of Physics.

Scanning Probe Lithography

This method utilizes a controlled movement of a sharp tip (probe) of a scanning tunneling microscope (STM) or atomic force microscope (AFM) to pattern surfaces. STM-based single atom manipulation is known as the ultimate bottom-up fabrication enabled by this technique.[42] As for the patterning of organic monolayers, scanning probe lithography can be carried out in three

different modes: elimination, substitution, or addition.[43] These modes are commonly referred to as nanoshaving,[44] nanografting,[45] and dip-pen nanolithography (DPN),[46] respectively.

Nanoshaving and nanografting are destructive approaches, which use an AFM tip to remove organic monolayers from a surface by mechanical scratching (Figure 1.4). By applying a force between the tip and the monolayer, molecules can be dislocated from the surface at a certain threshold (typically more than 30 nN), yielding a partially bare surface (nanoshaving).[44] The exposed area can be refilled with another monolayer (nanografting).[45] For example, Liu *et al*. has created an octadecanethiol/decanethiol alternating SAMs nanopattern on gold by nanografting with sub-20 nm resolution.[45b]
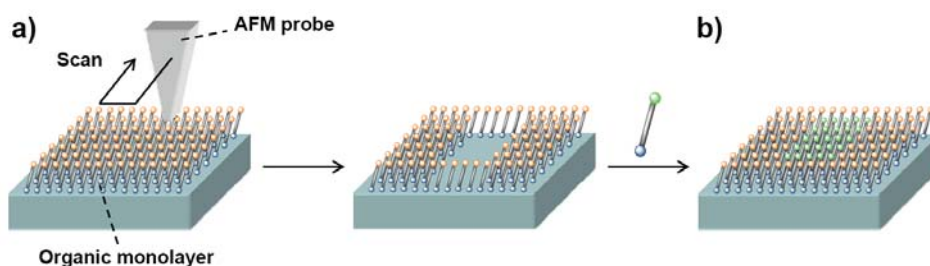
Figure 1.4. Schematic outlines of (a) nanoshaving and (b) nanografting.

DPN, on the other hand, generates patterns in a constructive fashion.[46] This technique was first invented by the Mirkin group in 1999.[46a] Molecules, absorbed on an AFM tip, are selectively delivered onto a surface through a water meniscus formed between the tip and the surface (Figure 1.5). A minimum resolution of 15 nm has been demonstrated with mercaptohexadecanoic acid-

based SAMs on gold.[46b] Offshoots of DPN include the use of a conductive AFM tip, and electrochemical deposition of alkyne molecules on hydrogen-terminated silicon surfaces has been performed.[47]
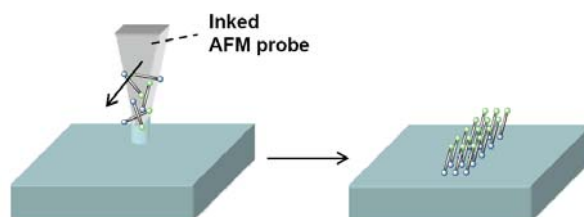
Figure 1.5. Schematic of DPN. Molecular inks, absorbed on an AFM probe, are delivered on a surface through a water meniscus, resulting in the formation of a patterned organic monolayer.

Because AFM and STM are commercially available with considerably less investment compared to photolithography or electron beam lithography, their utility as a nanofabrication tool is increasing at the laboratory level.[46b] DPN is already commercialized by NanoInk (http://www.nanoink.net). However, the slow process of scanning probe lithography needs to be improved from a practical point of view. To address this issue, parallel DPN patterning has been explored using 55,000 AFM cantilevers (Figure 1.6).[48] Related to parallel DPN, polymer pen lithography has been recently reported.[49]

Figure 1.6. An SEM image of a portion of a 2D array of 55,000 AFM tips. Reprinted with permission from ref. 48b. Copyright © 2007 American Chemical Society.

Soft Lithography (Microcontact Printing)

Soft lithography refers to a series of micro and nanofabrication techniques that utilize elastomeric materials as molds, masks, or stamps.[50] Originally proposed by Kumar and Whitesides in 1993,[51] microcontact printing (μCP) is the most intensively developed technique in soft lithography, while replica molding (REM), microtransfer molding (μTM), micromolding in capillaries (MIMIC), and solvent-assisted micromolding (SAMIM), are also known within the family of soft lithography techniques.[50a] In soft lithography, poly(dimethylsiloxane) (PDMS) is the most notably used material as the elastomer. Topographic patterns are usually formed on the surface of PDMS by molding from a rigid master, created by photolithography or electron beam lithography (Figure 1.7).[50c]
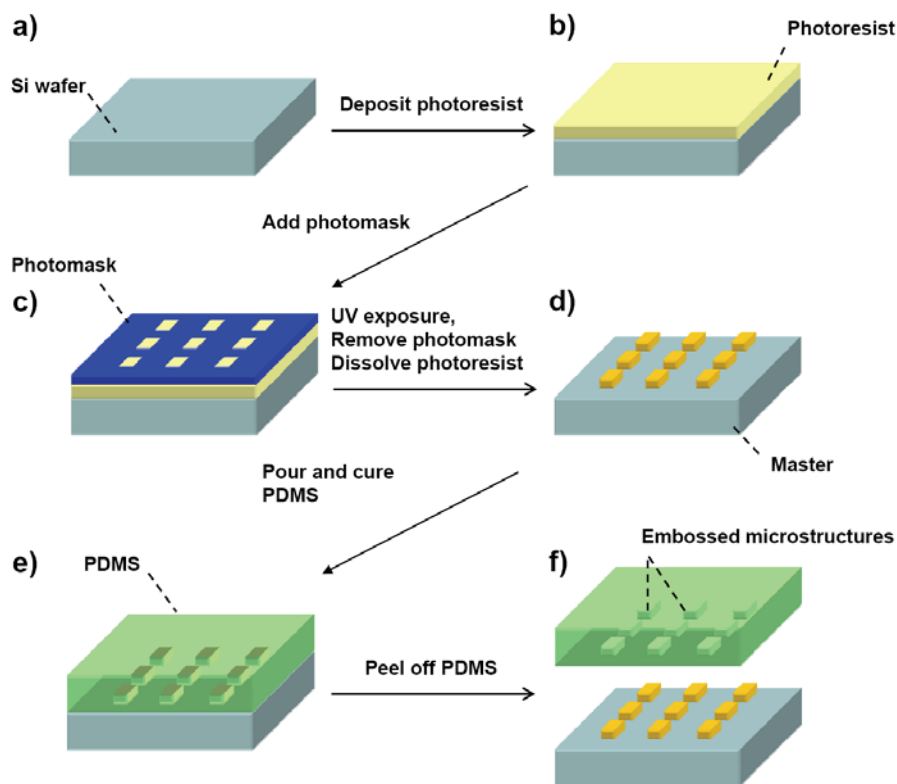
Figure 1.7. Fabrication of topographically patterned PDMS. (a-b) A flat silicon sample is spin-coated with photoresist. (c-d) Photolithography is performed to create a master consisting of a topographic pattern of photoresist on the flat silicon. (e-f) Liquid PDMS is poured on the master, thermally cured, and peeled away to yield topographically patterned PDMS.

Figure 1.8a shows a schematic illustration for the typical procedure of μCP.[51] A PDMS stamp is inked by covering its bas-relief surface with a solution of ink molecules. After the removal of the excess ink, the inked stamp is brought into contact with a surface to be modified. The conformal contact between the raised region of the PDMS stamp and the target surface provide high fidelity and

registration, when ink molecules are transferred onto the surface. While typical contact times are on the order of seconds, a high-quality monolayer can be produced on the surface upon removal of the PDMS stamp. Figure 1.8b shows SEM images of a series of gold patterns generated by μCP with a thiol ink, followed by selective chemical etching of unprotected regions of gold.[52] Other organic monolayer systems have also been patterned by μCP.[50,51]
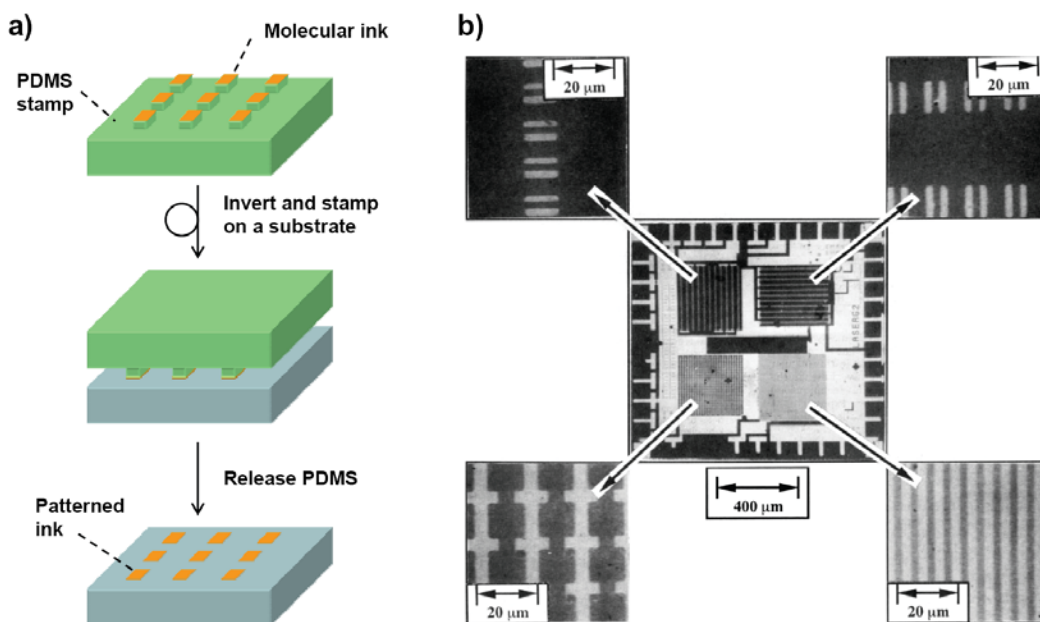
Figure 1.8. (a) Schematic outline for μCP. (b) SEM images of various types of gold features fabricated through μCP and subsequent selective chemical etching. Reprinted with permission from ref. 52. Copyright © 1994 American Chemical Society.

μCP has some unique capabilities that are challenging to achieve with other lithographic techniques described so far (photolithography, scanning beam

lithography, and scanning probe lithography). For example, the use of flexible elastomers allows patterning of non-planar (rough and curved) surfaces[53] and applications into ultrahigh-throughput schemes, such as a rolling stamp (Figure 1.9).[54] In addition, patterning can be carried out on a large surface area, and >50 cm^2 patterning has been demonstrated.[54] The operation can be carried out without the use of clean room and ultrahigh vacuum facilities, as long as a PDMS master is available. Because of these simple, efficient and low-cost procedures, μCP has been utilized in many disciplines beyond chemistry, such as microbiology.[50c]
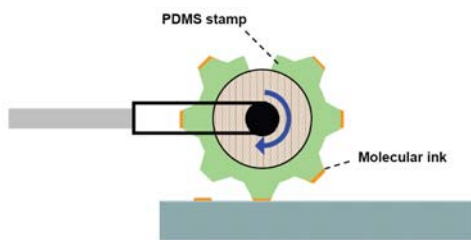
Figure 1.9. A rolling-stamp scheme for ultrahigh-throughput and large-area patterning of a planar surface.

In terms of the resolution limit of μCP, accurate pattern transfer is routinely applied on the microscale. While much smaller features have been demonstrated, it is technically challenging to achieve sub-100 nm patterning.[51d,55] Since conventional μCP generally relies on a spontaneous chemisorption or simple physisorption to deposit molecular inks onto target surfaces, the monolayer formation process can be significantly influenced by ink diffusion, including surface-mediated lateral diffusion and vapor phase transport (Figure

1.10a).[19c,56]   In addition, the capabilities of stamps to replicate the topographic features from photolithographically created masters and to maintain them without deformation (pairing, buckling, and roof collapse; Figure 1.10b) during the stamping procedure also play significant roles with regards to the final sizes of the transferred features.[51c,57]   It is apparent that these phenomena become more problematic if the lateral size of the patterned features reaches the nanoscale.   In order to facilitate nanoscale patterning by μCP, these ink and stamp-based challenges need to be overcome.
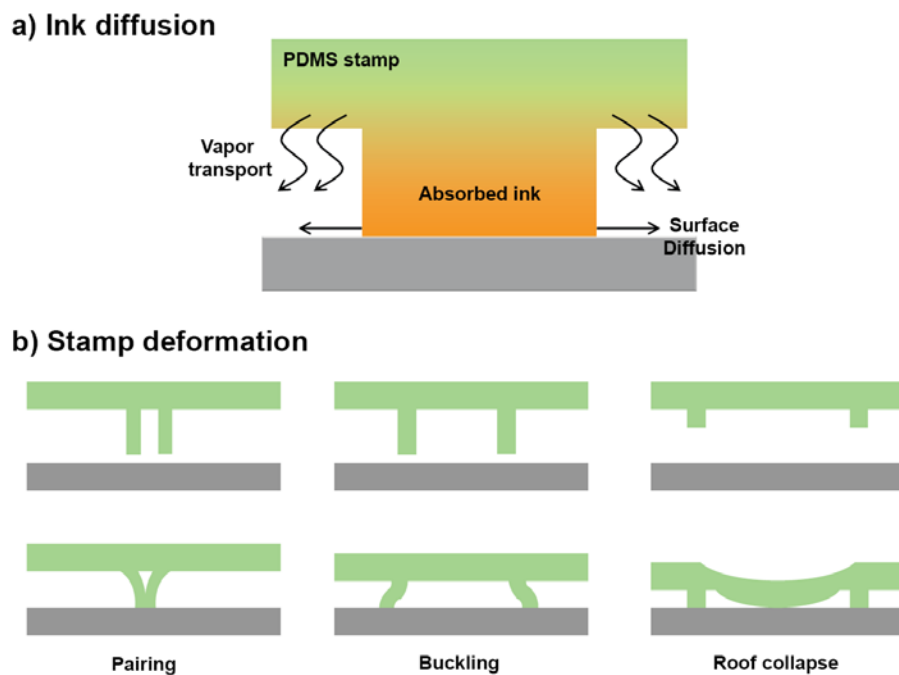
Figure 1.10.   Problems associated with patterning via μCP.   (a) Ink diffusion (surface-mediated lateral diffusion and vapor phase transport).   (b) Stamp deformation (pairing, buckling, and roof collapse).

Several approaches have been proposed to address these issues. For instance, to achieve a diffusion-free process, the use of high molecular weight materials as inks has been explored,[56a,58] and less-deformable composite structures have been developed to improve the stamp stability.[59] Huck and co-workers have performed "nanocontact" printing by combining these two approaches, where dendrimer-based sub-50 nm features were obtained (Figure 1.11).[60] Alternatively, topographically flat (but chemically patterned) stamps[61] have been also adopted in nanoscale patterning.[61d,f]
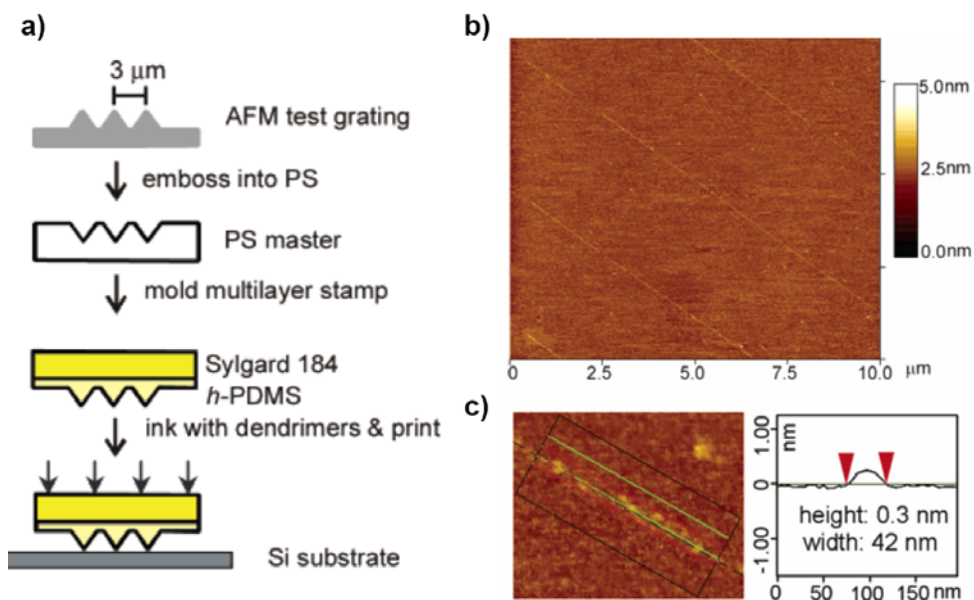
Figure 1.11. (a) Schematic illustration of nanocontact printing using a high molecular weight dendrimer and a less deformable composite PDMS stamp. (b) AFM images of patterned dendrimer lines on a silicon surface. (c) A magnified AFM image of part of (b) and a cross-sectional analysis. Reprinted with permission from ref. 60. Copyright © 2003 American Chemical Society.

1.3. Catalysis for High Resolution Patterning

A possible route to achieve nanoscale resolution patterning would be the utilization of more site-specific reactions, directed by heterogeneous (immobilized) catalysts, to formulate chemical patterns. Müller *et al.* first demonstrated catalytic transformations of surface species using catalytically activated scanning probes (Figure 1.12).[62] In this experiment, a platinum-coated AFM tip was prepared by electron beam evaporation of a platinum film onto a commercially available silicon AFM tip. By scanning the as-prepared tip over an azide-terminated organic monolayer in the presence of hydrogen (dissolved in 2-propanol), spatially-defined hydrogenation could be carried out to generate an amino-terminated moiety in the monolayer, and these amino groups were subsequently used as a reactive template to host aldehyde-modified latex beads. Following this report, other groups performed similar AFM-based approaches with Pd-catalyzed hydrogenation[63] and hydrosilylation,[63] acid-catalyzed hydrolysis,[64] and Pd-catalyzed C-C bond forming reactions (the Suzuki coupling and the Heck reaction)[65] to yield sub-100 nm scale patterns.

Figure 1.12. Schematic of site-selective hydrogenation of an azide-terminated surface using a Pt-coated AFM tip in the presence of hydrogen. The newly formed amino groups were then used to assemble aldehyde-modified latex beads. Reprinted with permission from ref. 62. Copyright © 1995 The American Association for the Advancement of Science.

Inspired by these catalytic scanning probe-based methods, the integration of catalysis and μCP has been also recently proposed. For example, Li *et al.* employed oxygen plasma treatment on a PDMS stamp to make its surface catalytically active by forming a thin layer of acidic silicon oxide.[66] Stamping of this surface-oxidized PDMS stamp onto a silyl ether-terminated self-assembled monolayer on gold led to a pattern formation via acid-catalyzed hydrolysis (Figure 1.13). Although the sizes of patterned features here were still within the microscale, the edge resolution (i.e., the degree of broadening) of those patterns was at the nanoscale due to the diffusion-free patterning process.
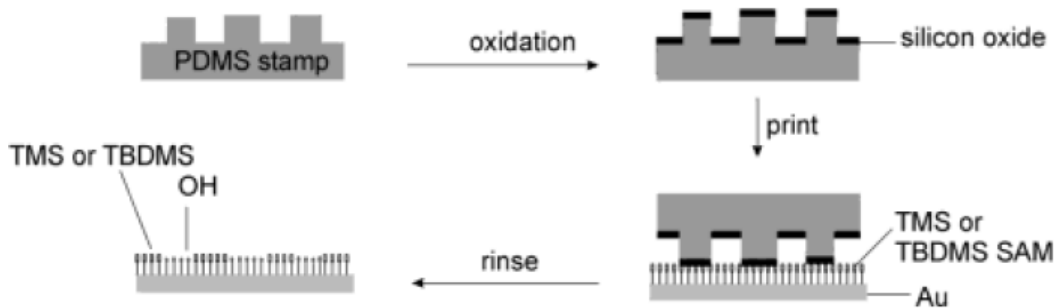
Figure 1.13. Schematic outline of pattern formation by acid-catalyzed hydrolysis induced by
μCP. A bas-relief PDMS stamp was first treated with oxygen plasma to catalytically activate
the surface by forming a silicon oxide layer. Printing of the oxidized stamp on a
trimethylsilyl (TMS)- or *tert*-butyldimethylsilyl (TBDMS)-ether terminated SAM resulted in
site-selective cleavage of TMS or TBDMS group, yielding a chemically patterned surface.
Reprinted with permission from ref. 66. Copyright © 2003 American Chemical Society.

Bio- and transition metal-catalysis were also utilized with μCP. Snyder
and co-workers have developed a procedure to incorporate enzymes on a
patterned poly(acrylamide)-based stamp and demonstrated site-selective
hydrolytic cleavage of fluorescent dye attached to DNA monolayer.[67] Spruell *et
al.* performed Cu-catalyzed azide-alkyne cyclization using Cu-coated PDMS
stamps to pattern azide-terminated surfaces (Figure 1.14).[68] These papers, again,
demonstrated an improved edge resolution in comparison to the observations of
chemisorptions-based μCP, confirming the utility of catalysis as a high resolution
patterning tool.
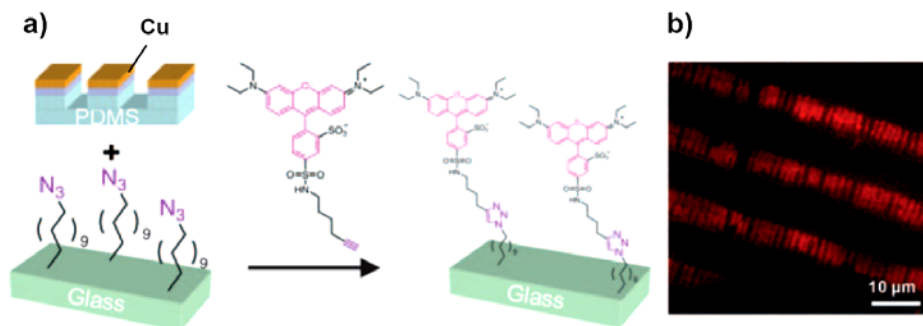
Figure 1.14. (a) Scheme for patterning an azide-terminated surface with fluorescent alkyne molecules using a Cu-coated PDMS stamp. (b) A fluorescent microscopy image of the resulting patterned surface. Reprinted with permission from ref. 68. Copyright © 2008 Wiley-VCH.

1.4. Development of Catalytic Stamp Lithography

From these pioneering works described *vide supra*, it was strongly suggested that patterning by heterogeneous catalysis provides an excellent route to suppress the ink diffusion problem even under static patterning conditions, such as stamping. Nanoscale patterning should be feasible by *localized catalysis* using a functional stamp whose surface is patterned with nanosized catalysts. With this stamp design, in addition, another critical issue of μCP – stamp deformation – would be simultaneously eliminated, since topographic features on a stamp are replaced by immobilized (deformation-free) solid catalyst in this case. Figure 1.15 schematically illustrates these points in comparison to conventional μCP. Thus, our strategy for stamp-based nanoscale patterning of organic monolayers, catalytic stamp lithography, was initiated through the design of a novel type of

patterning medium, a PDMS-based stamp patterned with an array of transition metal nanostructured catalysts.
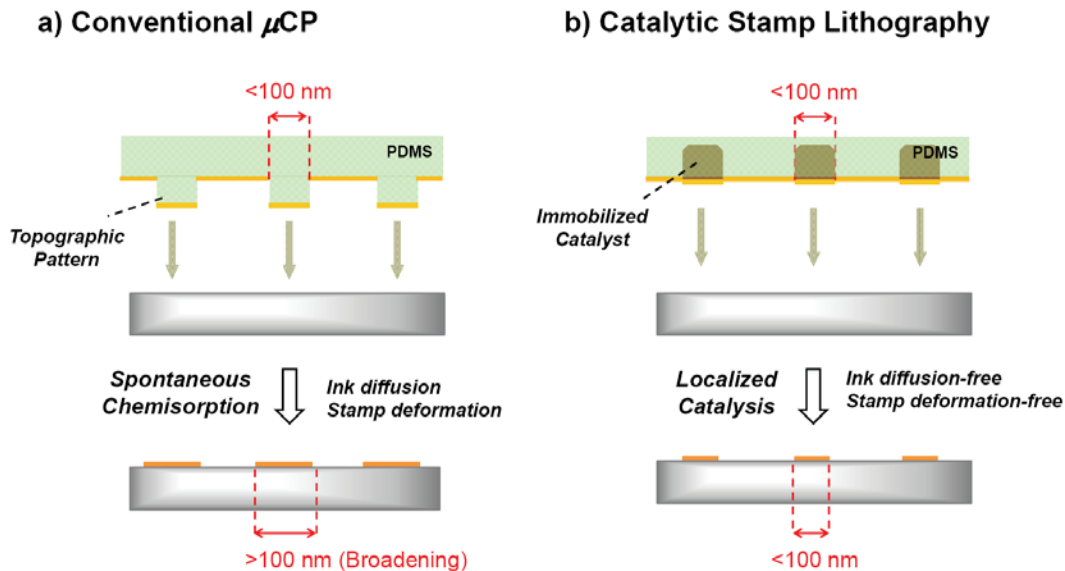
Figure 1.15. Nanoscale patterning by (a) conventional μCP and (b) catalytic stamp lithography. Even if a PDMS stamp with sub-100 nm topographic features is used, the resulting pattern generally results in broadening in conventional chemisorption-based μCP because of ink diffusion and/or stamp deformation. In contrast, in catalytic stamp lithography, pattern formation is mediated by localized catalysis derived from immobilized catalysts on PDMS. Therefore, the resulting pattern is less susceptible from ink diffusion and stamp deformation and mirrors the original size of the immobilized catalysts.

In order to integrate patterned nanoscale metallic catalysts with PDMS, we utilized block copolymer-based self-assembly to produce the desired patterns, and then incorporated them into a PDMS stamp. Via our approach, the metallic catalyst pattern is produced first on a rigid support, and then the flexible PDMS

mixed and cured over top, yielding a functional catalytic stamp. The use of the self-assembly-based process to produce catalytic stamps is inexpensive and efficient, since photolithography, e-beam lithography, and other techniques to produce the parent masters are avoided.

1.5. *Organization of the Thesis*

Based on the concept described above, this thesis presents catalytic stamp lithography with three varieties of catalytic reactions; hydrosilylation, hydrogenation, and the Heck reaction. These reactions have been well studied in molecular systems and utilized to modify surface properties of bulk materials.[62,63,65b] As for the target substrates to be patterned, technologically important silicon substrates were selected as an ideal starting point for a broad range of potential applications.[69]

Prior to the investigation of catalytic stamp lithography, however, the design and preparation of catalytic stamps needs to be clarified. Chapter 2 is devoted to this portion, and detailed strategy to fabricate catalytic stamps is presented. Because self-assembled block copolymers play a key role to produce these functional stamps, Chapter 2 starts with a general introduction of block copolymers. Catalytic stamps with Pd, Pt, and Au nanostructures were prepared with different morphologies, and were characterized by AFM, SEM, and XPS.

In Chapter 3, hydrosilylation-based catalytic stamp lithography is described. Using catalytic stamps patterned with Pd or Pt nanostructures,

catalytic hydrosilylation was performed on hydrogen-terminated Si surfaces with a series of alkene, alkyne, or aldehyde molecular inks. The resulting surfaces were analyzed mainly by AFM and XPS [We performed FTIR measurements as well, but no informative results were obtained because of the low surface coverage (typically <15%) of samples, patterned by catalytic stamp lithography],[70] and potential utility of as-chemically patterned surfaces was explored. Hydrosilylation on alkene-terminated surfaces using silane inks was also attempted [Chapter 2 and 3 were reproduced in part with permission from: (a) Mizuno, H.; Buriak, J. M. *J. Am. Chem. Soc.* **2008**, *130*, 17656-17657. Copyright © 2008 American Chemical Society. (b) Mizuno, H.; Buriak, J. M. *ACS Appl. Mater. Interfaces* **2009**, *1*, 2711-2700. Copyright © 2009 American Chemical Society].

Chapter 4 deals with hydrogenation- and the Heck reaction-based catalytic stamp lithography with the use of Pd catalytic stamps. Catalytic hydrogenation of azide-terminated oxide-capped silicon surfaces to yield amine-terminated patterns was first demonstrated. Secondly, C-C bond formation between aryl halides and alkenes were carried out in two systems: aryl halide inks/alkene-terminated surfaces or alkene inks/bromophenyl-terminated surfaces. AFM and XPS were again the primary analysis tools utilized to prove the chemical identities of resulting surfaces.

Finally, Chapter 5 describes the summary of each chapter (Chapters 2-4), followed by the potential research direction/perspectives of this thesis work.

1.6. References

1. *Nanoscience and nanotechnologies: opportunities and uncertainties*; The Royal Society, London, UK, 2004. http://www.nanotec.org.uk/final-Report.htm

2. (a) Moore, G. E. *Electronics* **1965**, *38*, 4-7. (b) Grifantini, K. *Technol. Rev.* **2009**, *112*, 30-39. (c) *International Technology Roadmap for Semiconductors, 2007 Edition*; The ITRS, 2007. http://www.itrs.net/Links/ 2007ITRS/Home2007.htm

3. Kostal, H.; Wang, J. *Laser Focus World* **2004**, *40*, 155-159.

4. Ho, C.-M. *14th IEEE International Conference on Micro Electro Mechanical Systems, Technical Digest* Interlaken, Switzerland, 2001, 375-384.

5. Lyshevski, S. E. *MEMS and NEMS: systems, devices, and structures*; CRC Press, Boca Raton, FL, 2002.

6. Truskett, V. N.; Watts, M. P. C. *Trends Biotechnol.* **2006**, *24*, 312-317.

7. (a) Cullis, A. G.; Canham, L. T. *Nature* **1991**, *353*, 335-338. (b) Tringides, M. C.; Jalochowski, M.; Bauer, E. *Phys. Today* **2007**, *60*, 50-54.

8. Salvetat, J. P.; Bonard, J. M.; Thomson, N. H.; Kulik, A. J.; Forro, L.; Benoit, W.; Zuppiroli, L. *Appl. Phys. A: Mater. Sci. Process.* **1999**, *69*, 255-260.

9. Savage, T.; Rao, A. M. *Thermal Conductivity* **2004**, 262-284.

10. Leslie-Pelecky, D. L.; Rieke, R. D. *Chem. Mater.* **1996**, *8*, 1770-1783.

11. Ishida, T.; Haruta, M. *Angew. Chem., Int. Ed.* **2007**, *46*, 7154-7156.

12. Brousseau, P.; Anderson, C. J. *Propell. Explos. Pyrot.* **2002**, *27*, 300-306.

13. Kroto, H. W.; Heath, J. R.; O'Brien, S. C.; Curl, R. F.; Smalley, R. E. *Nature* **1985**, *318*, 162-163.

14. Iijima, S. *Nature* **1991**, *354*, 56-58.

15. Novoselov, K. S.; Geim, A. K.; Morozov, S. V.; Jiang, D.; Zhang, Y.; Dubonos, S. V.; Grigorieva, I. V.; Firsov, A. A. *Science* **2004**, *306*, 666-669.

16. (a) Daniel, M.-C.; Astruc, D. *Chem. Rev.* **2003**, *104*, 293-346. (b) Kline, T. R.; Tian, M.; Wang, J.; Sen, A.; Chan, M. W. H.; Mallouk, T. E. *Inorg. Chem.* **2006**, *45*, 7555-7565.

17. (a) Wang, Y.; Herron, N. *J. Phys. Chem.* **1991**, *95*, 525-532. (b) Alivisatos, A. P. *Science* **1996**, *271*, 933-937.

18. Feynman, R. P. *Eng. Sci.* **1960**, *23*, 22-36.

19. (a) Ulman, A. *An Introduction to Ultrathin Organic Films*; Academic Press: Boston, 1991. (b) Ulman, A. *Chem. Rev.* **1996**, *96*, 1533-1554. (c) Love, J. C.; Estroff, L. A.; Kriebel, J. K.; Nuzzo, R. G.; Whitesides, G. M. *Chem. Rev.* **2005**, *105*, 1103-1169. (d) Hamers, R. J. *Annu. Rev. Anal. Chem.* **2008**, *1*, 707-736.

20. Buriak, J. M. *Chem. Rev.* **2002**, *102*, 1271-1308.

21. Niederhauser, T. L.; Lua, Y.-Y.; Jiang, G.; Davis, S. D.; Matheson, R.; Hess, D. A.; Mowat, I. A.; Linford, M. R. *Angew. Chem., Int. Ed.* **2002**, *41*, 2353-2356.

22. Laibinis, P. E.; Whitesides, G. M.; Allara, D. L.; Tao, Y. T.; Parikh, A. N.; Nuzzo, R. G. *J. Am. Chem. Soc.* **1991**, *113*, 7152-7167.

23. Effenberger, F.; Gotz, G.; Bidlingmaier, B.; Wezstein, M. *Angew. Chem., Int. Ed.* **1998**, *37*, 2462-2464.

24. Stewart, M. P.; Maya, F.; Kosynkin, D. V.; Dirk, S. M.; Stapleton, J. J.; McGuiness, C. L.; Allara, D. L.; Tour, J. M. *J. Am. Chem. Soc.* **2004**, *126*, 370-378.

25. Allara, D. L.; Nuzzo, R. G. *Langmuir* **1985**, *1*, 45-52.

26. Onclin, S.; Ravoo, B. J.; Reinhoudt, D. N. *Angew. Chem., Int. Ed.* **2005**, *44*, 6282-6304.

27. Benitez, J. J.; Kopta, S.; Ogletree, D. F.; Salmeron, M. *Langmuir* **2002**, *18*, 6096-6100.

28. (a) Hofer, R.; Textor, M.; Spencer, N. D. *Langmuir* **2001**, *17*, 4014-4020. (b) Gao, W.; Dickinson, L.; Grozinger, C.; Morin, F. G.; Reven, L. *Langmuir* **1996**, *12*, 6429-6435.

29. (a) Roberts, M. E.; Sokolov, A. N.; Bao, Z. *J. Mater. Chem.* **2009**, *19*, 3351-3363. (b) Menard, E.; Meitl, M. A.; Sun, Y.; Park, J. U.; Shir, D. J. L.; Nam, Y. S.; Jeon, S.; Rogers, J. A. *Chem. Rev.* **2007**, *107*, 1117-1160.

(c) Sarikaya, M.; Tamerler, C.; Jen, A. K. Y.; Schulten, K.; Baneyx, F. *Nat. Mater.* **2003**, *2*, 577-585.

30.   (a) Natan, A.; Kronik, L.; Haick, H.; Tung, R. T. *Adv. Mater.* **2007**, *19*, 4103-4117. (b) Aswal, D. K.; Lenfant, S.; Guerin, D.; Yakhmi, J. V.; Vuillaume, D. *Analytica Chimica Acta* **2006**, *568*, 84-108.

31.   (a) Koos, C.; Vorreau, P.; Vallaitis, T.; Dumon, P.; Bogaerts, W.; Baets, R.; Esembeson, B.; Biaggio, I.; Michinobu, T.; Diederich, F.; Freude, W.; Leuthold, J. *Nat. Photon.* **2009**, *3*, 216-219. (b) Hecht, J. *Laser Focus World* **2008**, *44*, 123-126.

32.   (a) Mela, P.; Onclin, S.; Goedbloed, M. H.; Levi, S.; Garcia-Parajo, M. F.; van Hulst, N. F.; Ravoo, B. J.; Reinhoudt, D. N.; van den Berg, A. *Lab Chip* **2005**, *5*, 163-170. (b) Knopf, D. A.; Cosman, L. M.; Mousavi, P.; Mokamati, S.; Bertram, A. K. *J. Phys. Chem. A* **2007**, *111*, 11021-11032. (c) Kreutz, J. E.; Li, L.; Roach, L. S.; Hatakeyama, T.; Ismagilov, R. F. *J. Am. Chem. Soc.* **2009**, *131*, 6042-6043.

33.   (a) Kim, P.; Du, Y.; Khademhosseini, A.; Langer, R.; Suh, K. Y. In *Unconventional Nanopatterning Techniques and Applications;* Rogers, J. A., Lee, H. L., Eds.; Wiley: Hoboken, NJ, 2009, 325-357. (b) Bhushan, B. *Micro. Engn.* **2007**, *84*, 387-412.

34.   (a) Lin, H.-Y.; Chen, H.-A.; Lin, H.-N. *Anal. Chem.* **2008**, *80*, 1937-1941. (b) Greibl, W.; Hayden, O.; Achatz, P.; Fischerauer, G.; Scholl, G.; Dickert, F. L. *Proc. SPIE* **2002**, *4576*, 160-168.   (c) Arakaki, A.;

Hideshima, S.; Nakagawa, T.; Niwa, D.; Tanaka, T.; Matsunaga, T.; Osaka, T. *Biotechnol. Bioeng.* **2004**, *88*, 543-546.

35.   (a) Har-Lavan, R.; Ron, I.; Thieblemont, F.; Cahen, D. *Appl. Phys. Lett.* **2009**, *94*, 0433081-0433083. (b) Hwang, E.; de Silva, K. M. N.; Seevers, C. B.; Li, J.-R.; Garno, J. C.; Nesterov, E. E. *Langmuir* **2008**, *24*, 9700-9706. (c) Grätzel, M. *Prog. Photovoltaics* **2006**, *14*, 429-442. (d) Imahori, H.; Fujimoto, A.; Kang, S.; Hotta, H.; Yoshida, K.; Umeyama, T.; Matano, Y.; Isoda, S.; Isosomppi, M.; Tkachenko, N. V.; Lemmetyinen, H. *Chem. Eur. J.* **2005**, *11*, 7265-7275.

36.   Gates, B. D.; Xu, Q.; Stewart, M.; Ryan, D.; Willson, C. G.; Whitesides, G. M. *Chem. Rev.* **2005**, *105*, 1171-1196.

37.   Geissler, M.; Xia, Y. *Adv. Mater.* **2004**, *16*, 1249-1269.

38.   (a) Pease, R. F.; Chou, S. Y. *Proc. IEEE* **2008**, *96*, 248-270. (b) Kapoor, R.; Adner, R. *Solid State Technol.* **2007**, *50*, 51-54.

39.   (a) Behm, J. M.; Lykke, K. R.; Pellin, M. J.; Hemminger, J. C. *Langmuir* **1996**, *12*, 2121-2124. (b) Shadnam, M. R.; Kirkwood, S. E.; Fedosejevs, R.; Amirfazli, A. *Langmuir* **2004**, *20*, 2667-2676. (c) Takakusagi, S.; Uosaki, K. *Jpn. J. Appl. Phys. 1* **2006**, *45*, 8961-8966. (d) Friebel, S.; Aizenberg, J.; Abad, S.; Wiltzius, P. *Appl. Phys. Lett.* **2000**, *77*, 2406-2408.

40.   (a) Zharnikov, M.; Grunze, M. *J. Vac. Sci. Technol., B* **2002**, *20*, 1793-1807. (b) Golzhauser, A.; Geyer, W.; Stadler, V.; Eck, W.; Grunze, M.;

Edinger, K.; Weimann, T.; Hinze, P. *J. Vac. Sci. Technol., B* **2000**, *18*, 3414-3418.

41.   (a) Chabinyc, M. L.; Love, J. C.; Thywissen, J. H.; Cervelli, F.; Prentiss, M. G.; Whitesides, G. M. *Langmuir* **2003**, *19*, 2201-2205. (b) Ada, E. T.; Hanley, L.; Etchin, S.; Melngailis, J.; Dressick, W. J.; Chen, M.-S.; Calvert, J. M. *J. Vac. Sci. Technol., B* **1995**, *13*, 2189-96.

42.   Hla, S.-W. *Jpn. J. Appl. Phys.* **2008**, *47*, 6063-6069.

43.   (a) Kramer, S.; Fuierer Ryan, R.; Gorman Christopher, B. *Chem. Rev.* **2003**, *103*, 4367-418. (b) Garcia, R.; Martinez Ramses, V.; Martinez, J. *Chem. Soc. Rev.* **2006**, *35*, 29-38.

44.   Liu, G.-Y.; Salmeron, M. B. *Langmuir* **1994**, *10*, 367-370.

45.   (a) Xu, S.; Liu, G.-Y. *Langmuir* **1997**, *13*, 127-129. (b) Liu, J.-F.; Von Ehr, J. R.; Baur, C.; Stallcup, R.; Randall, J.; Bray, K. *Appl. Phys. Lett.* **2004**, *84*, 1359-1361.

46.   (a) Piner, R. D.; Zhu, J.; Xu, F.; Hong, S.; Mirkin, C. A. *Science* **1999**, *283*, 661-663. (b) Ginger, D. S.; Zhang, H.; Mirkin, C. A. *Angew. Chem., Int. Ed.* **2004**, *43*, 30-35. (c) Salaita, K.; Wang, Y.; Mirkin, C. A. *Nat. Nanotechnol.* **2007**, *2*, 145-155.

47.   Hurley, P. T.; Ribbe, A. E.; Buriak, J. M. *J. Am. Chem. Soc.* **2003**, *125*, 11334-11339.

48.   (a) Salaita, K.; Wang, Y.; Fragala, J.; Vega, R. A.; Liu, C.; Mirkin, C. A. *Angew. Chem., Int. Ed.* **2006**, *45*, 7220-7223. (b) Mirkin, C. A. *ACS Nano* **2007**, *1*, 79-83.

49.   Huo, F.; Zheng, Z.; Zheng, G.; Giam, L. R.; Zhang, H.; Mirkin, C. A. *Science* **2008**, *321*, 1658-1660.

50.   (a) Xia, Y.; Whitesides, G. M. *Angew. Chem., Int. Ed.* **1998**, *37*, 550-575. (b) Rogers, J. A.; Nuzzo, R. G. *Mater. Today* **2005**, *8*, 50-56. (c) Weibel, D. B.; DiLuzio, W. R.; Whitesides, G. M. *Nat. Rev. Microbiol.* **2007**, *5*, 209-218.

51.   (a) Kumar, A.; Whitesides, G. M. *Appl. Phys. Lett.* **1993**, *63*, 2002-2004. (b) Ruiz, S. A.; Chen, C. S. *Soft Matter* **2007**, *3*, 168-177. (c) Quist, A. P.; Pavlovic, E.; Oscarsson, S. *Anal. Bioanal. Chem.* **2005**, *381*, 591-600. (d) Perl, A.; Reinhoudt, D. N.; Huskens, J. *Adv. Mater.* **2009**, *21*, 2257-2268.

52.   Kumar, A.; Biebuyck, H. A.; Whitesides, G. M. *Langmuir* **1994**, *10*, 1498-1511.

53.   Jackman, R. J.; Wilbur, J. L.; Whitesides, G. M. *Science* **1995**, *269*, 664-666.

54.   Xia, Y.; Qin, D.; Whitesides, G. M. *Adv. Mater.* **1996**, *8*, 1015-1017.

55.   Huck, W. T. S. *Angew. Chem., Int. Ed.* **2007**, *46*, 2754-2757.

56.   (a) Delamarche, E.; Schmid, H.; Bietsch, A.; Larsen, N. B.; Rothuizen, H.; Michel, B.; Biebuyck, H. *J. Phys. Chem. B* **1998**, *102*, 3324-3334. (b) Xia, Y.; Whitesides, G. M. *J. Am. Chem. Soc.* **1995**, *117*, 3274-3275. (c)

Gannon, G.; Larsson, J. A.; Greer, J. C.; Thompson, D. *Langmuir* **2009**, *25*, 242-247.

57.   (a) Delamarche, E.; Schmid, H.; Michel, B.; Biebuyck, H. *Adv. Mater.* **1997**, *9*, 741-746. (b) Hui, C. Y.; Jagota, A.; Lin, Y. Y.; Kramer, E. J. *Langmuir* **2002**, *18*, 1394-1407. (c) Sharp, K. G.; Blackman, G. S.; Glassmaker, N. J.; Jagota, A.; Hui, C.-Y. *Langmuir* **2004**, *20*, 6430-6438.

58.   (a) Liebau, M.; Huskens, J.; Reinhoudt, D. N. *Adv. Funct. Mater.* **2001**, *11*, 147-150. (b) Li, H.; Kang, D.-J.; Blamire, M. G.; Huck, W. T. S. *Nano Lett.* **2002**, *2*, 347-349. (c) Liebau, M.; Janssen, H. M.; Inoue, K.; Shinkai, S.; Huskens, J.; Sijbesma, R. P.; Meijer, E. W.; Reinhoudt, D. N. *Langmuir* **2002**, *18*, 674-682. (d) Perl, A.; Peter, M.; Ravoo, B. J.; Reinhoudt, D. N.; Huskens, J. *Langmuir* **2006**, *22*, 7568-7573.

59.   (a) James, C. D.; Davis, R. C.; Kam, L.; Craighead, H. G.; Isaacson, M.; Turner, J. N.; Shain, W. *Langmuir* **1998**, *14*, 741-744. (b) Tormen, M.; Borzenko, T.; Steffen, B.; Schmidt, G.; Molenkamp, L. W. *Appl. Phys. Lett.* **2002**, *81*, 2094-2096. (c) Schmid, H.; Michel, B. *Macromolecules* **2000**, *33*, 3042. (d) Odom, T. W.; Love, J. C.; Wolfe, D. B.; Paul, K. E.; Whitesides, G. M. *Langmuir* **2002**, *18*, 5314. (e) Choi, K. M.; Rogers, J. A. *J. Am. Chem. Soc.* **2003**, *125*, 4060-4061.

60.   Li, H. W.; Muir, B. V. O.; Fichet, G.; Huck, W. T. S. *Langmuir* **2003**, *19*, 1963-1965.

61. (a) Geissler, M.; Bernard, A.; Bietsch, A.; Schmid, H.; Michel, B.; Delamarche, E. *J. Am. Chem. Soc.* **2000**, *122*, 6303-6304. (b) Delamarche, E.; Donzel, C.; Kamounah, F. S.; Wolf, H.; Geissler, M.; Stutz, R.; Schmidt-Winkel, P.; Michel, B.; Mathieu, H. J.; Schaumburg, K. *Langmuir* **2003**, *19*, 8749-8758. (c) Sharpe, R. B. A.; Burdinski, D.; Huskens, J.; Zandvliet, H. J. W.; Reinhoudt, D. N.; Poelsema, B. *J. Am. Chem. Soc.* **2005**, *127*, 10344-10349. (d) Coyer, S. R.; Garcia, A. J.; Delamarche, E. *Angew. Chem., Int. Ed.* **2007**, *46*, 6837-6840. (e) Duan, X.; Sadhu, V. B.; Perl, A.; Peter, M.; Reinhoudt, D. N.; Huskens, J. *Langmuir* **2008**, *24*, 3621-3627. (f) Zheng, Z.; Jang, J.-W.; Zheng, G.; Mirkin, C. A. *Angew. Chem., Int. Ed.* **2008**, *47*, 9951-9954.

62. Müller, W. T.; Klein, D. L.; Lee, T.; Clarke, J.; McEuen, P. L.; Schultz, P. G. *Science* **1995**, *268*, 272-273.

63. Blackledge, C.; Engebretson, D. A.; McDonald, J. D. *Langmuir* **2000**, *16*, 8317-8323.

64. Peter, M.; Li, X. M.; Huskens, J.; Reinhoudt, D. N. *J. Am. Chem. Soc.* **2004**, *126*, 11684-11690.

65. (a) Davis, J. J.; Coleman, K. S.; Busuttil, K. L.; Bagshaw, C. B. *J. Am. Chem. Soc.* **2005**, *127*, 13082-13083. (b) Davis, J. J.; Bagshaw, C. B.; Busuttil, K. L.; Hanyu, Y.; Coleman, K. S. *J. Am. Chem. Soc.* **2006**, *128*, 14135-14141.

66.   Li, X. M.; Peter, M.; Huskens, J.; Reinhoudt, D. N. *Nano Lett.* **2003**, *3*, 1449-1453.

67.   Snyder, P. W.; Johannes, M. S.; Vogen, B. N.; Clark, R. L.; Toone, E. J. *J. Org. Chem.* **2007**, *72*, 7459-7461.

68.   Spruell, J. M.; Sheriff, B. A.; Rozkiewicz, D. I.; Dichtel, W. R.; Rohde, R. D.; Reinhoudt, D. N.; Stoddart, J. F.; Heath, J. R. *Angew. Chem., Int. Ed.* **2008**, *47*, 9927-9932.

69.   Sze, S. M. *Semiconductor Devices: Physics and Technology,* 2nd ed.; John Wiley & Sons: New York, 2002.

70.   Ishizaki, T.; Saito, N.; Lee, S.; Takai, O. *Nanotechnology* **2008**, *19*, 055601/1-055601/6.

Chapter 2
Fabrication of Catalytic Stamps

2.1. Introduction

This chapter describes the fabrication of catalytic stamps. As discussed in Chapter 1, our catalytic stamps were designed to lead to localized catalysis by nanostructured metals[1] upon stamping on an appropriate surface, where intimate contact is ensured by the elastomeric nature of PDMS.[2] In order to fabricate such hybrid nanostructures, we developed a two-step strategy consisting of 1) synthesis of metallic nanopatterns on rigid supports and 2) transfer of as-synthesized metallic nanopatterns onto PDMS surfaces through a simple peel-off method (Figure 2.1). For the first step, self-assembling block copolymers were particularly employed as templates to produce the desired metallic nanostructures.[3,4] We therefore start this chapter by introducing block copolymers and their use in nanolithography, with the emphasis on the work pioneered by the Buriak group.[4]
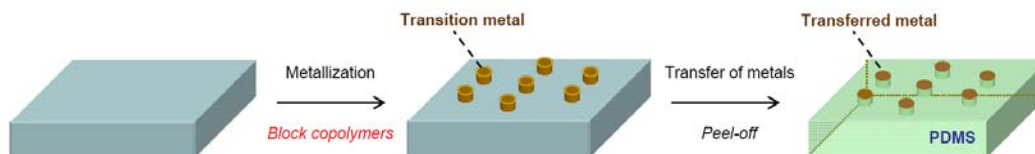
Figure 2.1. A two-step strategy for the fabrication of catalytic stamps. Metallic nanostructures, synthesized via the use of a block copolymer template, are transferred from a rigid substrate to a flexible PDMS support by peeling off.

Block Copolymers

Block copolymers are a special class of polymers that consist of two or more chemically distinct polymer fragments (blocks) covalently attached to each other.[5] Due to the incompatibility and the connectivity constraints of each blocks, they can spontaneously form regular structures at equilibrium. These structures are, for instance, spherical and cylindrical micelles in solutions, or phase-separated spherical, cylindrical, and lamellae patterns in thin films (Figure 2.2). More complicated structures, such as gyroid, can be also found in the bulk state.
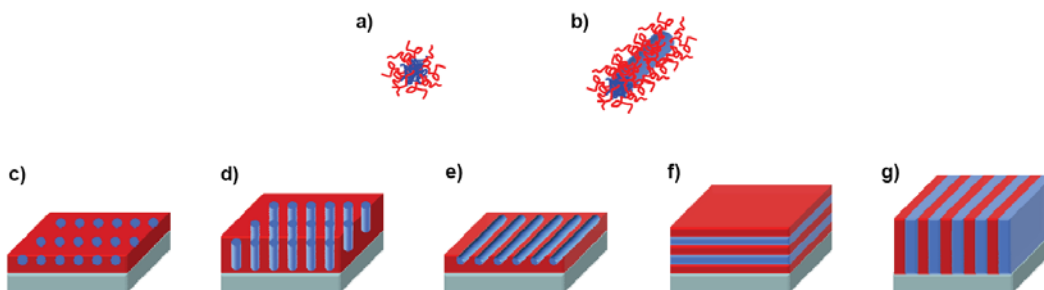
Figure 2.2. Examples of self-assembled block copolymers. (a,b) A spherical/cylindrical micelle in a solution. (c-g) In a thin film, the orientation of block copolymer domain to the surface can be (c) spheres, (d) cylinders lying perpendicular, (e) cylinders lying parallel, (f) lamellae lying parallel, and (g) lamellae lying perpendicular.

The size, periodicity, and morphology of formed structures are typically on the order of 10 to 100 nm, and can be tuned by modulating the molecular weights, the molar fraction, and the degree of interaction of constituent blocks (known as the Flory-Huggins parameter).[5] Because of these unique properties,

block copolymers have become promising materials in diverse applications,[6] including nanolithography.[7] It is considered that block copolymers are fully compatible with existing semiconductor manufacturing, since polymers are already ubiquitous as photoresists.[8]

Block Copolymer Nanolithography

One of the earliest demonstrations of the lithographic use of block copolymer thin film was reported by Park *et al.*[9] Here, polystyrene-*block*-polybutadiene (PS-*b*-PB) was self-assembled into hexagonally packed spherical arrays of PB cores (Figure 2.3a), that were then selectively stained with osmium tetraoxide or ozonated to make them etching-susceptible or resistant (Figure 2.3b,c). Subsequent reactive ion etching (RIE) treatments transformed them into positive or negative masks, respectively (Figure 2.3d). Further RIE treatments were carried out to produce ultradense ($\sim 10^{11}/cm^2$) nanodot or nanohole structures on silicon nitride surfaces (Figure 2.3e). Similar processes have been reported using different types of block copolymers, such as polystyrene-*block*-polymethylmethacrylate (PS-*b*-PMMA).[10]
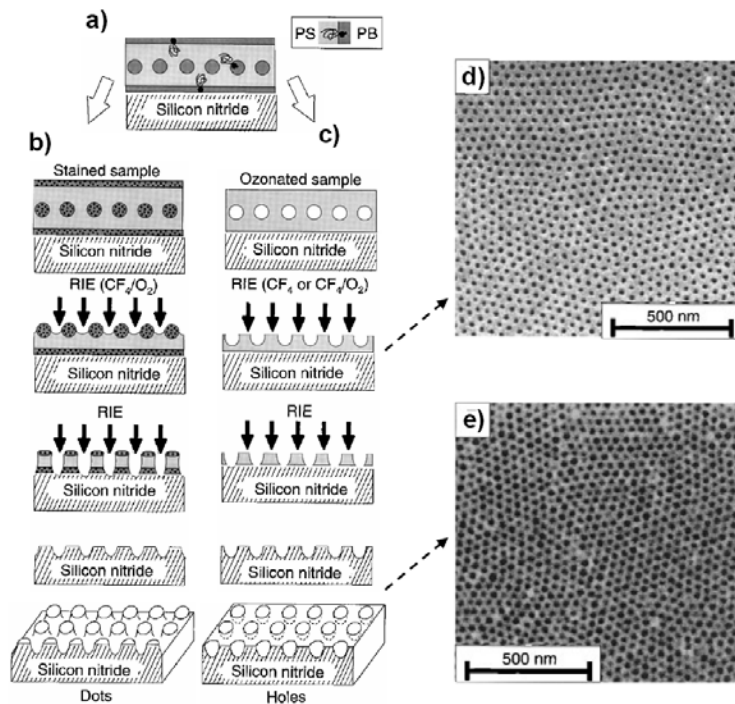
Figure 2.3. Schematic diagram of nanolithography with PS-*b*-PB. (a) Cross-sectional view of the template with spherical PB cores. (b) Outline for nanodot production via osmium tetraoxide treatment. (c) Outline for nanohole production on silicon nitride via ozone treatment. (d) An SEM image of a negative template prepared by ozonation and RIE. (e) An SEM image of a hexagonally ordered hole array on silicon nitride produced from the negative template shown in (d). Reprinted with permission from ref. 9. Copyright © 1997 The American Association for the Advancement of Science.

Kästle and co-workers demonstrated the block copolymer micelle-based nanolithography to pattern surfaces with metallic nanoparticles.[3c] In this case, self-assembled reverse micelles of polystyrene-*block*-poly-2-vinylpyridine (PS-*b*-P2VP) were first prepared in toluene, and the pyridyl groups of the P2VP cores

were complexed with metal ions, such as $HAuCl_4$. A monolayer of hexagonally arranged micelles was then transferred from toluene to solid surfaces via dip-coating. The following plasma treatment removed the PS-*b*-P2VP polymer and reduced metal ions, leaving elemental metallic nanoparticles with the parent hexagonal arrangement. A series of transition metal (Au, Pt, Pd, Co, and Ni) nanoparticle arrays have been obtained with this approach.

The Buriak group has also developed several approaches to nanopattern surfaces of semiconductors through the use of block copolymers.[4,11] These can be divided into three groups: redox-mediated metal patterning,[4a] plasma-mediated metal patterning,[4b-e] and site-selective etching.[11] In all cases, the use of amphiphilic block copolymers, mainly PS-*b*-P2VP or PS-*b*-P4VP, plays a key role.

In redox-mediated metal patterning (Figure 2.4), a semiconductor surface was first spin-coated with a solution of micellized block copolymers to prepare hexagonally packed P2VP (or P4VP) arrays, and then immersed into an aqueous solution containing metal ions. Because of the existence of pyridyl groups in the P2VP (or P4VP) domains, metal ions could be selectively captured and delivered to the semiconductor surface, where electrons were provided from the semiconductor surface to metal ions (Figure 2.4b).[4a] As a result of such surface redox reactions, called galvanic displacement, metals were deposited on the semiconductor interface, and metallic nanopatterns were produced upon the removal of the polymer template by dissolving it. With this wet chemical

approach, nanostructures of Au and Ag were produced on a series of semiconductor surfaces, including Si, Ge, InP, and GaAs (Figure 2.4c).
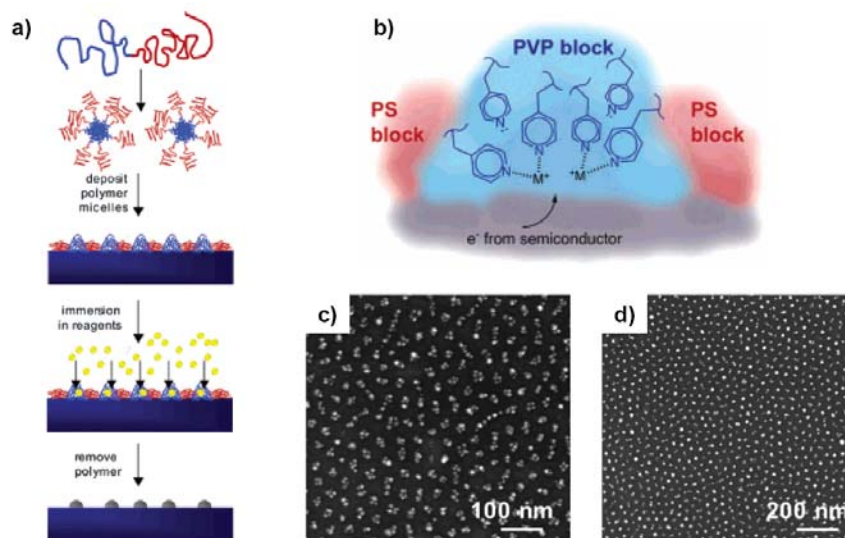
Figure 2.4. (a) Outline for the PS-*b*-P4VP templated deposition of metal nanoparticles onto a substrate. (b) Pyridyl groups in the P4VP cores can capture metal ions and deliver them to a substrate, where galvanic displacement takes place. (c,d) SEM images of Au nanoparticles on (c) GaAs(100) and (d) Si(100). Reprinted with permission from ref. 4a. Copyright © 2005 American Chemical Society.

While the use of galvanic displacement to deposit metals permitted a convenient wet chemical approach to sub-100 nm patterning, it was revealed that some important class of metals, such as Pt and Pd, are incompatible with this method.[4b] In this case, plasma treatment could be applied to reduce metal ions (and to remove polymers simultaneously).[3,4b-e] By performing thermal annealing

and graphoepitaxy,[4c,d] more versatile patterns (fingerprint or aligned lines) beyond the simple hexagonal arrangement could be obtained with a broad range of metals, including Au, Pt, Pd, Fe, Co, Cu, and Ni (Figure 2.5).[4c,d] Some representative SEM images are shown in Figure 2.5c and d.
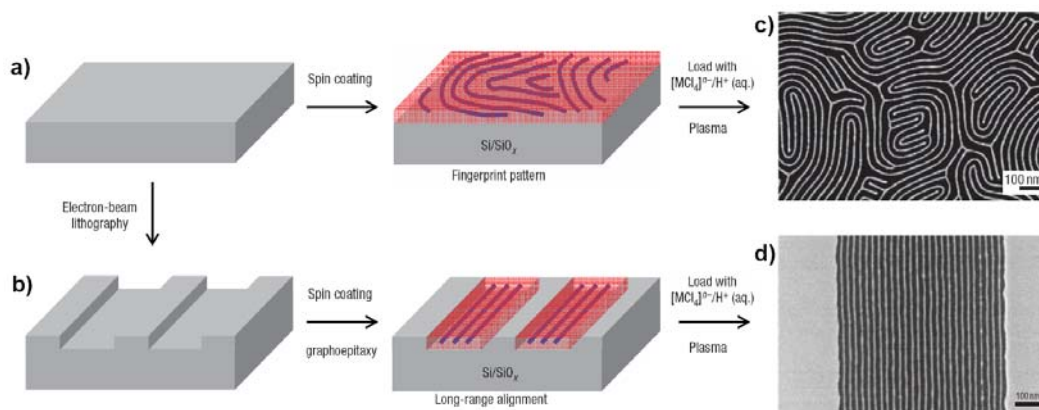
Figure 2.5. Schematic diagrams of metal deposition with cylindrical PS-*b*-P2VP templates lying parallel to surfaces. (a) Fingerprint pattern formation on a flat surface. (b) Aligned linear pattern formation on a trenched surface (graphoepitaxy). (c,d) SEM images of fingerprint (c) and aligned linear pattern (d) consisting of Pt. Reprinted with permission from ref. 4c. Copyright © 2007 Nature Publishing Group.

Site-selective etching of silicon surfaces was carried out using the same idea as the redox-mediated metal patterning; here, fluoride ions were selectively delivered to the surface instead of metal ions through the P4VP domains (Figure 2.6a).[11] Depending on the orientation of the crystalline planes within the silicon wafers used, etched pits showed specific shapes and bottoms due to the

anisotropic etching by *in situ* formed poly(pyridinium)fluoride (Figure 2.6b,c). It was also demonstrated that the interiors of the produced etched pits could be further functionalized with organic molecules and metal nanoparticles.
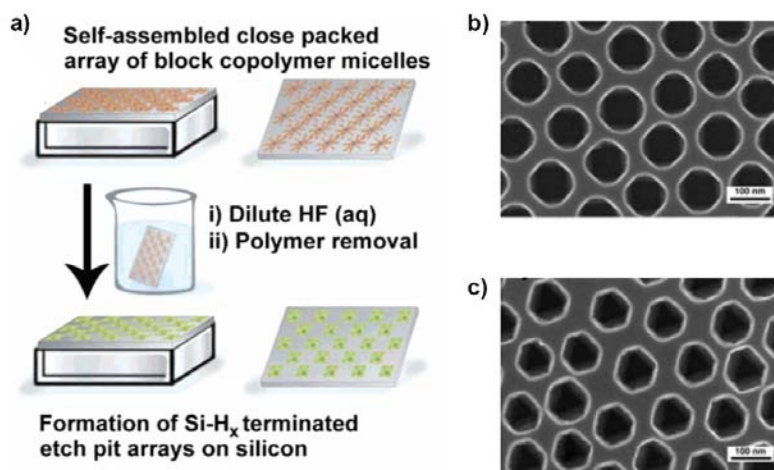
Figure 2.6. (a) Outline for the selective etching of a Si surface using a block copolymer micelle template (PS-*b*-P4VP). (b,c) SEM images of resulting pits arrays on Si(111) (b, square holes) and Si(100) (c, hexagonal holes). Reprinted with permission from ref. 11. Copyright © 2007 American Chemical Society.

Strategy towards Catalytic Stamps

As discussed, block copolymers offer an efficient way to build nanoscale metallic patterns without the use of photolithography or e-beam lithography. Since we intended to prepare catalytically active transition metal nanostructures[1] on PDMS, Pd and Pt were of particular interest. As a result, plasma-mediated metal patterning was adopted to synthesize metallic nanostructures on flat oxide-

capped silicon substrates. Before transferring the thus-produced metals onto the surface of the PDMS, a surface treatment with fluoroalkylsilane was also incorporated to prevent the potential adhesion between SiO_x and PDMS.[12] Figure 2.7 outlines the entire procedure to fabricate catalytic stamps. The details of each step will be discussed in the following section.
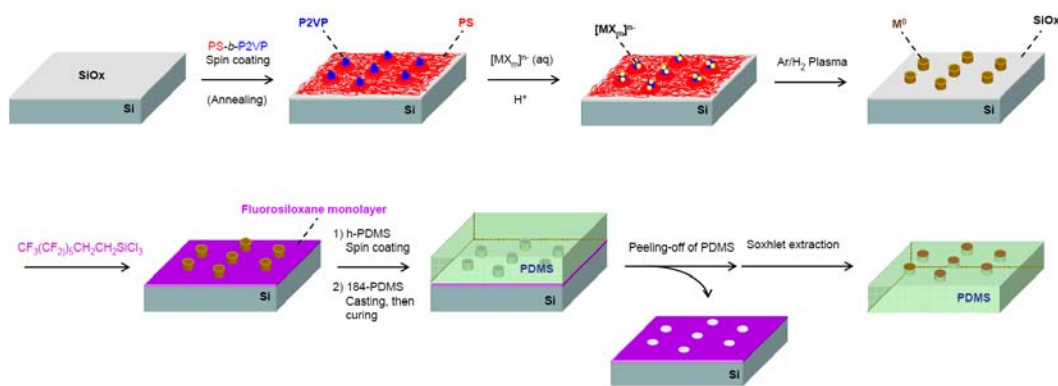
Figure 2.7. Schematic outline for the fabrication of catalytic stamps. (Top row) Block copolymer (PS-*b*-P2VP)-templated synthesis of a metallic nanopattern on oxide-capped Si. (Bottom row) Transfer of the metallic nanopattern onto PDMS surface through a peel-off approach.

2.2.   Results and Discussion

Block Copolymer Templates

The block copolymers used here were all PS-*b*-P2VP, with molecular weights (g/mol) of PS/P2VP = 48500/70000, 91500/105000, 190000/190000, and 125000/58500. In order to self-assemble these PS-*b*-P2VP into spherical reverse micelles (i.e., P2VP cores and PS coronas), *o*-xylene was used to prepare 0.60 wt% solutions of PS_{48500}-*b*-$P2VP_{70000}$, PS_{91500}-*b*-$P2VP_{105000}$, and PS_{190000}-*b*-$P2VP_{190000}$,[4b,13] while toluene was used to prepare a 1.0 wt% solution of PS_{125000}-*b*-$P2VP_{58500}$[4e] (Figure 2.8).
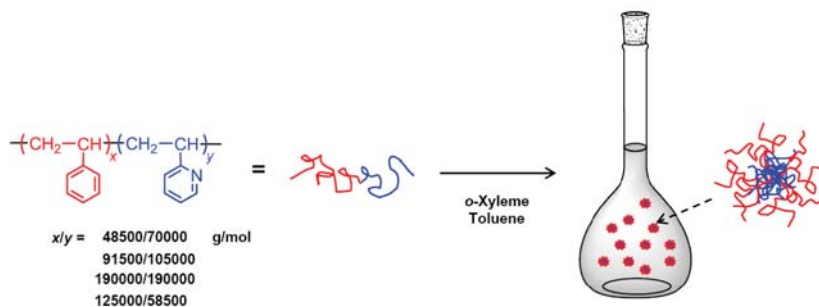
Figure 2.8. Formation of reverse micelles with PS-*b*-P2VP in *o*-xylene or toluene.

Thin film templates of block copolymers were prepared on flat oxide-capped silicon substrates by spin coating of PS-*b*-P2VP solutions at 6000 rpm for 40 s. Because of the rapid evaporation of solvents upon spin coating, the spherical micelles spontaneously organized into pseudo-hexagonally packed patterns with P2VP cores surrounded by a PS matrix (Figure 2.9).
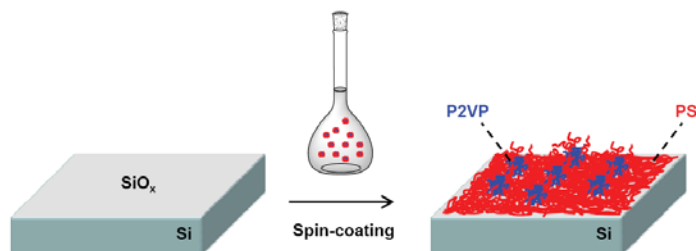
Figure 2.9. Preparation of a thin film from block copolymer micelles by spin coating. Spherical micelles are spontaneously organized into a hexagonally packed structure.

Figure 2.10 shows AFM images of the PS-*b*-P2VP thin films obtained from the *o*-xylene solutions (a: PS$_{48500}$-*b*-P2VP$_{70000}$, b: PS$_{91500}$-*b*-P2VP$_{105000}$, and c: PS$_{190000}$-*b*-P2VP$_{190000}$). In all cases, pseudo-hexagonal arrays consisting of P2VP domains were observed. As summarized in Table 2.1, there was a clear tendency that polymers with higher molecular weights afforded patterns with increased domain height, lateral size and center-to-center spacing. For example, approximately 50 nm increases in center-to-center spacing were observed as the polymers were changed from PS$_{48500}$-*b*-P2VP$_{70000}$ (~76 nm), to PS$_{91500}$-*b*-P2VP$_{105000}$ (~124 nm), to PS$_{190000}$-*b*-P2VP$_{190000}$ (~180 nm). Since the thin films obtained from *o*-xylene solutions had good ordering, they could be directly utilized as templates in the next metallization step, as discussed later.
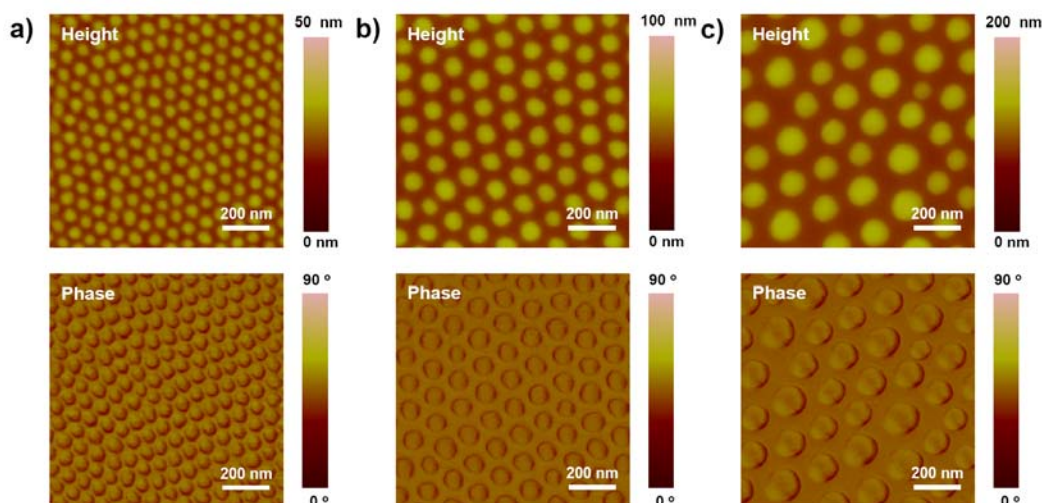
Figure 2.10. Tapping-mode AFM images of PS-*b*-P2VP thin films formed on oxide-capped Si surfaces. (a) PS$_{48500}$-*b*-P2VP$_{70000}$. (b) PS$_{91500}$-*b*-P2VP$_{105000}$. (c) PS$_{190000}$-*b*-P2VP$_{190000}$.

PS-*b*-P2VP	Height (nm)	Domain size (nm)	Spacing (nm)
PS$_{48500}$-*b*-P2VP$_{70000}$	10 ± 1^{a}	29 ± 4	76 ± 6
PS$_{91500}$-*b*-P2VP$_{105000}$	24 ± 1	49 ± 4	124 ± 8
PS$_{190000}$-*b*-P2VP$_{190000}$	44 ± 6	73 ± 14	180 ± 15

Table 2.1. Summary of the height, domain size, and center-to-center spacing of P2VP cores in PS-*b*-P2VP thin film. [a] Standard deviation (1σ).

When a thin film of PS$_{125000}$-*b*-P2VP$_{58500}$ was prepared from a toluene solution, however, the resulting pattern had a less ordered structure compared to those produced from *o*-xylene solutions (Figure 2.11a). In this case, solvent-assisted annealing was carried out to enhance its order.[4e] Figure 2.11b shows AFM images of the spin coated PS$_{125000}$-*b*-P2VP$_{58500}$ thin film followed by THF annealing for 20 h in a *loosely* sealed annealing chamber (see Experimental Section). Because THF is a slightly selective solvent for PS (solubility

parameters of PS, P2VP, and THF are 18.5, 21.2, and 18.6 MPa$^{1/2}$, respectively),[14] the PS block was preferentially swollen under these conditions, leading to selective enhancement of PS chain mobility. As a result of the following reorganization of the PS matrix, the improved hexagonal array was achieved compared to the as-spin-coated film (Figure 2.12a).[15] The domain sizes and center-to-center spacing of the resulting pattern was 18 nm and 66 nm, respectively (Table 2.2, top).
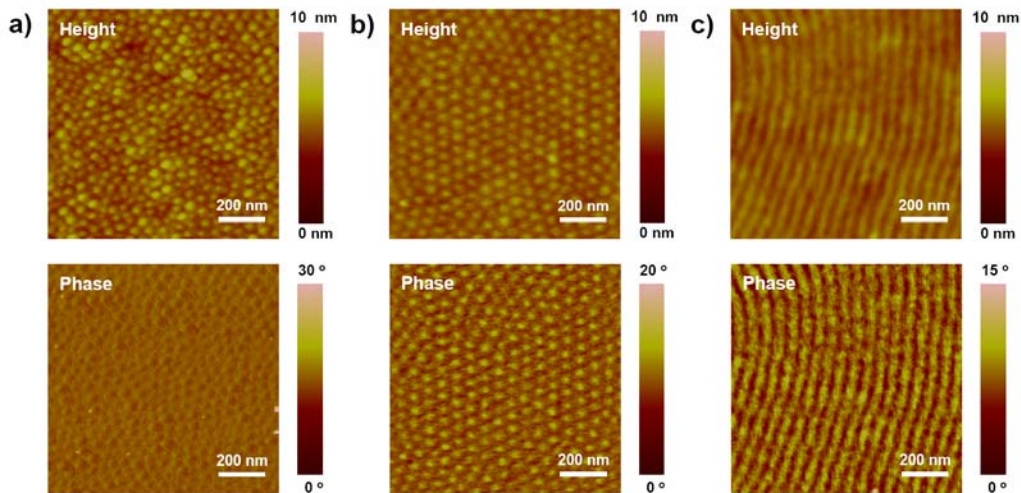
Figure 2.11. Tapping-mode AFM images of PS$_{125000}$-b-P2VP$_{58500}$ thin films formed on oxide-capped Si. (a) Before THF annealing. (b,c) After THF annealing.

PS$_{125000}$-b-P2VP$_{58500}$	Height (nm)	Size/Width (nm)	Spacing (nm)
Hexagonal array	1.4 ± 0.3^{a}	18 ± 3	66 ± 7
Linear array	1.0 ± 0.2	17 ± 2	58 ± 4

Table 2.2. Summary of the height, domain size/width, and center-to-center spacing of P2VP cores in PS$_{125000}$-b-P2VP$_{58500}$ thin film. ^{a} Standard deviation (1σ).
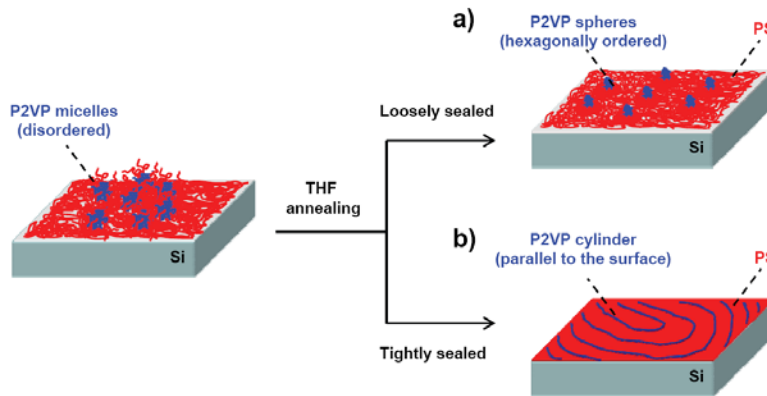
Figure 2.12. Formation of cylindrical domains from PS-*b*-P2VP micelles via THF annealing. When THF annealing was performed in a loosely sealed chamber, hexagonally patterned P2VP domains with a better order were obtained. When annealing was performed in a tightly sealed chamber, on the other hand, parallel cylinders were obtained to form a fingerprint pattern.

Other than the hexagonal template, a linear template was also produced from the PS$_{125000}$-*b*-P2VP$_{58500}$ thin film (Figure 2.11c). THF annealing in a *tightly* sealed chamber was required to create such a template with cylindrical P2VP domains parallel to the surface (Figure 2.12b). Due to the richer THF atmosphere produced by tight sealing of the annealing system, both PS and P2VP blocks were swollen in this case. In addition to the reorganization of the PS matrix described above, the swelling of the P2VP domains induced the coalescence between neighboring P2VP domains to yield continuous cylindrical structures. This type of morphological change is known as mortensitic-type phase transition.[16] The

domain width and center-to-center spacing of the resulting pattern were 17 and 58 nm, respectively (Table 2.2, bottom).

Metallic Nanostructures on SiO$_x$/Si.

The five templates described in the previous section were then transformed into a series of transition metal nanostructures (Pd, Pt, and Au). In general, desired metal ions were loaded selectively on P2VP domains using electrostatic interactions between protonated pyridyl groups (positive) and anionic metal complexes (negative).[4] The conditions for metal loading were, however, metal- and template-dependent. After metal ions were loaded onto the templated samples, Ar/H$_2$ plasma treatment was carried out to reduce the metal ions and remove the PS-*b*-P2VP template (Figure 2.13).[3,4]
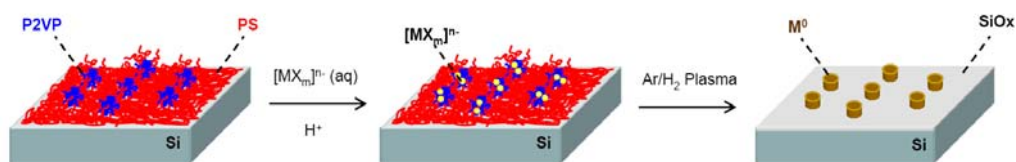
Figure 2.13. PS-*b*-P2VP-templated synthesis of metallic nanostructures on oxide-capped Si. Template samples were immersed in an aqueous metal salt solution (acidic) for a given time to electrostatically load anionic metal complexes within P2VP domains. After loading, an Ar/H$_2$ plasma was applied to reduce the metal ions and remove the polymer template.

1) Palladium

Pd nanostructures on SiO_x/Si were produced using aqueous Na_2PdCl_4 as a Pd^{2+} source. Two loading conditions were developed, depending on how PS-*b*-P2VP templates were prepared. For the three templates prepared without THF annealing (PS_{48500}-*b*-$P2VP_{70000}$, PS_{91500}-*b*-$P2VP_{105000}$, and PS_{190000}-*b*-$P2VP_{190000}$, see Figure 2.10), templated samples were immersed in a 1 mM Na_2PdCl_4 (aq) for 10 min followed by the Ar/H_2 plasma treatment. Since the pH of the solution employed was 3.8 (measured), nearly all the pyridyl groups were considered to be protonated, therefore forming complexes with anionic $[PdCl_4]^{2-}$ (pK_a of P2VP in aqueous solution is 4~4.5).[17] As shown in Figure 2.14, SEM images of the resulting samples confirmed that the original hexagonal arrays of P2VP domains were translated into metallic Pd (a, b, and c are obtained from the PS_{48500}-*b*-$P2VP_{70000}$, PS_{91500}-*b*-$P2VP_{105000}$, and PS_{190000}-*b*-$P2VP_{190000}$ template, respectively).
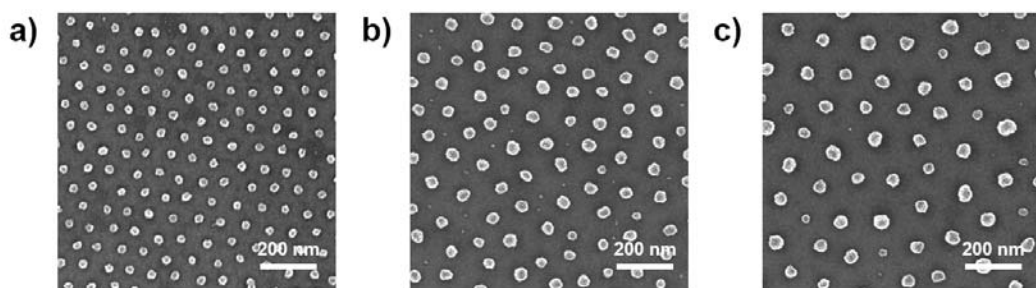
Figure 2.14. SEM images of Pd nanostructures on SiO_x/Si, obtained from (a) PS_{48500}-*b*-$P2VP_{70000}$, (b) PS_{91500}-*b*-$P2VP_{105000}$, and (c) PS_{190000}-*b*-$P2VP_{190000}$, respectively.

For the two templates prepared from the toluene solution of PS_{125000}-b-$P2VP_{58500}$ with THF annealing (see Figure 2.11b,c), 10 mM of Na_2PdCl_4 (aq) containing 0.9% (v/v) HCl was used for the Pd^{2+} loading (time: 3 h). The higher concentration of Pd^{2+} and H^+ as well as the longer deposition time were necessary to fully load Pd^{2+} into the P2VP domains. The reason for this difference might be the result of THF annealing, which significantly changes the spatial conformation of the polymer chains,[18] including pyridyl groups in the P2VP domains. SEM images of Pd nanostructures produced from hexagonal and linear templates are shown in Figure 2.15.
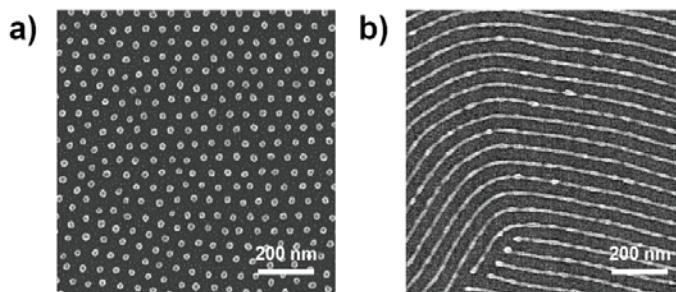
Figure 2.15. SEM images of Pd nanostructures on SiO_x/Si, obtained from THF-annealed PS_{125000}-b-$P2VP_{58500}$ templates. (a) A hexagonal array. (b) A linear array.

2) *Platinum*

Pt nanostructures on SiO_x/Si were prepared with two templates from annealed PS_{125000}-b-$P2VP_{58500}$ thin films. The loading conditions were similar to the Pd samples: 10 mM Na_2PtCl_4 (aq) containing 0.9% (v/v) HCl with a 3 hour deposition time. Ar/H_2 plasma was used to reduce the Pt^{2+} to Pt^0 and to remove

the polymer templates. The SEM images of the resulting hexagonal and linear Pt

nanostructures are shown in Figure 2.16.
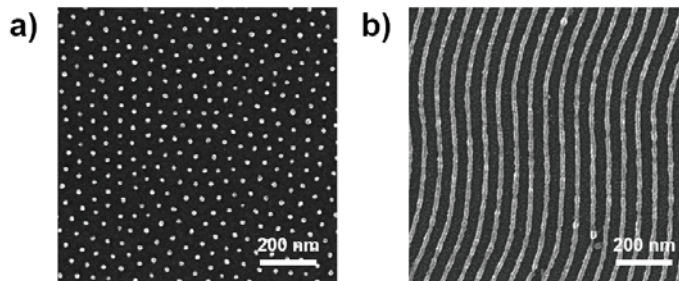
Figure 2.16. SEM images of Pt nanostructures on SiO_x/Si, obtained from THF-annealed

PS_{125000}-*b*-$P2VP_{58500}$ templates. (a) A hexagonal array. (b) A linear array.

3) Gold

A hexagonal Au nanoarray was prepared on SiO_x/Si from the PS_{190000}-*b*-

$P2VP_{190000}$ template using 10 mM $KAuCl_4$ (aq) as an Au^{3+} source (loading time:

10 min). Figure 2.17 shows the SEM image of the resulting pattern.
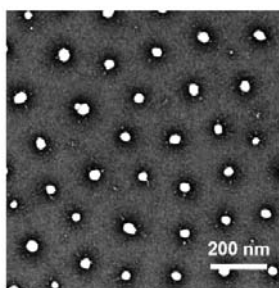
Figure 2.17. A SEM image of Au nanostructures on SiO_x/Si, obtained from the PS_{190000}-*b*-

$P2VP_{190000}$ template.

Metallic Nanostructures on PDMS: Catalytic Stamps

Finally, the metallic nanostructures produced on SiO_x/Si were transferred onto PDMS surfaces via peel-off to afford catalytic stamps. Regardless of the types of metals, the same procedure was adopted as outlined in Figure 2.18.
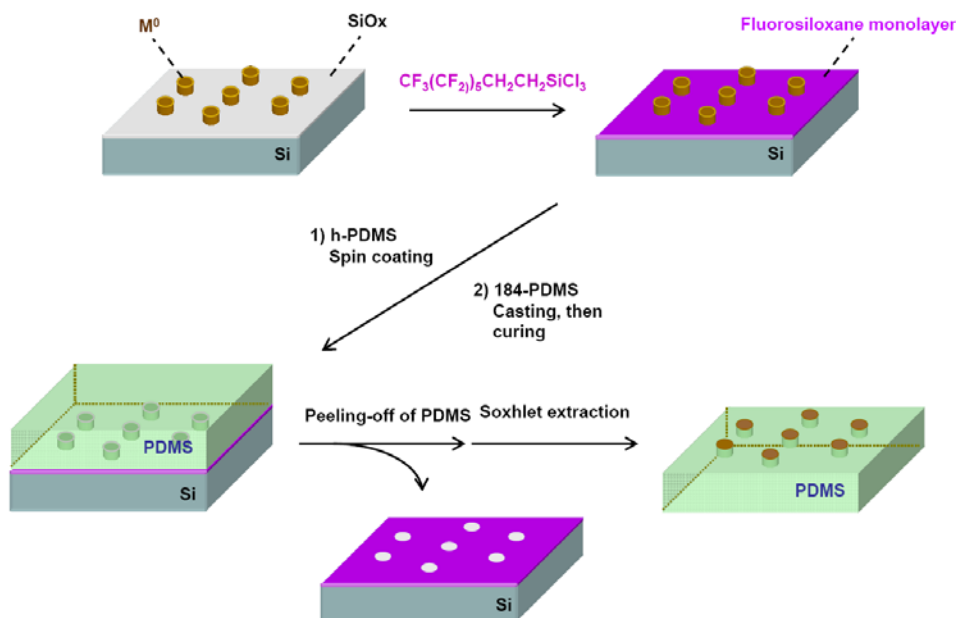
Figure 2.18. Transfer of a metallic nanostructures onto a PDMS surface. A fluoroalkylsiloxane monolayer was prepared on the SiO_x region of the plasma treated sample. Composite PDMS (h- and 184 PDMS) was then prepared on the surface. After thermal curing, the PDMS was peeled off from the SiO_x/Si substrate, yielding a catalytic stamp and a metal-dislocated surface. Finally, the catalytic stamp was washed by Soxhlet extraction.

After the Ar/H_2 plasma treatment, the metal-patterned sample was exposed to a vapor of trichloro(1*H*,1*H*,2*H*,2*H*-perfluorooctyl)silane under reduced pressure

to prepare a fluorinated alkylsiloxane monolayer on the exposed SiO_x regions.[19] Subsequently, two kinds of PDMS, termed h- and 184-PDMS, were solidified on the sample by spin coating the h-PDMS, and pouring of 184-PDMS, to form double-layered PDMS.[20] After thermally curing at 65 ^{o}C for 3 h, the composite PDMS was carefully peeled away from the SiO_x/Si surface to afford a catalytic stamp. Because of the highly fluorinated monolayer on SiO_x, the master could be smoothly separated from the PDMS stamp,[19] while the metallic nanostructure was physically captured by h-PDMS and dislocated from the original SiO_x interface. It was found that the use of h-PDMS was essential to facilitate transfer of the metallic nanostructure; partial transfer of metals occurred when only 184-PDMS was used. The higher Young's modulus of h-PDMS (~9 MPa),[20a] compared to 184-PDMS (~3 MPa),[20a] assisted in firmly taking hold of the metallic nanostructures produced on SiO_x/Si. Finally, the catalytic stamp prepared through this approach was submitted to Soxhlet extraction using hexane to remove low-molecular weight PDMS.[21] It should be emphasized that no disappearance of the metallic nanostructure from PDMS was observed by AFM even after this harsh cleaning process.

Figure 2.19 represents AFM images of a Pd catalytic stamp (a) and the corresponding Pd-removed SiO_x/Si surface (b), obtained via this simple peeling-off approach (original template: PS_{190000}-b-$P2VP_{190000}$). It was confirmed that nearly the entire Pd nanoarray was transferred from SiO_x/Si to PDMS. As a comparison, Figure 2.19c shows an AFM image of a Pd catalytic stamp fabricated

with 184-PDMS. As noted previously, incomplete transfer of Pd resulted in the formation of defects (holes) on PDMS, proving the necessity of h-PDMS layer to achieve high-quality catalytic stamps.
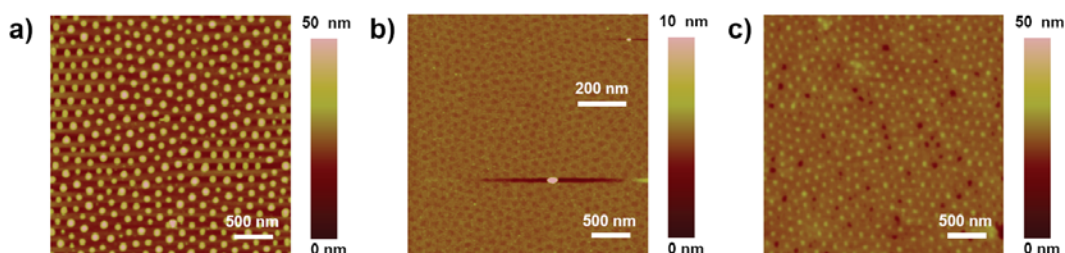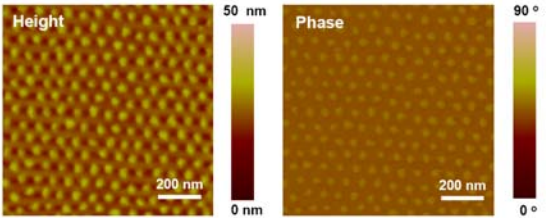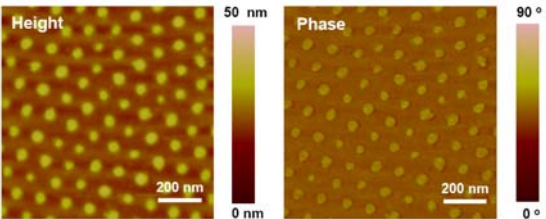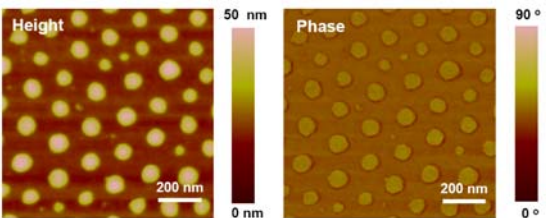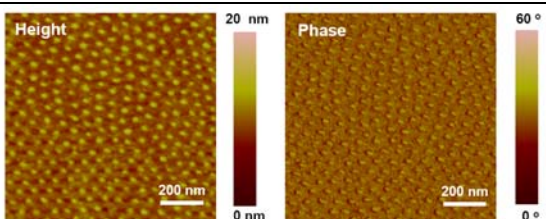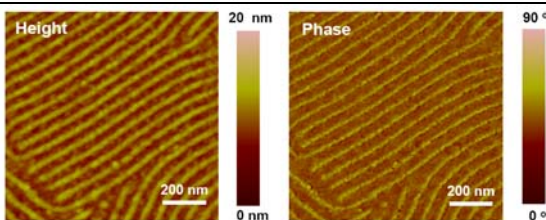
Figure 2.19.   (a) An AFM image of a representative Pd catalytic stamp (i.e., Pd nanostructures patterned on the h- and 184-PDMS composite) prepared from PS_{190000}-b-$P2VP_{190000}$ template. (b) An AFM image of a Pd-removed SiO_x/Si substrate. Traces of a hexagonal array are observed. (c) An AFM image of a Pd catalytic stamp fabricated using 184-PDMS. Defects are confirmed as dark spots due to the incomplete transfer of Pd.

Table 2.3 summarizes AFM images and parameters (size/width of metal and center-to-center spacing) of all the catalytic stamps fabricated through the approach described here. Depending on the starting PS-b-P2VP template, various patterns of Pd, Pt, and Au could be obtained with sizes/widths of 15-54 nm and center-to-center spacings of 59-168 nm. Because of the potential difference in the shape of metallic nanoparticles produced, the final size/width of patterned metals on PDMS could differ from the parent template, keeping all other parameters equal. In fact, such difference could be confirmed by comparing the Pd and Au

catalytic stamps prepared from the PS_{190000}-b-$P2VP_{190000}$ template: the size of Pd (54 nm) was ~10 nm larger than that of Au (44 nm). Thus, the choice of metal can serve as an additional factor in designing nanopatterned metal/soft material architectures based on the use of block copolymer templates.

Metal[Template]	AFM images	Size/Width (nm)	Spacing (nm)
Pd[a]		20 ± 2^{f}	76 ± 6
Pd[b]		33 ± 6	116 ± 12
Pd[c]		54 ± 11	168 ± 14
Pd[d]		16 ± 3	70 ± 10
Pd[e]		15 ± 2	59 ± 2
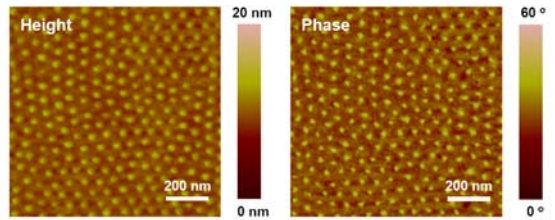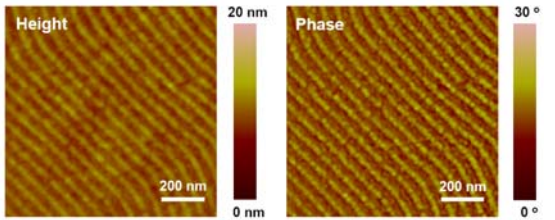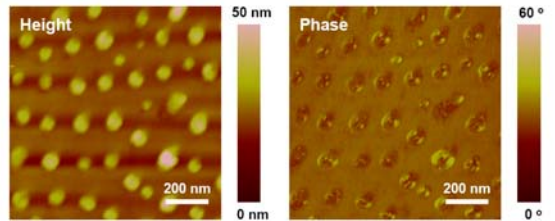
	Height / Phase images	domain size/width	center-to-center spacing
Pt[d]		18 ± 2	64 ± 6
Pt[e]		15 ± 2	59 ± 3
Au[c]		44 ± 8	158 ± 25

Table 2.3. Summary of AFM images, domain size/width, and center-to-center spacing of Pd, Pt, and Au catalytic stamps. [a] From PS_{48500}-b-$P2VP_{70000}$. [b] From PS_{91500}-b-$P2VP_{105000}$. [c] From PS_{190000}-b-$P2VP_{190000}$. [d] From PS_{125000}-b-$P2VP_{58500}$ (hexagonal array). [e] From PS_{125000}-b-$P2VP_{58500}$ (linear array). [f] Standard deviation (1σ).

Interfacial Morphologies of Metals on Catalytic Stamps

Because good and consistent contact between the metallic nanopattern on the PDMS stamp and the surface is a necessity while stamping, the morphology of the metallic nanostructures is particularly important. Although the height profiles of a typical catalytic stamp by AFM could not reveal the precise morphology of the metal surfaces because of tip convolution effects[22] (metal = Pd, Figure 2.20a), cross-sectional SEM images of the bare Pd nanostructures on the SiO_x/Si interface reveal the truncated shape of the nanoparticles, with a flat Pd face that forms on

the smooth single crystal silicon surface (Figure 2.20b). When the liquid prepolymer of PDMS infiltrated these metals on the silicon substrate, it uniformly grasps the metals upon thermal curing (Figure 2.20c). As a result, the morphology of the metals on PDMS is nearly flat upon removal from the silicon (Figure 2.20d: the cross-sectional SEM image showed somewhat recessed metals in PDMS, which may be due to the swelling of PDMS upon exposure to the electron beam).[23] This flatness of metallic nanostructure on PDMS leads to good contact with a surface upon stamping, as confirmed in later chapters (Chapters 3 and 4).
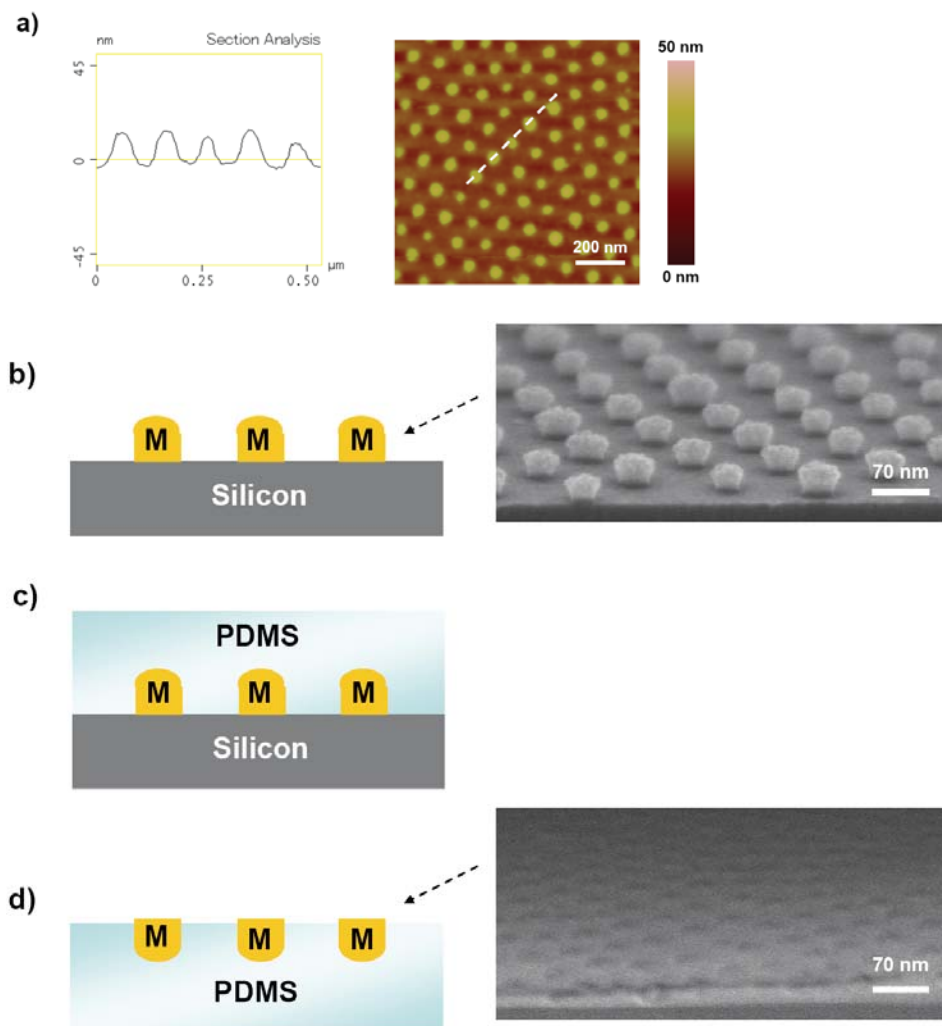
Figure 2.20. (a) AFM cross-sectional analysis of a Pd catalytic stamp (template = PS$_{91500}$-*b*-P2VP$_{105000}$). (b) Cartoon schematic of metals on SiO$_x$/Si and cross-sectional SEM image of Pd nanostructures on SiO$_x$/Si (template = PS$_{91500}$-*b*-P2VP$_{105000}$). (c) Cartoon schematic of filling of PDMS on the metals-on-silicon. (d) Cartoon schematic of metals on PDMS and cross-sectional SEM image of Pd nanostructures on PDMS obtained from (b).

X-Ray Photoelectron Spectroscopy of Catalytic Stamps

X-Ray Photoelectron Spectroscopy (XPS) measurement was carried out on catalytic stamps to investigate the oxidation status of metallic nanostructures embedded on PDMS supports. The main peaks found in the survey scan of, for instance, a Pd catalytic stamp (Figure 2.21a) were Si(2p) (102 eV), and C(1s) (284 eV) and O(1s) (532 eV), all of which were derived from bulk PDMS.[24] The same peaks were found with Pt and Au catalytic stamps. Although the signals from each metal in the survey scans were too small to characterize their oxidation states, high resolution XPS spectra for the Pd(3d), Pt(4f), and Au(4f) regions (Figure 2.21b, c, and d, respectively) revealed the binding energies of $Pd(3d_{5/2})$ = 335.4 eV, $Pt(4f_{7/2})$ = 71.4 eV, and $Au(4f_{7/2})$ = 84.1 eV, all of which were in good agreement with their elemental states (i.e., Pd^0, Pt^0, and Au^0).[25] According to the present analysis, formation of corresponding metal oxides was not detected despite the handling of catalytic stamps under ambient atmosphere, although the formation of thin-layer oxides cannot be ruled out.
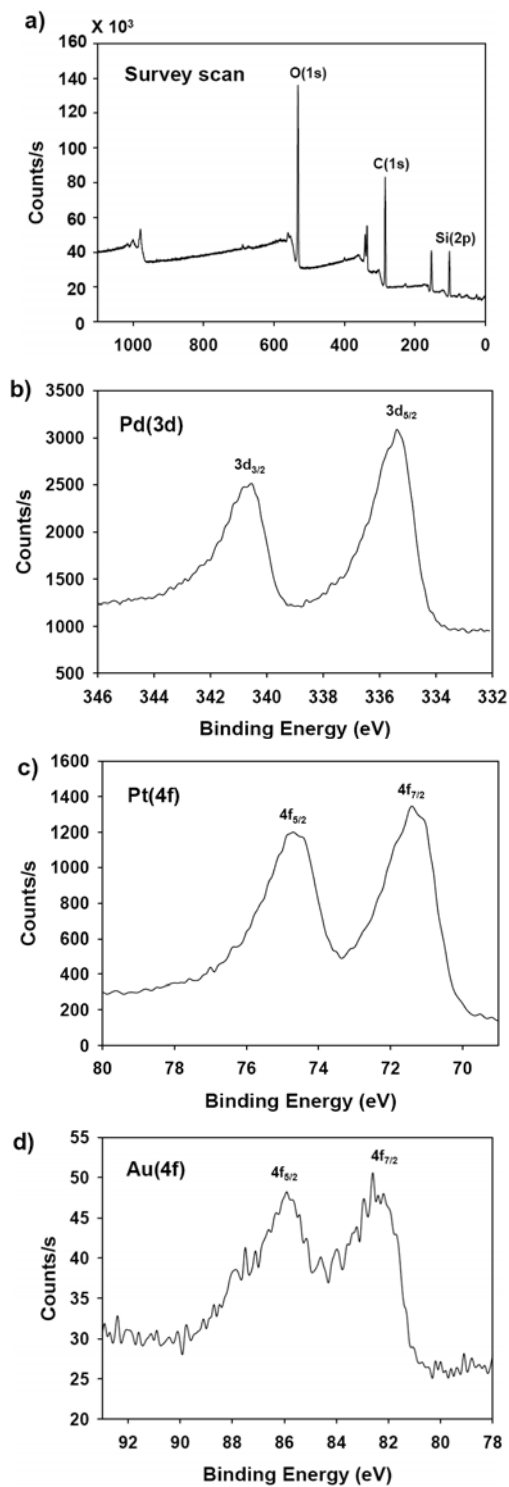
Figure 2.21. XPS spectra of catalytic stamps. (a) Survey scan of a Pd catalytic stamp. (b-d)

High resolution XPS spectra of Pd(3d) (b), Pt (4f) (c), and Au (4f) (d) regions.

2.3. Conclusion

In this chapter, the strategy for the fabrication of catalytic stamps was discussed. Using self-assembled block copolymer (PS-*b*-P2VP) templates, nanoscale arrays of Pd, Pt, and Au with different geometries (hexagonal/linear), size, and spacing were first created on oxide-capped silicon substrates, and those structures were transferred onto surfaces of PDMS through a peel-off procedure. In order to assist the separation of PDMS from SiO_x/Si substrates, a fluorinated alkylsiloxane monolayer was necessary on the SiO_x region. In addition, the use of composite PDMS (h- and 184-PDMS) system was important to enhance the efficiency of transferring metals from the SiO_x/Si substrates. It was suggested by SEM and XPS that those resulting metals on PDMS have flat interfaces and elemental (zero-valent) states. This block copolymer-mediated method provides a convenient, flexible, and cost-effective approach to construct metallic nanostructures on soft materials without the use of costly techniques, such as photolithography and electron beam lithography.

Note: During the course of this work, Spatz and co-workers demonstrated a similar approach using block copolymers to produce arrays of gold nanoparticles on hydrogels for a cell adhesion study.[26]

2.4. Experimental Section

Generalities.

Unless otherwise noted, all the experiments were performed under ambient conditions. Teflon beakers and tweezers were used exclusively during the cleaning of the Si wafers. Si(111) (p-type, B-doped, ρ = 1-10 Ω-cm, thickness = 600-650 μm) and Si(100) (p-type, B-doped, ρ = 0.01-0.02 Ω-cm, thickness = 600-650 μm) wafers were purchased from MEMC Electronic Materials, Inc. Water was obtained from a Millipore system (resistivity = 18.2 MΩ). Aqueous HCl (36.5-38%, BAKER ANALYZED ACS Reagent), NH$_4$OH (29%, Finyte), H$_2$O$_2$ (30%, CMOS) were purchased from J. T. Baker. Block copolymers used in this study were polystyrene-*block*-poly-2-vinylpyridine (PS$_x$-*b*-P2VP$_y$), with molecular weights (g/mol) of x/y = 48500/70000, 91500/105000, 190000/190000, and 125000/58500, obtained from Polymer Source, Inc. Two kinds of poly(dimethysiloxane) (PDMS), termed h- and 184-PDMS, were used in this study, and the prepolymers of h-PDMS (VDT-731, HMS-301, and SIP6831.1) were obtained from Gelest Corp., while those of 184-PDMS (Sylgard 184) were obtained from Dow Corning. Trichloro(1*H*,1*H*,2*H*,2*H*-perfluorooctyl)silane (98%), 2,4,6,8-tetramethyl-2,4,6,8-tetravinylcyclotetra-siloxane, toluene (>99.9%, CHROMASOLV$^®$, for HPLC), and *o*-xylene (98%, CHROMASOLV$^®$ Plus, for HPLC) were purchased from Sigma-Aldrich. Na$_2$PdCl$_4$·3H$_2$O (99%), Na$_2$PtCl$_4$·xH$_2$O and KAuCl$_4$·xH$_2$O were obtained from Strem Chemicals. Optima

grade hexane and THF were purchased from Fisher. All reagents listed above were used as-received.

Silicon Cleaning Procedures.

Pieces of Si(111) or Si(100) ($\sim$1 cm^2) were degreased in methanol using an ultrasonic bath for 15 min. The wafers were then cleaned via standard RCA cleaning procedures:[27] the wafers were first immersed in a solution of $H_2O/NH_4OH/H_2O_2$ (5/1/1) and heated (80 ^{o}C) for 15 min. After the wafers were rinsed with excess water, they were immersed in another solution of $H_2O/HCl/H_2O_2$ (6/1/1) and reheated (80 ^{o}C) for 15 min. The wafers were again rinsed with an excess amount of water and dried with a stream of N_2 gas.

Preparation of Block Copolymer Solutions.

Block copolymers (PS_x-b-$P2VP_y$; x/y = 48500/70000, 91500/105000, and 190000/190000) were dissolved in o-xylene and stirred for 1 h at room temperature to make 0.60 wt% solutions. In the case of PS_{125000}-b-$P2VP_{58500}$, the polymer was dissolved in toluene and stirred for 1 h at room temperature to make a 1.0 wt% solution. All solutions were allowed to sit for 24 h prior to use to complete the micelle formation.

Preparation of Block Copolymer thin film templates on SiO$_x$/Si Substrates.

A RCA cleaned Si(111) or (100) sample was spin-coated (model WS-400B-6NPP-Lite, Laurell Technologies) with 10 μL of a block copolymer solution at 6000 rpm for 40 s. Templates from PS$_x$-*b*-P2VP$_y$, where x/y = 48500/70000, 91500/105000, and 190000/190000, were directly used for the next step. In the case of PS$_{125000}$-*b*-P2VP$_{58500}$, solvent annealing was carried out for ~20 h in a chamber, an inverted 500 mL crystallization dish and 5 mL of THF in a small beaker placed on top of an aluminum foil covered papers (Figure 2.22).[28] By controlling the degree of sealing of the annealing system, either a pseudohexagonal or a linear template was produced. To obtain the pseudohexagonal pattern, the polymer-coated sample was placed in the chamber, and a 500 g mass was placed on top of the inverted dish to loosely seal the chamber. Alternatively, a 2 kg mass was used to prepare the linearly patterned template by sealing the chamber tightly. Although both pseudohexagonal and linear structures are considered to be kinetically trapped states, it should be noted that the selective production of hexagonal/linear morphology was completely reproducible by simply changing the weight of the mass.
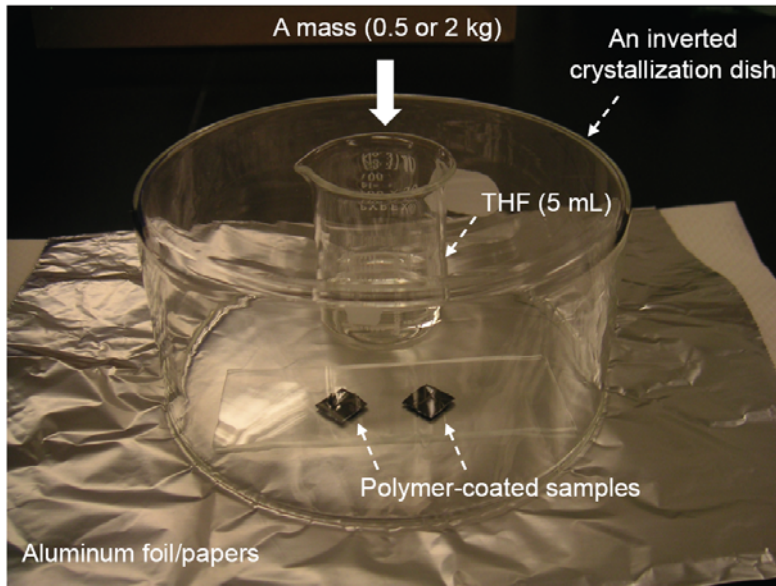
Figure 2.22. Photograph of the solvent (THF) annealing system. In addition to this setup, a 500 g or 2 kg mass was placed on top of the inverted crystallization dish to control the degree of sealing, as indicated by a thick white arrow.

Preparation of Pd and Au Nanostructures on SiO$_x$/Si Substrates with PS$_x$-b-P2VP$_y$ templates (x/y = 48500/70000, 91500/105000, and 190000/190000).

A cleaned Si sample was spin-coated with ~10 μL of a block copolymer solution at 6000 rpm for 40 s. The polymer-coated sample was then immersed in 10 mL of 1 mM aq. Na$_2$PdCl$_4$ or 10 mM aq. KAuCl$_4$ for 10 min, rinsed thoroughly with a copious amount of water, and dried with a stream of nitrogen gas. The metal ion (M^{n+})-loaded sample was treated with Ar/H$_2$ plasma (Harrick PDC 32G, 18W) at 1.5 Torr for 20 min to reduce M^{n+} to M^0 and to remove block copolymer templates.

Preparation of Pd and Pt Nanostructures on SiO_x/Si Substrates with Annealed

PS₁₂₅₀₀₀-b-P2VP₅₈₅₀₀ templates.

A block polymer-templated sample was immersed in 10 mM a metal salt (aq) containing 0.9% (v/v) HCl and 3 h, rinsed thoroughly with a copious amount of water, and dried with a stream of N_2 gas. The M^{n+}-loaded sample was then treated with Ar/H_2 plasma (Harrick PDC 32G, 18W) at 1.5 torr for 30 min to reduce M^{n+} to M^0 and to remove block copolymer templates.

Preparation of Catalytic Stamps.

A patterned SiO_x/Si substrate was immediately transferred into a desiccator containing an open vial of trichloro(1*H*,1*H*,2*H*,2*H*-perfluorooctyl)silane (15 μL), after the plasma treatment. The desiccator was closed and pumped to ~1 torr to carry out vapor phase deposition of the corresponding siloxane monolayer on SiO_x. After 1 h with static vacuum, the sample was exposed to ambient atmosphere and washed with ethanol and water to remove polymerized siloxane residues. The sample was next spin-coated with h-PDMS, a mixture of 0.38 g of a vinyl silane prepolymer (VDT-731), 2 μL of a Pt catalyst (platinum divinyltetramethyldisiloxane, SIP6831.1), 12 μL of a modulator (2,4,6,8-tetramethyltetravinylcyclotetrasiloxane), and 0.12 mL of a hydrosilane prepolymer (HMS-301), at 1000 rpm for 40 s, and then cured at 65 ^{o}C for 30 min. After the first curing, degassed 184-PDMS, a 10:1 (w/w) mixture of Sylgard 184 prepolymer and curing agent, was poured onto the h-PDMS-covered sample,

degassed, and cured again at 65 ^{o}C at least for 3 h. After the second curing, the whole sample was allowed to cool to room temperature, and then the composite PDMS was carefully and slowly peeled off from the SiO$_x$/Si substrate at room temperature. In order to remove low molecular weight PDMS, the catalytic stamps were extracted overnight with hexane, dried under vacuum, and sonicated three times using a freshly prepared ethanol/water = 2/1 (v/v) solution for 5 min. These extraction and sonication processes were repeated three times, and the washed catalytic stamps were kept under vacuum until use.

Surface Characterization.

The samples obtained in this study were characterized by atomic force microscopy (AFM), scanning electron microscopy (SEM), and X-ray photoelectron spectroscopy (XPS). AFM images were taken with a Digital Instruments/Vecco Nanoscope IV (tapping mode) using commercially available Si cantilevers (PPP-NCHR probe, purchased from Nanosensors, http://www.nanosensors.com/PPP-NCHR.htm) under ambient conditions. Prior to the measurement, AFM probes were treated with oxygen plasma (O$_2$ pressure: 0.2 Torr, time: 30 s) to clean and make the surfaces hydrophilic. This treatment was important to obtain consistent results especially for phase imaging. Because the surface of Si AFM probes is hydrophilic, the attractive interaction with surface hydrophilic species was detected as positive (brighter) features in the phase images, while negative (darker) features emerged when the repulsive

interaction with surface hydrophobic species was dominant.[29]   The mean sizes, center-to-center spacings, and standard deviations (1σ) of P2VP or metal domains were calculated by counting the sizes (distances) of 200 domains, randomly picked from AFM height images (1 μm × 1 μm) of five different samples (i.e., 40 domains/sample).   SEM was performed with Hitachi S-4800 FE-SEM using an electron energy of 10k eV under high vacuum conditions ($<10^{-8}$ Torr).   XPS was taken on a Kratos Axis 165 X-ray photoelectron spectrometer using a monochromatic Al Kα with a photon energy of 1486.6eV under high vacuum conditions ($<10^{-8}$ Torr), and ejected X-rays were measured 0° from the surface normal.   To avoid surface charging for PDMS samples, the charge neutralizer was used.   The XPS signals were calibrated on the basis of the O(1s) (532.0 eV).

2.5. References

1. (a) Yang, W.; Yang, C.; Sun, M.; Yang, F.; Ma, Y.; Zhang, Z.; Yang, X. *Talanta* **2009**, *78*, 557-564. (b) Shiju, N. R.; Guliants, V. V. *Appl. Catal. A: Gen.* **2009**, *356*, 1-17. (c) Rostovshchikova, T. N.; Smirnov, V. V.; Gurevich, S. A.; Kozhevin, V. M.; Yavsin, D. A.; Nevskaya, S. M.; Nikolaev, S. A.; Lokteva, E. S. *Catal. Today* **2005**, *105*, 344-349.

2. (a) Xia, Y.; Whitesides, G. M. *Annu. Rev. Mater. Sci.* **1998**, *28*, 153-184. (b) Xia, Y.; Whitesides, G. M. *Angew. Chem., Int. Ed.* **1998**, *37*, 550-575.

3. (a) Glass, R.; Moeller, M.; Spatz, J. P. *Nanotechnology* **2003**, *14*, 1153-1160. (b) Spatz, J. P.; Mossmer, S.; Hartmann, C.; Moller, M.; Herzog, T.; Krieger, M.; Boyen, H.-G.; Ziemann, P.; Kabius, B. *Langmuir* **2000**, *16*, 407-415. (c) Käestle, G.; Boyen, H.-G.; Weigl, F.; Lengl, G.; Herzog, T.; Ziemann, P.; Riethmueller, S.; Mayer, O.; Hartmann, C.; Spatz, J. P.; Moeller, M.; Ozawa, M.; Banhart, F.; Garnier, M. G.; Oelhafen, P. *Adv. Funct. Mater.* **2003**, *13*, 853-861 (d) Glass, R.; Moeller, M.; Spatz, J. P. *Nanotechnology* **2003**, *14*, 1153-1160.

4. (a) Aizawa, M.; Buriak, J. M. *J. Am. Chem. Soc.* **2005**, *127*, 8932-8933. (b) Aizawa, M.; Buriak, J. M. *Chem. Mater.* **2007**, *19*, 5090-5101. (c) Chai, J.; Wang, D.; Fan, X.; Buriak, J. M. *Nat. Nanotechnol.* **2007**, *2*, 500-506. (d) Chai, J.; Buriak, J. M. *ACS Nano* **2008**, *2*, 489-501. (e) Chai, J.; Taschuk, M. T.; Brett, M. J.; Buriak, J. M. *Proc. SPIE* **2008**, *7041*, 704111.

5.	(a) Bates, F. S.; Fredrickson, G. H. *Phys. Today* **1999**, *52*, 32-38. (b) *Amphiphilic Block Copolymers*; Alexandridis, P., Ed.; Elsevier: Amsterdam, Netherland, 2000. (c) Hamley, I. W. In *Developments in Block Copolymer Science and Technology*; Hamley, I. W., Ed.; Wiley-VCH: Weinheim, Germany, 2004, 1-29. (d) Gohy, J.-F. *Adv. Polym. Sci.* **2005**, *190*, 65-136. (e) Ozin, G. A.; Arsenault, A. C. *Nanochemistry: A Chemistry Approach to Nanomaterials*; Royal Society of Chemistry, Cambridge, UK, 2005; Chapter 9, 435-467. (f) Segalman, R. A. *Mater. Sci. Eng., R.* **2005**, *48*, 191-226.

6.	(a) Kataoka, K.; Harada, A.; Nagasaki, Y. *Adv. Drug Deliver. Rev.* **2001**, *47*, 113-131. (b) *Block Copolymers in Nanoscience*; Lazzari M.; Liu, G.; Lecommandoux, S., Ed.; Wiley-VCH, Weinheim, Germany, 2006. (c) Blanazs, A.; Armes, S. P.; Ryan, A. J. *Macromol. Rapid Commun.* **2009**, *30*, 267-277. (d) Hamley, I. W. *Angew. Chem. Int. Ed.* **2003**, *42*, 1692-1712.

7.	(a) Forster, S.; Antonietti, M. *Adv. Mater.* **1998**, *10*, 195-217. (b) Hamley, I. W. *Nanotechnology* **2003**, *14*, 39-54. (c) Park, C.; Yoon, J.; Thomas, E. L. *Polymer* **2003**, *44*, 6725-6760. (d) Stoykovich, M. P.; Nealey, P. F. *Mater. Today* **2006**, *9*, 20-29. (e) Li, M.; Ober, C. K. *Mater. Today* **2006**, *9*, 30-39. (f) Krishnamoorthy, S.; Hinderling, C.; Heinzelmann, H. *Mater. Today* **2006**, *9*, 40-47.

8.	Black, C. T. *ACS Nano* **2007**, *1*, 147-150.

9.   Park, M.; Harrison, C.; Chaikin, P. M.; Register, R. A.; Adamson, D. H. *Science* **1997**, *276*, 1401-1404.

10.   Xu, T.; Kim, H.-C.; DeRouchey, J.; Seney, C.; Levesque, C.; Martin, P.; Stafford, C. M.; Russell, T. P. *Polymer* **2001**, *42*, 9091-9095.

11.   Qiao, Y.; Wang, D.; Buriak, J. M. *Nano Lett.* **2007**, *7*, 464-469.

12.   Duffy, D. C.; McDonald, J. C.; Schueller, O. J. A.; Whitesides, G. M. *Anal. Chem.* **1998**, *70*, 4974.

13.   Krishnamoorthy, S.; Pugin, R.; Brugger, J.; Heinzelmann, H.; Hinderling, C. *Adv. Funct. Mater.* **2006**, *16*, 1469-1475.

14.   (a) *Polymer Handbook*, 4th ed.; Brandrup, J.; Immergut, E. H.; Grulke, E. A., Ed.; John Wiley & Sons: New York, NY, 1999. (b) Arichi, S.; Matsuura, H.; Tanimoto, Y.; Murata, H. *Bull. Chem. Soc. Jpn.* **1966**, *39*, 434-439.

15.   Bosworth, J. K.; Paik, M. Y.; Ruiz, R.; Schwartz, E. L.; Huang, J. Q.; Ko, A. W.; Smilgies, D.-M.; Black, C. T.; Ober, C. K. *ACS Nano* **2008**, *2*, 1396-1402.

16.   (a) Breulmann, M.; Forster, S.; Antonietti, M. *Macromol. Chem. Phys.* **2000**, *201*, 204-211. (b) Chen, Y.; Huang, H.; Hu, Z.; He, T. *Langmuir* **2004**, *20*, 3805-3808.

17.   (a) Ripoll, C.; Muller, G.; Selegny, E. *Eur. Polym. J.* **1971**, *7*, 1393-1409. (b) Nisit Tantavichet, M. D. P. C. M. B. *J. Appl. Polym. Sci.* **2001**, *81*, 1493-1497.

18. (a) Niihara, K.; Nishikawa, Y.; Nishi, T.; Jinnai, H. *Trans. Mater. Res. Soc. Jpn.* **2005**, *30*, 617-622. (b) Yokoyama, H.; Sugiyama, K. *Langmuir* **2004**, *20*, 10001-10006. (c) Cohen, R. E.; Bellare, A.; Drzewinski, M. A. *Macromolecules* **1994**, *27*, 2321-2323.

19. Jung, G.-Y.; Li, Z.; Wu, W.; Chen, Y.; Olynick, D. L.; Wang, S.-Y.; Tong, W. M.; Williams, R. S. *Langmuir* **2005**, *21*, 1158-1161.

20. (a) Schmid, H.; Michel, B. *Macromolecules* **2000**, *33*, 3042. (b) Odom, T. W.; Love, J. C.; Wolfe, D. B.; Paul, K. E.; Whitesides, G. M. *Langmuir* **2002**, *18*, 5314.

21. Graham, D. J.; Price, D. D.; Ratner, B. D. *Langmuir* **2002,** *18,* 1518-1527.

22. Hulteen, J. C.; Treichel, D. A.; Smith, M. T.; Duval, M. L.; Jensen, T. R.; Van Duyne, R. P. *J. Phys. Chem. B* **1999**, *103*, 3854-3863.

23. Because PDMS is not conductive, the charging up of a sample occurs by an electron beam irradiation. This causes the heating of the sample, resulting in the swelling of PDMS. See: Echlin, P. In *Handbook of Sample Preparation for Scanning Electron Microscopy and X-Ray Microanalysis*; Echlin, P., Ed.; Springer: New York, 2009, 299-306.

24. Louette, P.; Bodino, F.; Pireaux, J.-J. *Surf. Sci. Spectra* **2006**, *12*, 38-43.

25. Wagner, C. D.; Naumkin, A. V.; Kraut-Vass, A.; Allison, J. W.; Powell, C. J.; Rumble, J. R., NIST X-ray Photoelectron Spectroscopy Database. In *NIST Standard Reference Database 20, Version 3.5*, National Institute of Standards and Technology, Gaithersburg: 2007. http://srdata.nist.gov/xps/

26. Graeter, S. V.; Huang, J.; Perschmann, N.; Lopez-Garcia, M.; Kessler, H.; Ding, J.; Spatz, J. P. *Nano Lett.* **2007**, *7*, 1413-1418.

27. Kern, W. Overview and Evolution of Semiconductor Wafer Contamination and Cleaning Technology. In *Handbook of Semiconductor Wafer Cleaning Technology*; Kern, W., Ed.; Noyes Publications: Park Ridge, NJ, 1993, 3.

28. Rider, D. A.; Cavicchi, K. A.; Vanderark, L.; Russell, T. P.; Manners, I. *Macromolecules* **2007**, *40*, 3790-3796.

29. Garcia, R.; Magerle, R.; Perez, R. *Nat. Mater.* **2007**, *6*, 405-411.

Chapter 3
Catalytic Stamp Lithography 1: Hydrosilylation

3.1. Introduction

Using the catalytic stamps fabricated via the procedure described in Chapter 2, nanoscale patterning of organic monolayers, termed catalytic stamp lithography, was performed. As a first demonstration, this chapter focuses on hydrosilylation-based patterning of hydrogen-terminated crystalline flat silicon surfaces and shows that our proposed system is effectively able to achieve patterned organic monolayers, even at the sub-20 nm resolution.

In terms of the design of the experiment, we selected the hydrosilylation of hydrogen-terminated crystalline silicon surfaces for the following reasons: (1) crystalline silicon is ubiquitous in a broad range of existing technologies,[1] therefore direct modification of silicon substrates would become an ideal starting point with wide interest, (2) a hydrogen-terminated, atomically flat crystalline silicon surface is readily available,[2] (3) hydrosilylation is an extremely efficient reaction for forming a chemically stable Si-C bond, and the catalytic mechanism is well established in molecular systems,[3] and (4) significant progress was made on surface hydrosilylation over the past 15 years.[4] These points are more clearly stated in the next section.

3.2. Review of Related Topics

Single Crystalline Silicon

Single crystalline silicon is one of the most important materials in modern technologies, ranging from electronics[1a] and optics,[1b] to photovoltaics.[1c] Crystal orientations of (100) and (111) are most common, among others, and commercially available at relatively low cost.[5] Because the surface is susceptible to oxidation, it is usually covered by a thin layer of native oxide (SiO_x) upon exposure to air.[5] Most of the conventional silicon-based applications rely on thermally grown SiO_x as an effective passivating layer.[1a] However, there is increasing demand for methods that control a greater variety of the surface characteristics of this material for existing technologies, and for emerging applications (such as molecular electronics). Thus, a number of surface functionalization methods for oxide-free crystalline silicon have been proposed to date, including hydrosilylation (*vide infra*).[4]

Hydrogen-Terminated Crystalline Silicon Surfaces

Hydrogen termination on crystalline silicon surfaces can be readily achieved by treating cleaned native oxide-capped silicon substrates with fluoride-containing aqueous solutions for 4-6 min (Figure 3.1).[2] Depending on the crystal orientations, either HF or NH_4F is used as a fluoride source. For Si(100), diluted (1-2%) aqueous HF is usually employed to yield a mainly dihydride surface with nanoscale roughness (Figure 3.1a), although it is known that mono- and trihydride

groups also exist on the resulting surface.[2a] For Si(111), on the other hand, degassed 40% aqueous NH$_4$F is used to produce a monohydride surface with atomic-flatness (Figure 3.1b).[2] These surfaces are commonly expressed as Si(100)-H$_x$ and Si(111)-H, respectively, and can be handled in air for a few tens of minutes.[2]
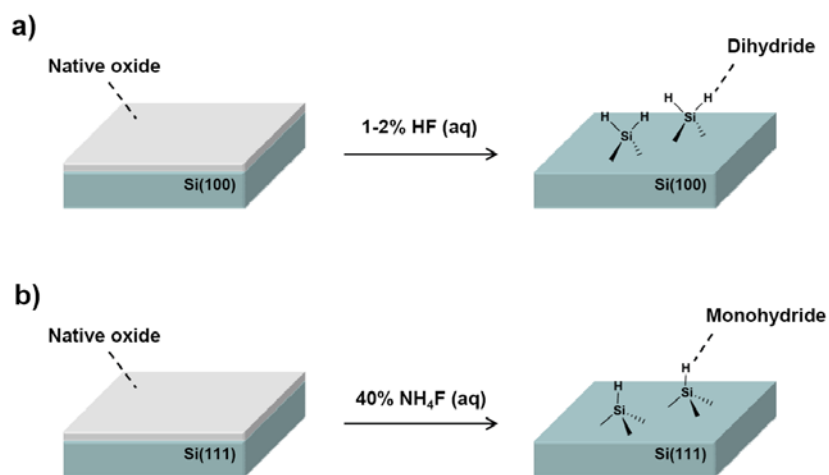
Figure 3.1. Outline for hydrogen-termination of flat Si(100) and Si(111) surfaces. (a) A dihydride surface is produced from Si(100) with HF (aq). (b) A monohydride surface is obtained from Si(111) and NH$_4$F (aq).

A proposed mechanism for hydrogen-termination of crystalline silicon surfaces by HF is shown in Figure 3.2.[6] After the dissolution of native silicon oxide, the topmost silicon atom (Si$_I$) is considered to have fluorine termination. Since the fluorine atom has the greatest electronegativity, the bond between the Si$_I$ and the second topmost silicon atom (Si$_{II}$) becomes highly polarized as Si$_I^+$– Si$_{II}^-$. This polarization makes Si$_I^+$ susceptible towards nucleophilic attack from F$^-$,

leading to the elimination of the Si_I atom from the surface as H_2SiF_6 (aq) or SiF_4

(aq). Finally, the newly formed topmost Si_{II}^- is protonated, yielding Si-H

terminations.
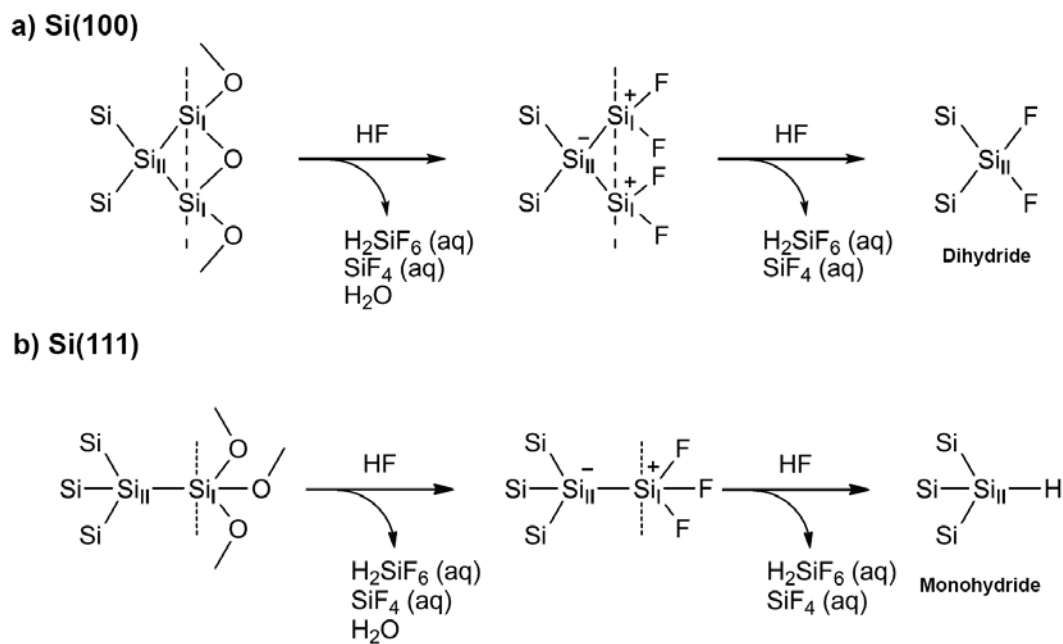
a) Si(100)

b) Si(111)

Figure 3.2. A possible mechanism for hydrogen termination of crystalline silicon surfaces

using HF as an etchant. (a) Dihydride termination on Si(100). (b) Monohydride termination

on Si(111).

Hydrosilylation with Molecular Si-H Bonds

Hydrosilylation is an addition reaction of a Si-H bond across an

unsaturated (π) bond and is well studied in the molecular system (that is, typical

Si-H precursors are small silane molecules/oligomers/polymers) (Figure 3.3).[3]

Because no byproduct is produced, this reaction is truly atom-economical.

Normally, the bond is a C=C or C≡C bond, although carbon-heteroatom (nitrogen or oxygen) and heteroatom-heteroatom multiple bonds are also included.[3] Various pathways are known for this reaction, including transition metal- and Lewis acid-catalysis, and thermal- or photo-induced radicals with an initiator.[7]

$$R_3Si-H \quad + \quad R^1\text{===}R^2 \quad \xrightarrow{\text{Metal catalysis or Radical}} \quad \underset{R_3Si}{\overset{R^1}{>}}=\underset{H}{\overset{R^2}{<}}$$
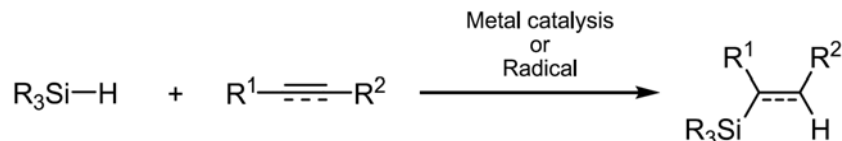
Figure 3.3. A representative chemical equation for hydrosilylation of a carbon-carbon multiple bond.

This reaction has played a significant role in organic synthesis due to the utility of the resulting organosilicon compounds.[3] Many useful transformations have been developed, in particular, through catalytic hydrosilylation of carbon-carbon multiple bonds. For example, Pd-catalyzed asymmetric hydrosilylation of alkenes is known as an efficient route to produce chiral organosilanes, which can be converted into optically active alcohols.[8] In addition, a variety of functional silicones are industrially produced via hydrosilylation.[9] Thermal curing of commercially available PDMS, such as Sylgard-184 of Dow Corning, is based on the hydrosilylation between vinyl- and hydride-containing siloxane prepolymers, induced by a Pt catalyst.

Figure 3.4 shows a generally accepted classic mechanism for transition metal-catalyzed hydrosilylation of alkenes: the Chalk-Harrod mechanism.[10] This

consists of (1) coordination of an alkene to a metal center, (2) oxidative addition

of a Si-H bond to the metal center, (3) migration of the hydrogen onto the

coordinated alkene, and (4) reductive elimination of the alkyl group from the

metal to form a Si-C bond.
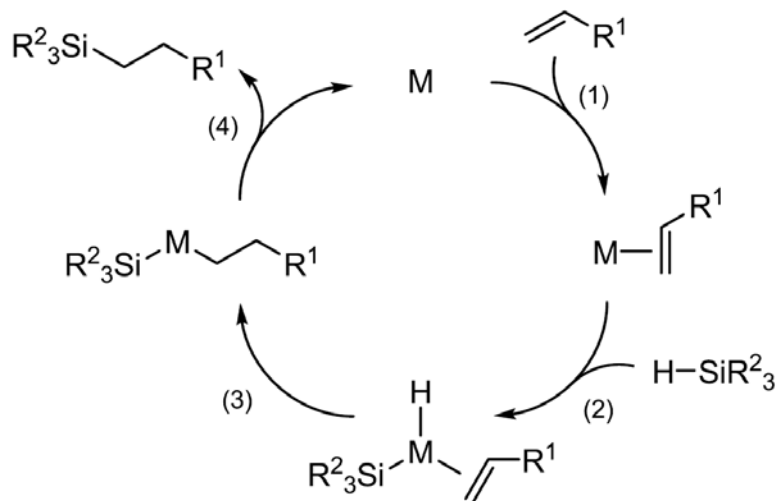
Figure 3.4. The Chalk-Harrod hydrosilylation mechanism of alkenes. (1) alkene

coordination to a metal catalyst. (2) Oxidative addition of a Si-H bond to the catalyst. (3)

Hydrogen migration to the alkene. (4) Reductive elimination of alkyl ligand to form Si-C

bond and regenerate the catalyst.

Although the Chalk-Harrod mechanism well-substantiates homogeneous

hydrosilylation catalysis, colloid-[11] and Lewis acid-catalyzed[12] hydrosilylation are

also reported with their own proposed mechanisms.

Hydrosilylation with Surface Si-H Bonds

It has been revealed that hydrosilylation takes place on bulk silicon materials, including hydrogen-terminated single crystalline flat silicon (and nanostructured silicon materials, such as porous silicon and silicon nanoparticles/nanowires, although they are not covered in this thesis).[4] Because a Si-C bond is stable both thermodynamically and kinetically,[3] surface hydrosilylation offers an attractive method to modify metastable H-terminated Si surfaces with a variety of functionalities. As in the case of molecular systems, both radical[13] and metal-catalyzed[14] approaches have been developed.

In the case of radical-based surface hydrosilylation, the key step includes the generation of a surface silicon radical through the use of either radical initiators,[13a] heat,[13b] or light (UV).[13c] In 1993, Linford and Chidsey for the first time demonstrated hydrosilylation of crystalline Si surfaces using radical initiators.[13a] Alkyl radicals are thermally (100 ^{o}C) produced from diacyl peroxides to induce a hydrogen abstraction from a silicon surface, yielding a silicon radical on the surface. It was later found that surface radicals can be produced without radical initiators, if carried out at higher temperatures (>150 ^{o}C)[13b] or under UV irradiation.[13c] In these cases, hemolytic cleavage of Si-H bonds yielded surface Si radicals. Once the surface radicals are generated, a monolayer can be formed as follows: (1) Si-C bond formation between a surface Si radical and an alkene (or alkyne) molecule to yield a carbon radical, (2) hydrogen transfer from neighboring Si-H to the carbon radical to create a new Si

radical, and (3) repeating of a and b until a densely packed monolayer is formed on the entire surface (Figure 3.5).
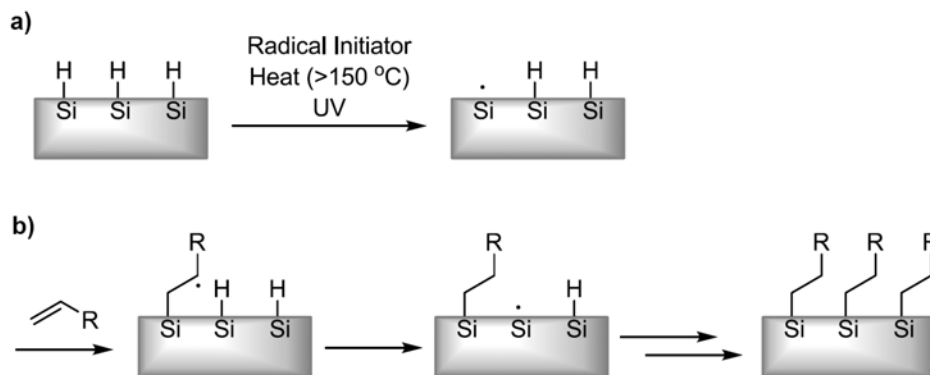
Figure 3.5. A proposed mechanism for the radical-mediated surface hydrosilylation. (a) Surface silicon radical formation by radical initiator/heat/UV. (b) Si-C bond formation between the surface radical and an alkene and radical propagation to form the next Si-C bond.

Because transition metals are extremely effective catalysts in the case of molecular hydrosilylation, their use in surface hydrosilylation have also been investigated. In general, however, transition metal systems cause unfavored surface oxidation in addition to surface hydrosilylation.[14] For instance, when platinum divinyltetramethylsiloxane and 3,4-dichlorobutane were used as the catalyst and a monolayer precursor, respectively, both hydrosilylation of the precursor and oxide formation were observed on Si(100)-H_x, as confirmed by XPS and TOF-SIMS.[14a] A similar result was observed in the reaction between an indene-derivative and a Si(111)-H using H_2PtCl_6 as the catalyst.[14c] Related to metal-catalyzed reactions, Lewis acid-catalyzed surface hydrosilylation has also

been demonstrated on Si(111)-H surfaces.[15]   Although this Lewis acid-based hydrosilylation had been proven to be highly effective for the modification of porous silicon surfaces, it was found that monolayers formed on flat Si(111) were not as stable as those made from other routes (UV hydrosilylation).   Different from the molecular system, metal catalysis-based hydrosilylation has not been harnessed in the surface system.

Patterning of Organic Monolayers via Catalytic Hydrosilylation

Although H-terminated Si surfaces were not involved, there is only one report by Blackledge *et al*. that employed catalytic hydrosilylation to generate chemically patterned surfaces (Figure 3.6).[16]   Here, an alkene-terminated surface was used as a substrate, and an aminoalkylsilane molecule was hydrosilylated by the use of a Pd-coated AFM tip (Figure 3.6a).   The resulting amine-terminated line was treated with biotin, followed by the attachment of streptavidin-coated gold nanoparticles, to clearly visualize the created pattern by AFM (Figure 3.6b,c).
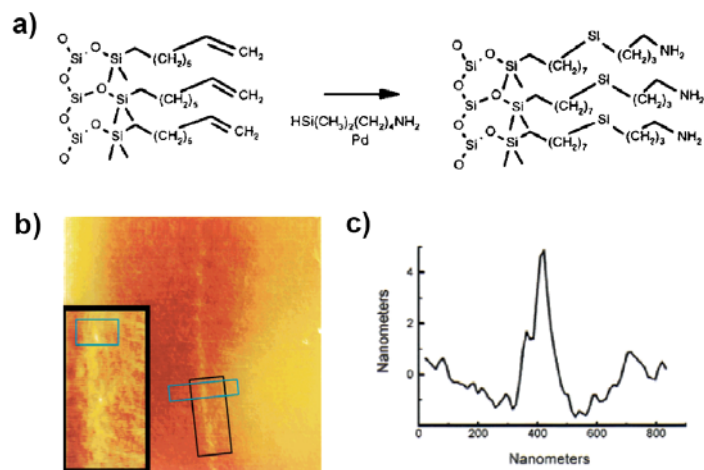
Figure 3.6. (a) Schematic of Pd-catalyzed hydrosilylation of surface alkene groups with aminobutyldimethylsilane. (b) AFM image of a single line produced via the AFM tip-induced surface reaction shown (a), followed by the modification with biotin and streptavidin-coated gold nanoparticles. (c) Cross-section analysis of a part of the line in the cyan box. Reprinted with permission from ref. 16. Copyright © 2000 American Chemical Society.

3.3. Results and Discussion

Figure 3.7 illustrates the typical conditions of catalytic stamp lithography: a catalytic stamp (Pd or Pt) was inked with a dilute solution of terminal alkenes/alkynes for 1 min, and then applied to freshly-prepared flat H-terminated Si [either (100) or (111)] under ambient laboratory conditions. Stamping was normally carried out for 20 min under light continuous pressure (see Experimental Section). The subsequent release of the catalytic stamp resulted in a duplication of the original pattern of metallic nanostructures on the silicon surface with arrays of alkyl/alkenyl groups covalently attached to a Si surface (localized catalysis); the released stamp was reusable for subsequent inking/ stamping.
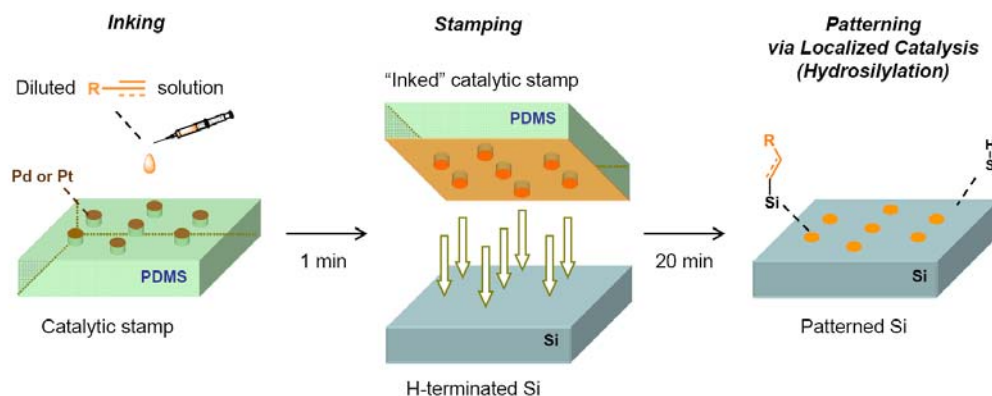
Figure 3.7. Outline for catalytic stamp lithography. In the typical procedure, a diluted molecular ink in 1,4-dioxane was first applied on a Pd or Pt catalytic stamp and let sit for 1 min. After the remaining ink was gently blown off by a nitrogen stream, the inked stamp was brought into contact with a freshly prepared H-teminated Si(111) or (100) surface for 20 min at room temperature. During this stamping, molecular patterns were formed by catalytic hydrosilylation, which took place only underneath the patterned metals (localized catalysis).

Hydrosilylation with Pd catalytic stamps[17]

The first demonstration of catalytic stamp lithography was carried out with the use of Pd catalytic stamps. Heterogeneous hydrosilylation by solid Pd is known.[11c,16] Figure 3.8 summarizes the results using a 5 mM 1,4-dioxane solution of 1-octadecyne as an ink. Tapping mode AFM height images of a Pd catalytic stamp and a stamped Si(111)-H surface show pseudo-hexagonal arrays of (a) Pd and (b) hydrosilylated 1-octadecyne molecules, with center-to-center spacings of ~120 nm in both the stamp and resulting surface pattern. The AFM phase image (c), simultaneously recorded with the height image (b), suggest the existence of hydrophobic 1-octadecenyl groups surrounded by H-terminated Si.[18] The section analysis (d) along the dashed line in b showed that each domain is approximately 1.3 nm tall, suggesting the molecules are loosely packed and significantly tilted from the surface normal (the theoretical length of 1-octadecenyl group with all *trans* conformations is ~2.2 nm).
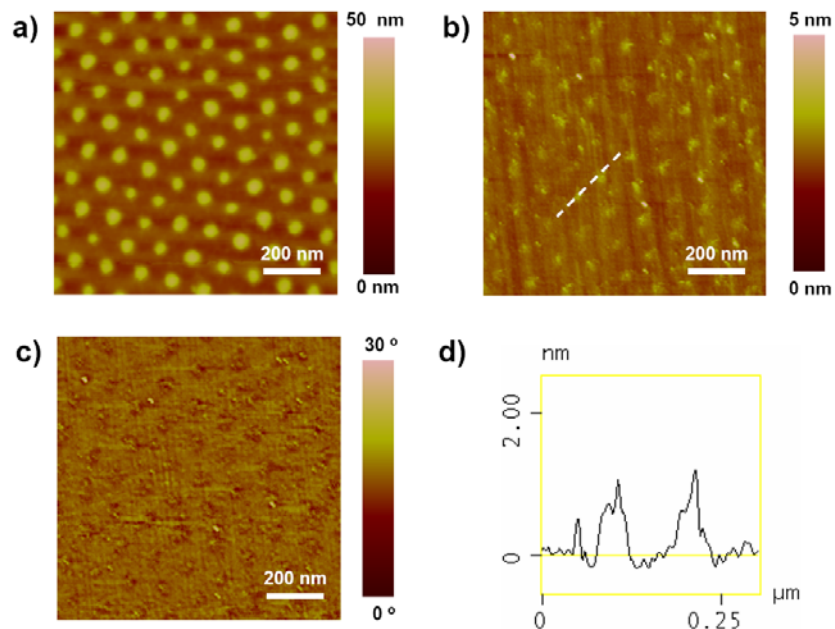
Figure 3.8. (a) AFM height image of a parent Pd catalytic stamp with NP diameters of 40 nm, and a center-to-center spacing of 110 nm. (b) 1- octadecyne-stamped Si(111)-H surface and corresponding phase image (c). (d) Section analysis along the dashed line in (b).

Figure 3.9 shows the AFM and SEM images of the 1-octadecyne-stamped sample tested in a series of etching solutions. The hexagonal pattern was still visible after aggressive etching with 40% NH_4F (aq) for 5 min (a). The greater topographic contrast after etching was enough to be observed by SEM as well (b). Similar stability results could be achieved using 1% HF (aq) for 30 s (c) and 1 M KOH (aq, containing 15% 2-propanol) for 60 s (d), indicating that the 1-octadecyne molecules were bonded via covalent Si-C bonds.
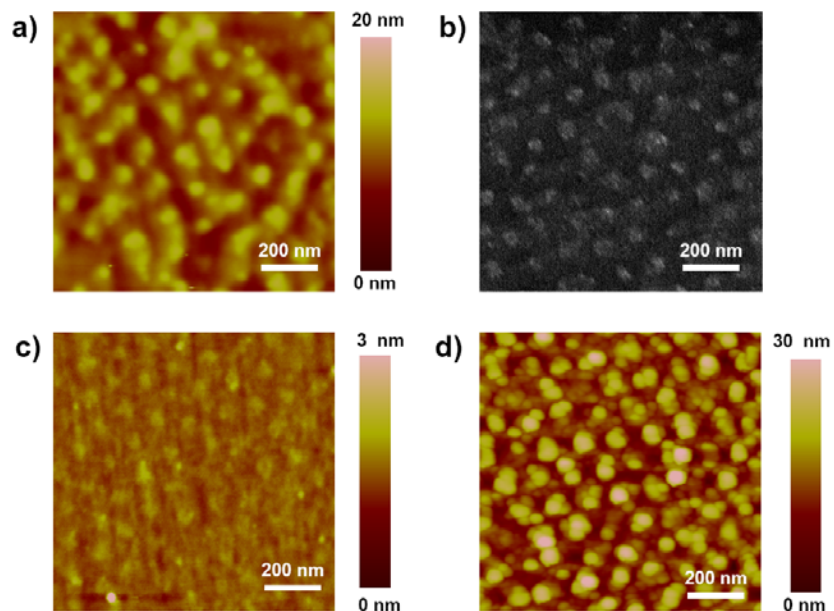
Figure 3.9. (a) AFM height image of a 1-octadecyne-stamped Si(111)-H surface, followed by wet chemical etching with 40% NH_4F (aq) for 5 min. (b) SEM image of the sample from (a). (c) AFM height image of a 1-octadecyne-stamped Si(111)-H, followed by the treatment with 1% HF (aq) for 30s. (d) AFM height image of a 1-octadecyne-stamped Si(100)-H_x, followed by the treatment with 1 M KOH (aq, containing 15% 2-propanol) for 1 min.

Additional evidence was collected to prove the pattern formation by catalytic stamping. First, a series of control stamping experiments resulted in no visible patterns, as shown by AFM: (a) the use of neat 1,4-dioxane (no alkenes/alkynes included) (Figure 3.10a), (b) stamping with the standard alkene/alkyne ink solution on oxide-capped Si(111) surface (no Si-H bonds) (Figure 3.10b), (c) use of catalytically inactive Au patterned stamps with the standard alkene/alkyne ink solution (Figure 3.10c).

a)

1,4-Dioxane only

Pd

PDMS

Catalytic stamp

1 min

"Inked" catalytic stamp

PDMS

Si

H-terminated Si

20 min

H
Si

Si

Patterned Si

5 nm

200 nm

0 nm

b)

Diluted R solution

Pd

PDMS

Catalytic stamp

1 min

"Inked" catalytic stamp

PDMS

Si

SiOx

Oxide-capped Si

20 min

SiOx

Si

Patterned oxide-capped Si

5 nm

200 nm

0 nm
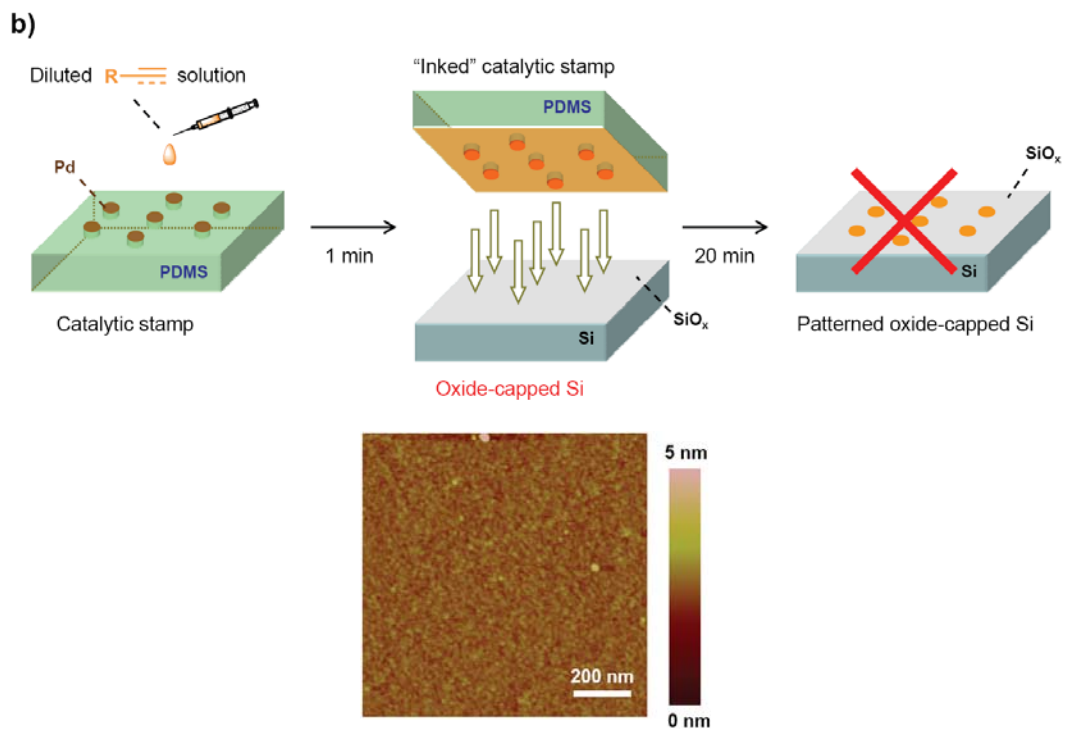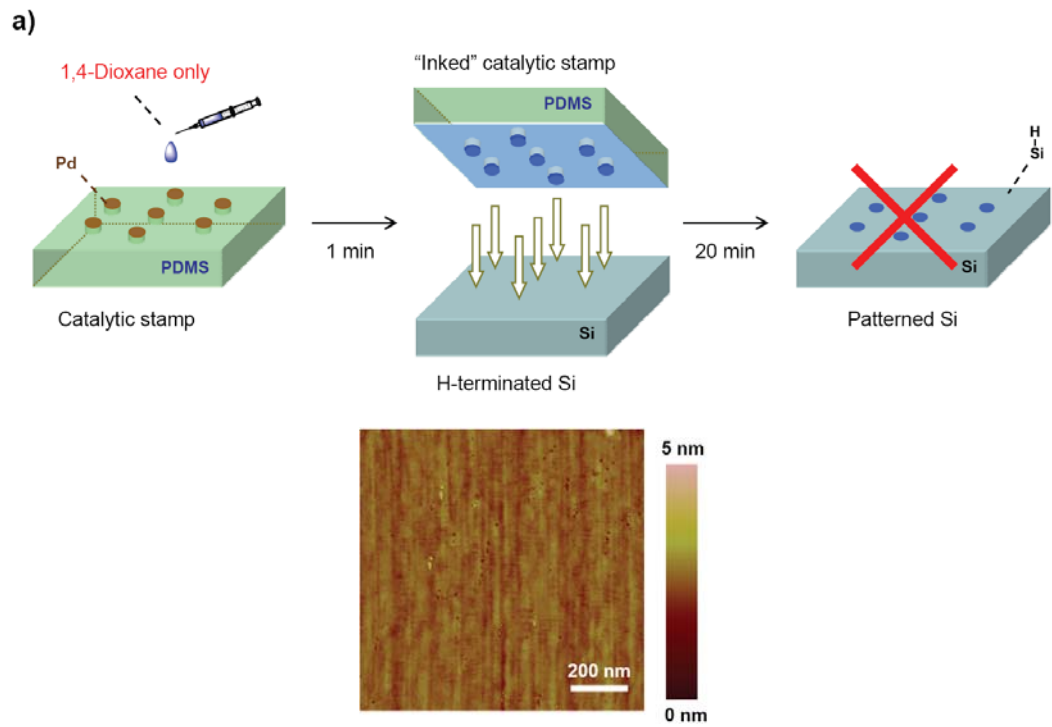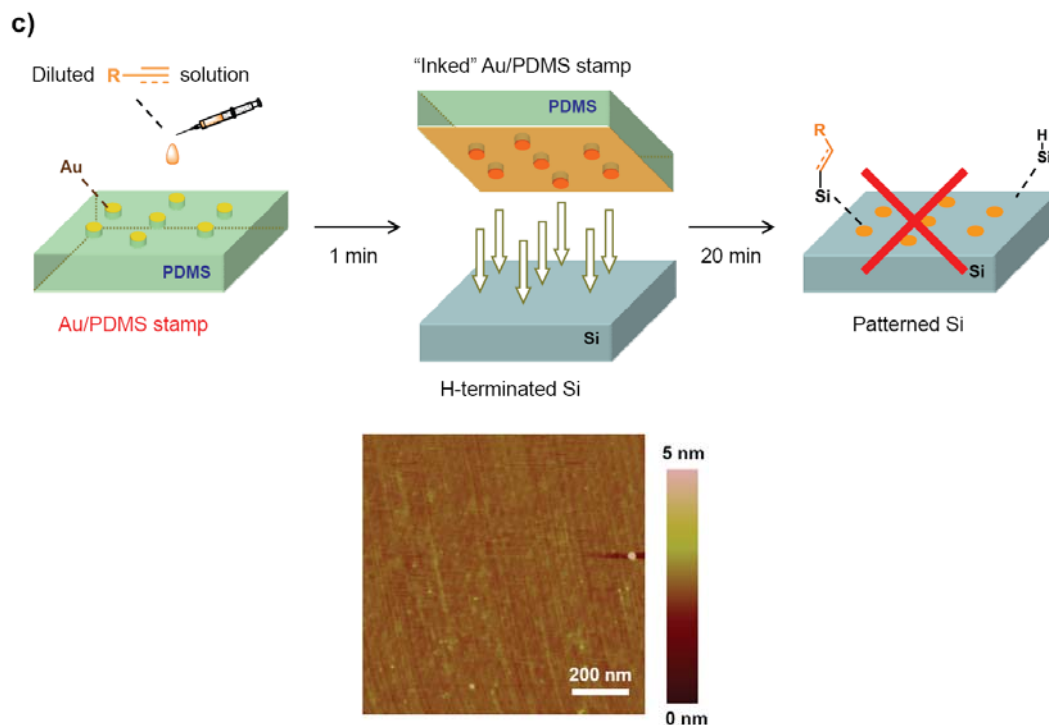
Figure 3.10. Outline for control experiments and corresponding AFM height images. No patterns were observed on the resulting surfaces when catalytic stamping was attempted using (a) solvent (1,4-dioxane) only, (b) a native oxide-capped silicon surface, and (c) a gold/PDMS stamp.

Second, each stamp could be reused multiple times (at least 12 times, Figure 3.11) with no apparent degradation of the quality of the surface patterns, suggesting the catalytic nature of Pd NPs on PDMS.
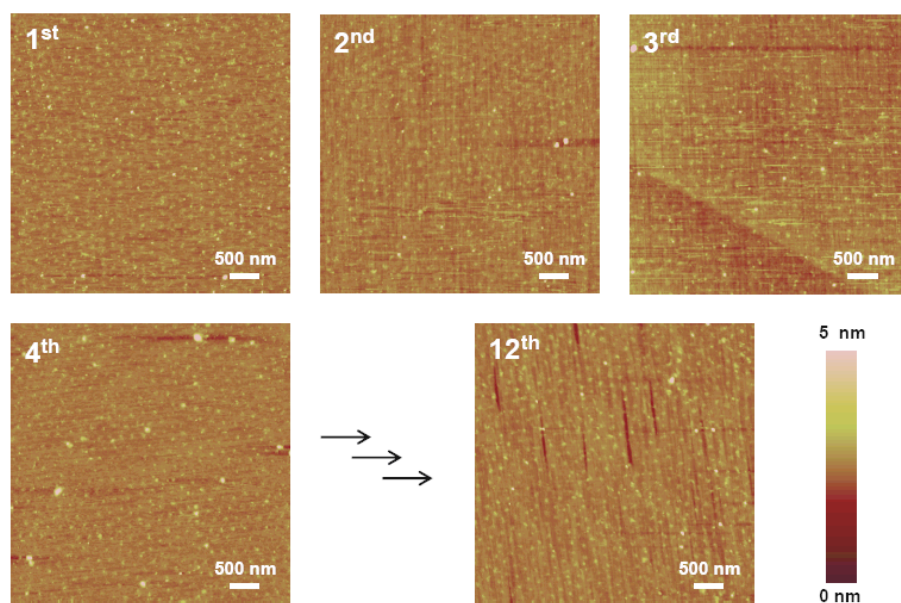
Figure 3.11. Reusability test (up to 12 times) of a Pd catalytic stamp (NP diameter of 40 nm and center-to-center spacing of 110 nm) using Si(111)-H as substrates and 1-octadecyne as an ink.

Furthermore, XPS analysis of the stamped sample revealed neither the formation of silicon oxides (Figure 3.12a), which is known to be facilitated in the presence of transition metals,[14a,b] nor the contamination by PDMS[19] and/or Pd (Figure 3.12a,b respectively). All of these observations strongly support the premise of localized catalytic hydrosilylation-induced pattern formation.
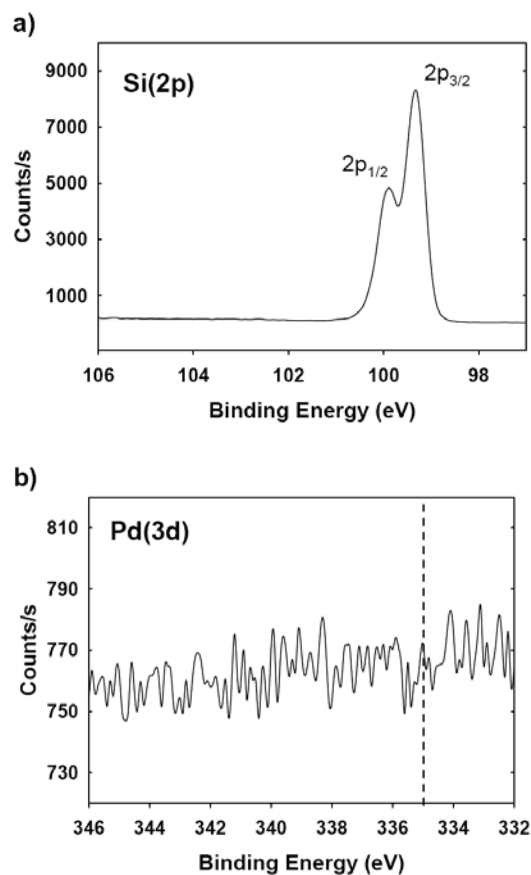
Figure 3.12. XPS of Si(111)-H surface stamped with 1-octadecyne. (a) Si(2p) region (b) Pd(3d) region. No signals from silicon oxide (~103 eV), PDMS (~102 eV) or Pd^0 (~335 eV) were observed. The dashed line in (b) corresponds to metallic Pd (335.4 eV).

The resulting silicon surface patterns are tunable with respect to sizes/spacings and properties, using different Pd catalytic stamps and inks, respectively. AFM height images in Figure 3.13 show the Pd catalytic stamps with the NP diameters of ~20 nm and center-to-center spacing of ~60 nm (a) and the stamped Si(111)-H surface (b) using 5-hexyn-1-ol (5 mM in dioxane) as the ink. Again, clear pattern transfer was observed, and in this case, hydrophilicity of

the OH termination in the ink molecule was also suggested by the phase image (c). Thus, wide varieties of functional molecules with terminal C=C or C≡C groups are compatible with this method.
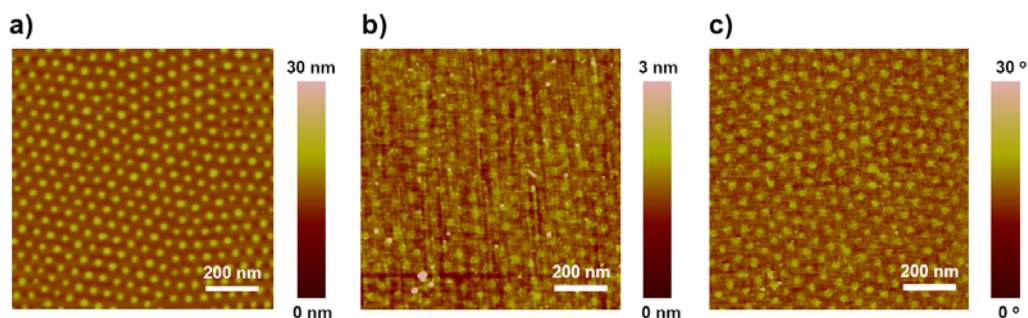
Figure 3.13. (a) AFM height image of a Pd catalytic stamp with NP diameters of 20 nm and a center-to-center spacing of 60 nm. (b,c) AFM height (b) and phase (c) images of the 5-hexyn-1-ol stamped Si(111) surface.

To further demonstrate the scope of catalytic stamp lithography, subsequent modification of the patterned surfaces was performed (Figure 3.14a). After the patterned stamping of 1,7-octadiene on Si(100)-H_x, the remaining blank hydride-terminated regions between the alkene-terminated surface were etched with 4 M KOH (aq) for 30 s, and then soaked in O_2-saturated H_2O overnight to remove any residual Si-H groups that could react in the next step.[20] Next, a UV-mediated thiol-ene reaction[21] with 1,9-nonanedithiol was carried out to produce thiol-terminated patterns. Immersion in a toluene solution of tetraoctylammonium bromide-capped Au NPs (diameter: ~5 nm) resulted in selective assembly of Au NPs on surface thiol groups (Figure 3.14b,c).[22]
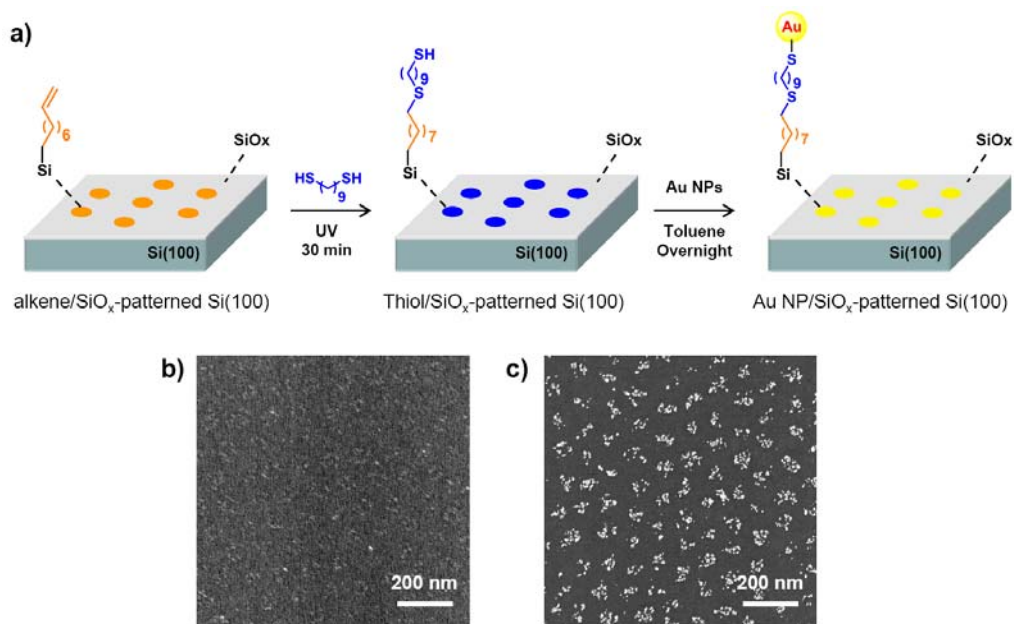
Figure 3.14. (a) Outline of the procedure for modification of alkene/SiO$_x$-patterned Si(100).

(b) SEM images of Si(100)-H$_x$ patterned with hexagonal arrangements of regions of thiol terminated-groups. (c) Assembly of 5 nm Au NPs on the surface shown in (b).

Hydrosilylation with Pt catalytic stamps[23]

In order to expand the scope for catalytic stamp lithography with regard to hydrosilylation, we next utilized Pt catalytic stamps, since Pt is historically the most actively investigated metal for hydrosilylation catalysis.[11a,b,24] In addition, an aldehyde functionality[25] was included in the list of molecular inks to complement alkenes and alkynes.

Figure 3.15 shows the tapping-mode AFM height and phase images of stamped Si(111)-H or Si(100)-H_x surfaces, using hexagonally or linearly patterned Pt catalytic stamps (a and b, respectively). Eight varieties of molecular inks were tested under the same conditions as Pd catalytic stamps, containing terminal C=C, C≡C, or C=O groups, to produce the corresponding hydrosilylated alkyl, alkenyl, or alkoxy groups; all the resulting patterns appeared as positive features in the height mode in the AFM images. As mentioned in Chapter 2, the surfaces of Pt nanostructures are believed to be flat and therefore able to make good contact with the precursor H-terminated Si surfaces. Because highly localized catalysis took place exclusively underneath the nanopatterned Pt during stamping, the size (~18 nm) and center-to-center spacing (~64 nm) for the hexagonal pattern, or the width (~15 nm) and interline distance (~59 nm) for linear patterns were nearly identical to the original Pt patterns of catalytic stamp (see Chapter 2), and thus not apparently affected by ink diffusion or stamp deformation. Depending on the chemical nature of terminal functional groups in the stamped molecules relative to the surrounding H-terminated Si, negative

(more hydrophobic) patterns[17] were obtained in the case of 1-dodecene (c), 1*H*,1*H*,2*H*-perfluoro-1-dodecene (e) phenylacetylene (f), undecanal (h), and benzaldehyde (i) in the phase images, while positive (more hydrophilic) patterns[17] were obtained in the case of 4-vinylpyridine (d) and 10-undecynoic acid (g).

e) $\diagup\diagdown(CF_2)_9\diagup CF_3$

Height
5 nm
0 nm
200 nm

Phase
20 °
0 °
200 nm

f) $\equiv\diagdown$⬡

Height
5 nm
0 nm
200 nm

Phase
15 °
0 °
200 nm

g) $\equiv\diagdown(\;)_9$COOH

Height
5 nm
0 nm
200 nm

Phase
30 °
0 °
200 nm

h) O$=\diagdown(\;)_9\diagdown$

Height
5 nm
0 nm
200 nm
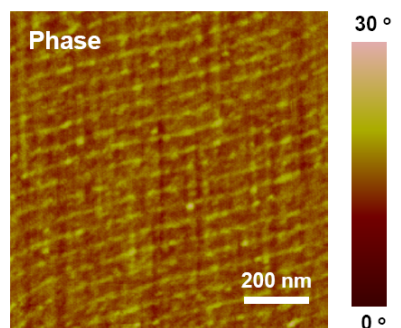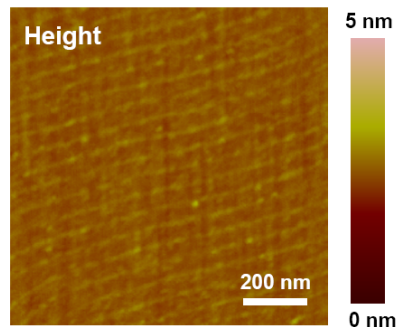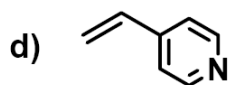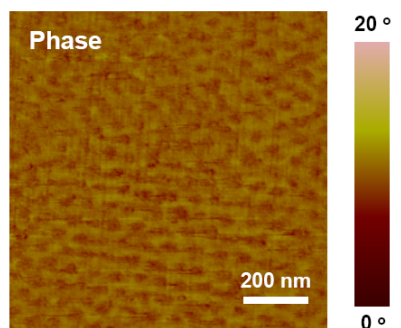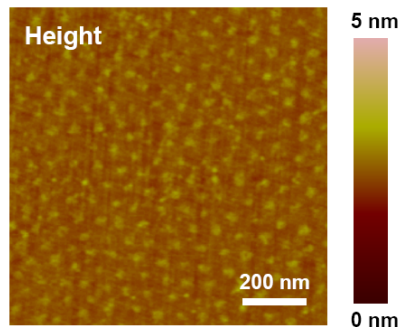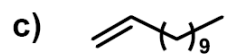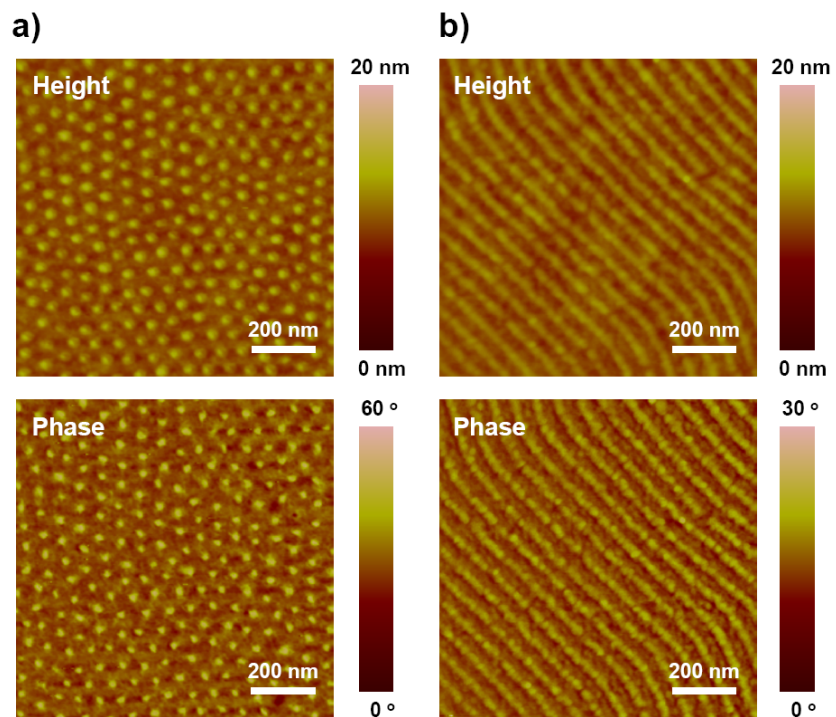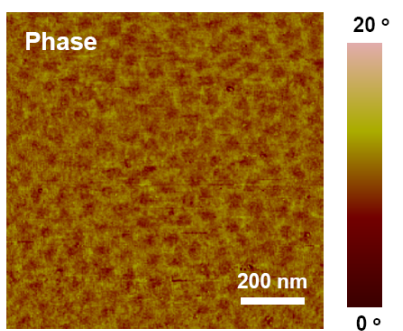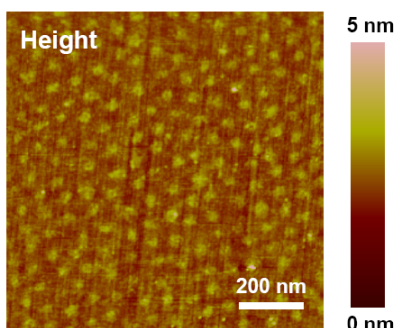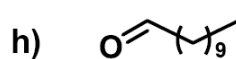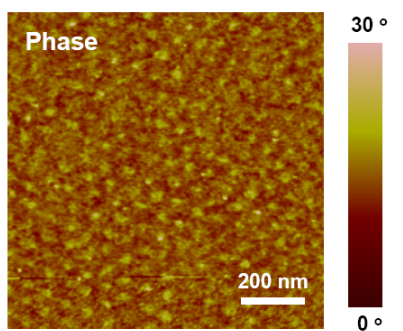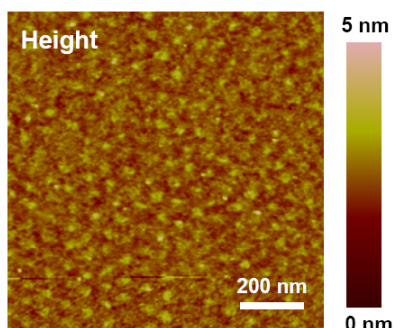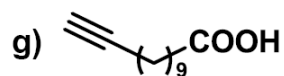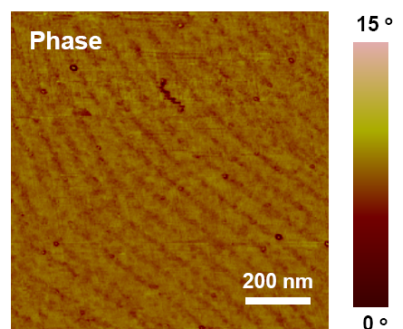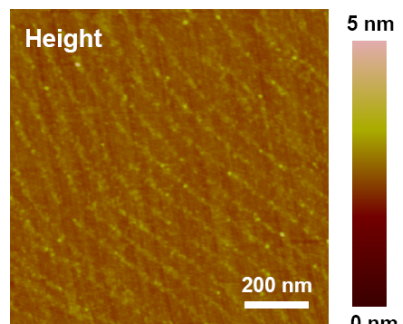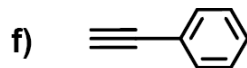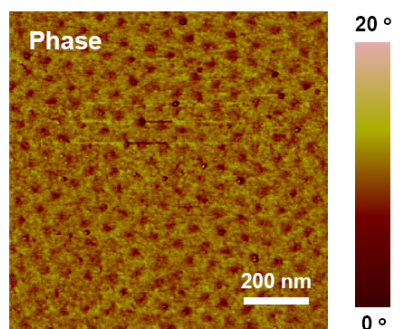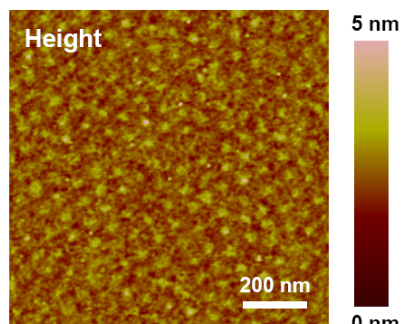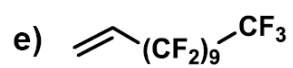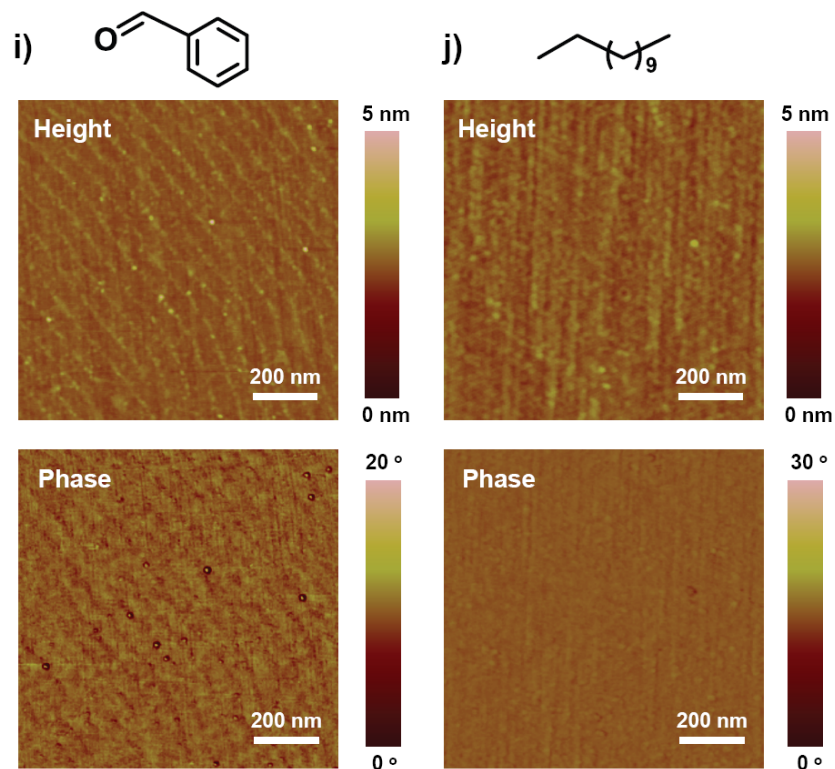
Phase
20 °
0 °
200 nm

Figure 3.15. AFM height and phase images of Pt catalytic stamps and H-terminated Si surfaces stamped with various molecular inks. (a) A pseudohexagonally patterned Pt catalytic stamp. (b) A linearly patterned Pt catalytic stamp. (c) Si(111)-H stamped with 1-dodecene. (d) Si(111)-H stamped with 4-vinylpyridine. (e) Si(100)-H_x stamped with 1H,1H,2H-perfluoro-1-decene. (f) Si(111)-H stamped with phenylacetylene. (g) Si(100)-H_x stamped with 10-undecynoic acid. (h) Si(111)-H stamped with undecanal. (i) Si(111)-H stamped with benzaldehyde. (j) Si(111)-H stamped with dodecane.

In contrast, when dodecane was used as an ink, pattern transfer did not take place, as confirmed by both the height and phase images (Figure 3.15j). This observation clearly indicates that inked molecules need to possess C-X multiple

bonds (X = C or O) to undergo hydrosilylation with surface H-Si groups. Further support for catalytic hydrosilylation-mediated pattern formation was gathered based upon the following observations: 1) when a SiO_x/Si surface was used in place of a H-terminated Si surface, no pattern was observed. Because of the lack of surface H-Si groups, alkene/alkyne/aldehyde molecules cannot link to the surface through hydrosilylation; 2) the Pt catalytic stamp could be reused multiple times without significant loss of the stamping quality (14 times, Figure 3.16); and 3) the catalytic nature of Pt nanostructures could be chemically deactivated. When a Pt catalytic stamp was immersed in a 1 mM ethanolic solution of 1-octadecanethiol for 24 h, followed by thorough rinsing with EtOH, no pattern was observed on the stamped surface due to the formation of a self-assembled monolayer on Pt,[26] which blocks contact between the Pt catalyst, the ink molecules, and the surface H-Si groups.
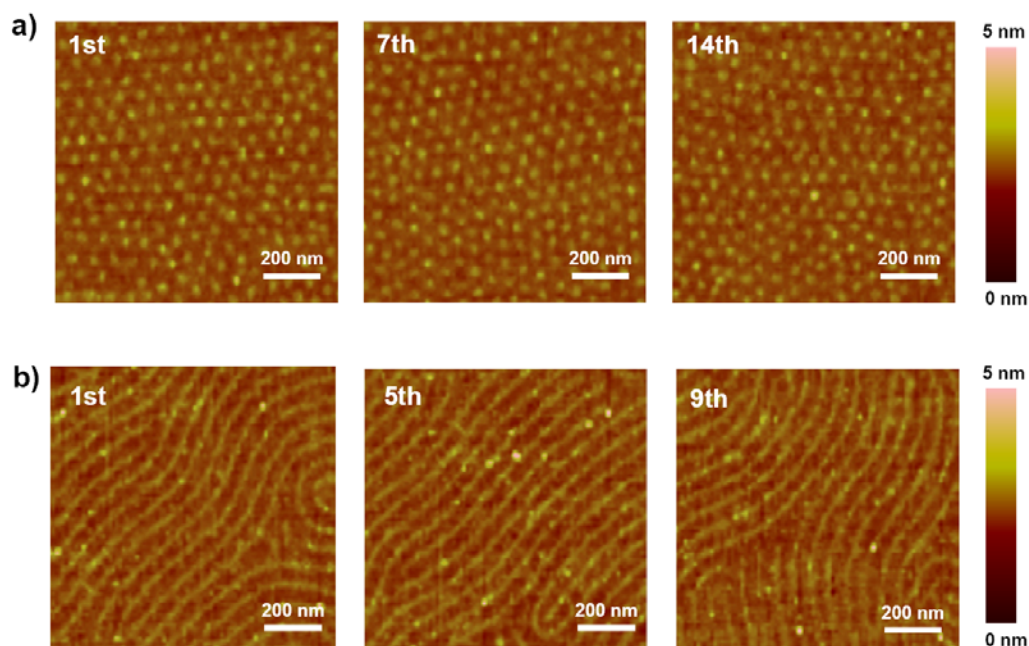
Figure 3.16. Reusability tests of Pt catalytic stamps with (a) a pseudohexagnal array (up to 14 times) and (b) a linear array (up to 9 times), using Si(111)-H as substrates and 1-dodecene as an ink.

XPS analysis also indicated the incorporation of molecules on the H-terminated Si surface via catalytic hydrosilylation. We used 1H,1H,2H-perfluoro-1-decene as a demonstrative molecule because of the high loading of fluorine atoms that are distinguishable from adventitious C(1s) and O(1s). In addition, fluorine has a greater sensitivity factor (1) than that of other hetero atoms (0.42 for nitrogen, for example),[27] which makes the detection easier even with the low coverage of the stamped molecules relative to the entire area of a surface. After stamping 1H,1H,2H-perfluoro-1-decene on an Si(111)-H surface, the sample was rinsed with CH_2Cl_2 to eliminate any physisorbed molecules on the surface and

immediately loaded on a sample holder, and then the XPS spectra were recorded (Figure 3.17). As shown in Figure 3.17a, an expected single peak appeared at 688 eV, a typical value for F(1s).[28] This peak was not observed with a control sample, where 1*H*,1*H*,2*H*-perfluoro-1-dodecene was stamped with a flat PDMS stamp having no imbedded Pt catalysts, indicating that the simple physisorption is not sufficient to produce this level of peak intensity. In Figure 3.17b, the Si(2p) peak found at 99.3 eV was attributed to bulk Si,[29] and no significant peaks from Si oxide (~103 eV)[29] and PDMS (~102 eV)[30] were detected. Furthermore, significant Pt leaching was not observed in the Pt (4f) spectrum (Figure 3.17c). Thus, all of these results point to a hydrosilylation-mediated pattern formation event, catalyzed by Pt nanostructures on PDMS.
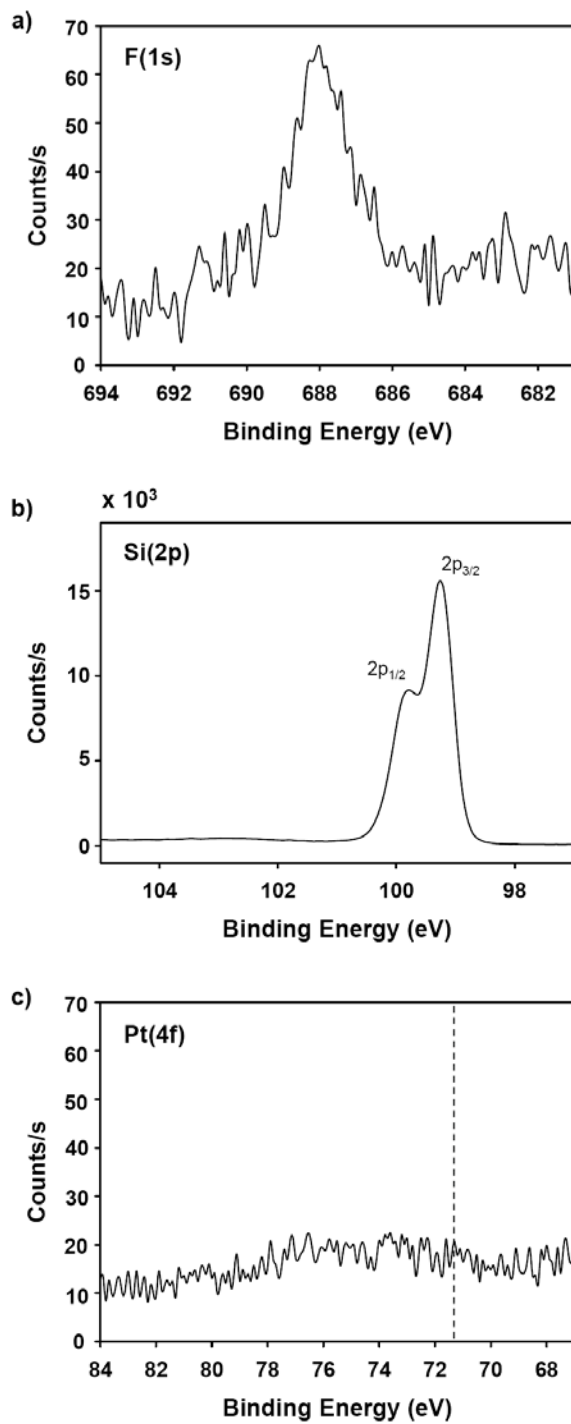
Figure 3.17. High resolution XPS spectra of an H-terminated Si(111) surface stamped with

1*H*,1*H*,2*H*-perfluoro-1-decene. (a) F(1s) region. (b) Si(2p) region. (c) Pt(4f) region. The

dashed line in (c) corresponds to metallic Pt (71.4 eV).

It should be noted that successful stamping is dependent upon a number of specific conditions. First, 1,4-dioxane was used as a diluent of ink molecules to avoid 1) PDMS swelling (significant catalytic stamp expansion was observed with hexane, toluene, or THF, for instance)[31] and 2) potentially competing reactions with hydrosilylation (such as alcoholysis of silanes when alcohols were used).[32] As for the concentration of molecular inks, 2-5 mM was found to be ideal for 1 min inking (Figure 3.18a), and higher or lower than this range resulted in a poor pattern formation. In particular, no pattern was obtained when a 15 mM solution of molecular ink was used (Figure 3.18b), probably due to the excess population of inked molecules on the catalytic stamp, inhibiting sufficient contact between Pt catalysts and H-Si groups on the surface. 20 min of stamping was enough to bring about catalysis regardless of the type of molecule, and longer times did not improve or affect the quality of patterning, based upon the AFM images (Figure 3.18c). Shorter times, however, often resulted in poor patterning (Figure 3.18d,e).
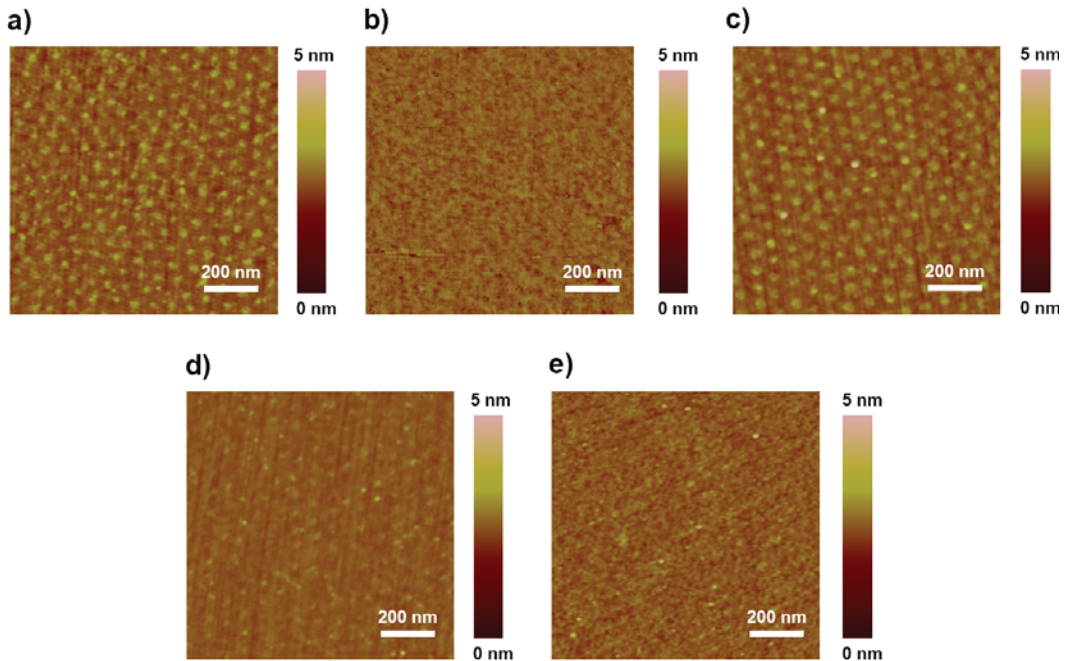
Figure 3.18. AFM height images of various control experiments. (a) A patterned Si(111)-H sample stamped for 20 min with 2 mM 1,4-dioxane solution of 1-dodecene. (b) Freshly etched Si(111)-H sample stamped for 20 min with 15 mM 1,4-dioxane solution of 4-vinylpyridine (hexagonal pattern expected). (c) A patterned Si(111)-H sample stamped for 30 min with 2 mM 1,4-dioxane solution of 1-dodecene. (d) A poorly patterned Si(111)-H sample stamped for 10 min with 5 mM 1,4-dioxane solution of 1-dodecene (hexagonal pattern expected). (b) A poorly patterned Si(100)-H_x sample stamped for 5 min with 5 mM 1,4-dioxane solution of phenylacetylene (linear pattern expected).

The stability of the patterns produced by catalytic stamping to a variety of organic and aqueous solvents and solutions was examined by AFM to give a sense of how robust the films are. First, all the patterns obtained with terminal alkene/alkyne/aldehyde molecules (shown in Figure 3.15) withstood immersion in

boiling mesitylene (165 $^{\circ}$C) for 3 h under Ar, indicating the strongly bonded covalent nature of these monolayers. Secondly, the treatment of patterned samples with a 1/1 (v/v) mixed solution of 49% HF (aq)/EtOH[18] had differing effects, depending upon the molecular precursors: 1) Alkene/alkyne-stamped samples maintain the original patterns after immersion in the solution for 30 s, due to the stability of the Si-C bond under these conditions. 2) When aldehyde-stamped samples were tested under the same conditions, however, the original patterns vanished because of the lability of the Si-O bonds in the presence of HF.[25b] Similar trends were observed with the treatment of a silicon etching solution. Figure 3.19a shows typical AFM height images of stamped Si(100)-H$_x$ surfaces followed by etching treatment for 30 s with 4 M KOH (aq) containing 15% 2-propanol.[33] In Figure 3.19a, lines produced through hydrosilylation of phenylacetylene were observed to act as a crude etch stop, with the AFM line profiles showing trench formation between the organic monolayer lines.[17] No original linear features were visible with a benzaldehyde-stamped sample, as shown in Figure 3.19b.
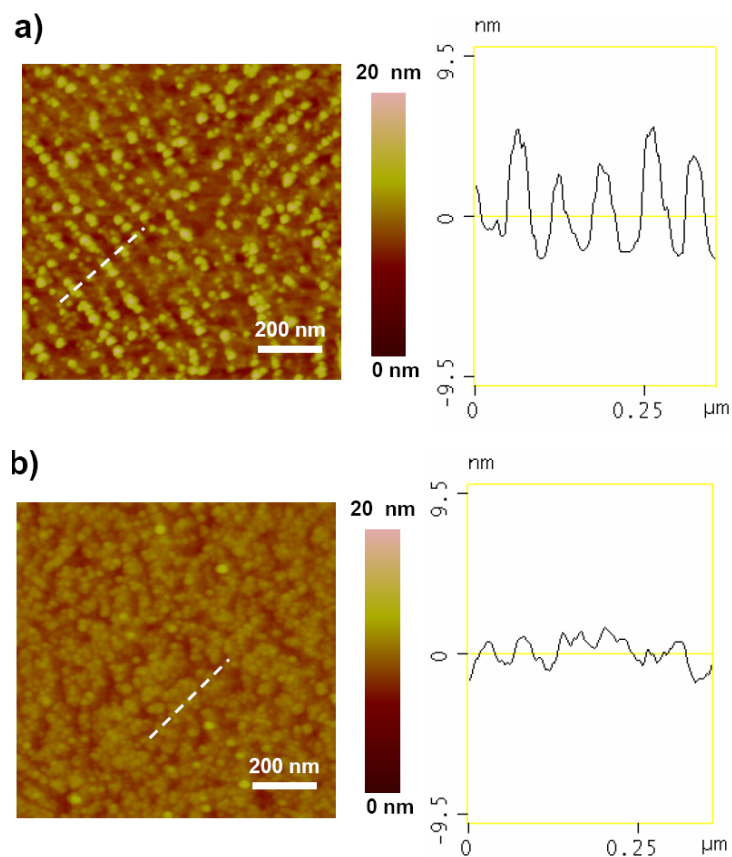
Figure 3.19. AFM height images and section analyses of H-terminated Si(100) surfaces stamped with (a) phenylacetylene and (b) benzaldehyde, followed by etching with 4 M KOH (aq) containing 15% 2-propanol for 30 s.

Finally, "inverted" catalytic stamp lithography was attempted on alkene-terminated surfaces using silanes as molecular inks. This inverted system, in principle, should also produce patterned surfaces via hydrosilylation mediated by the Pt catalytic stamp. An alkene-terminated surface was prepared through monolayer formation of octenyltrichlorosilane on an oxide capped-Si(100) substrate in toluene. This alkene-terminated SiO_x/Si(100) was stamped for 20

min, under ambient conditions, with a Pt catalytic stamp inked for 1 min with a 5 mM solution of phenylsilane in 1,4-dioxane (Figure 3.20). Interestingly, we observed no pattern formation with this system. Neither stamping for longer time (1 h) nor at elevated temperature (65 $^{\circ}$C) resulted in pattern formation.
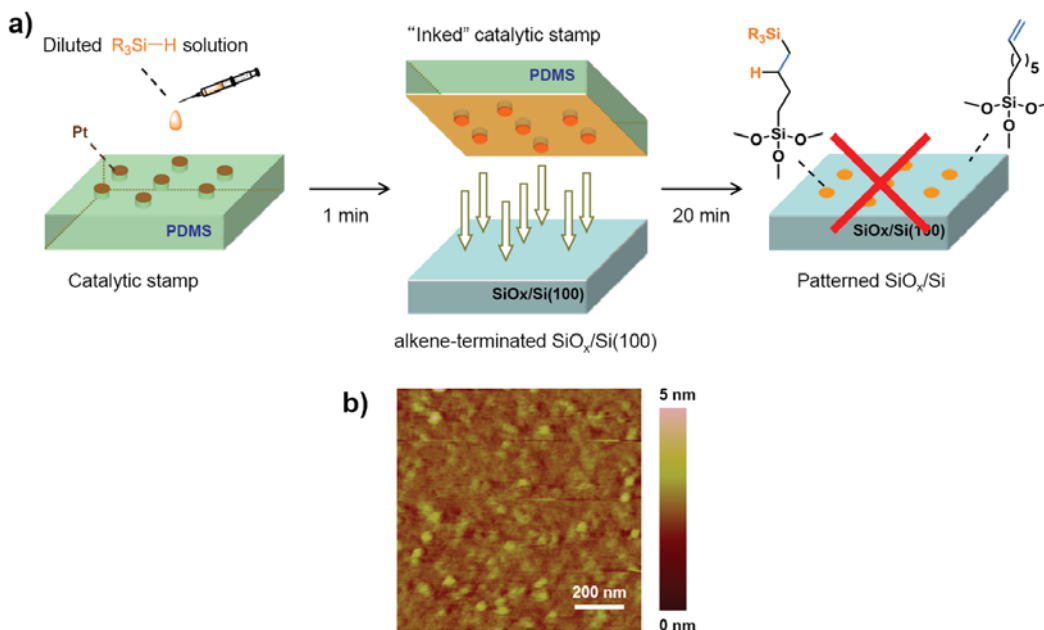
Figure 3.20. (a) Outline for catalytic stamp lithography on an alkene-terminated surface. A Pt catalytic stamp was inked with phenylsilane (5 mM in 1,4-dioxane) for 1 min and stamped on an alkene-terminated SiO$_x$/Si surface for 20 min. In this case, however, no pattern formation was observed, as shown in the resulting AFM height image (b).

A plausible explanation for this result might be dehydrogenative condensation of silanes in the presence of Pt catalyst.[34] What is clear is that the Pt catalytic stamp, after stamping, was covered by a significant amount of

unidentified materials as observed by AFM, possibly oligomerized/polymerized phenylsilane due to dehydrogenative coupling (Figure 3.21).
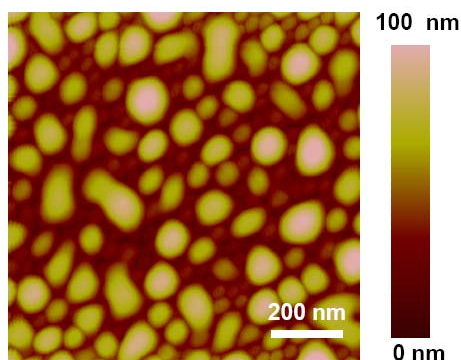
Figure 3.21. An AFM height image of a Pt catalytic stamp inked with phenylsilane (5 mM in 1,4-dioxane) for 1 min. Large unidentified "blobs" of material (possibly oligomerized/ polymerized phenylsilane) were observed.

A related reason could be catalyst poisoning by *in-situ* formation of di- and trihydride silane, as described in earlier reports.[24] Replacement of phenylsilane with less reactive monosilanes, such as dimethylphenylsilane or dimethyloctadecylsilane, again did not produce patterned surfaces. As with any catalytic reaction, the potential of competing reactions and catalyst poisoning or deactivation are always factors to consider, and thus it is necessary to carefully consider each combination of inks and surfaces to obtain successful patterning.

3.4. Conclusion

This chapter described a proof-of-concept demonstration of a stamp-based nanoscale patterning technique of organic monolayers, termed catalytic stamp lithography. Using hexagonally or linearly patterned Pd or Pt catalytic stamps, catalytic hydrosilylation were performed on H-terminated Si surfaces and attempted on alkene-terminated oxide-capped Si surfaces.

When alkenes/alkynes/aldehydes were used as molecular inks, covalently attached monolayers were patterned on H-terminated Si(111) and Si(100) surfaces. Since the reaction takes place exclusively underneath the patterned Pd or Pt nanostructures, the pattern formation is less susceptible to ink diffusion and stamp deformation, even at the sub-20 nm scale. A range of different molecular inks could be utilized to produce monolayer patterns of different chemical functionalities, and the stamps could be reused multiple times. The potential utility of resulting patterned surfaces was demonstrated through gold nanoparticle capture, and a series of chemical stability tests.

When silanes were used as molecular inks, on the other hand, no patterns were formed on alkene-terminated surfaces. Because competing reactions and catalyst deactivation can be inevitable in any metal-catalyzed reactions, rational designs for inks, surfaces, and stamping conditions are critical for the success of catalytic stamp lithography.

Note: In terms of the ultimate resolution limit of catalytic stamp lithography, sub-10 nm (or down to single molecular) patterning should be possible if catalytic stamps with such metallic nanostructures could be fabricated. However, because of tip convolution effects,[35] the actual feature sizes may not be accurately determined by AFM (Figure 3.22). With this respect, STM would be more useful to observe the accurate size of created features.[36]
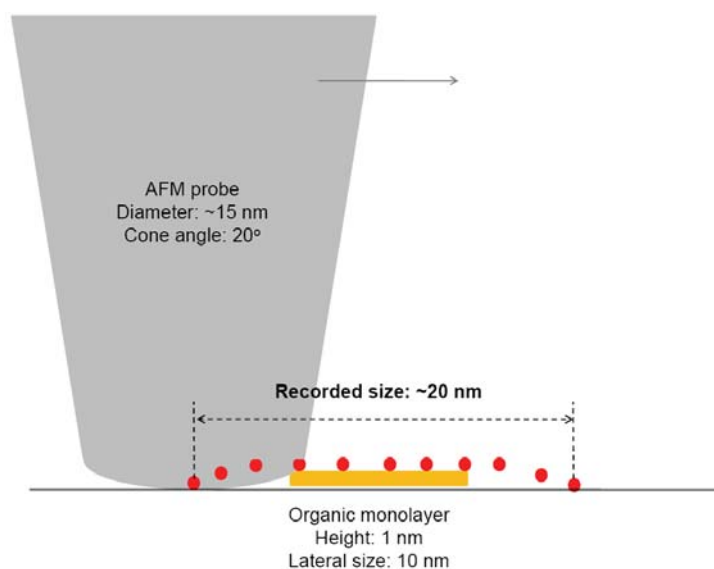
Figure 3.22. Schematic representation of an AFM tip convolution effect. For instance, when an organic monolayer domain with 1 nm height and 10 nm lateral size is scanned with an AFM probe with ~15 nm tip diameter and 20° cone angle, the image is in fact convoluted, leading to an observed lateral size of ~20 nm.

3.5. *Experimental Section*

Generalities.

Unless otherwise noted, all the experiments were performed under ambient conditions. Teflon beakers and tweezers were used exclusively during the cleaning of the Si wafers. Si(111) (p-type, B-doped, ρ = 1-10 Ω-cm, thickness = 600-650 μm) and Si(100) (p-type, B-doped, ρ = 0.01-0.02 Ω-cm, thickness = 600-650 μm) wafers were purchased from MEMC Electronic Materials, Inc. Water was obtained from a Millipore system (resistivity = 18.2 MΩ). Aqueous HCl (36.5-38%, BAKER ANALYZED ACS Reagent), NH$_4$OH (29%, Finyte), H$_2$O$_2$ (30%, CMOS), HF (49%, CMOS), and NH$_4$F (40%, CMOS) were purchased from J. T. Baker. HAuCl$_4$·xH$_2$O (99.999%), tetraoctylammonium bromide (98%), sodium borohydride, 1H,1H,2H-perfluoro-1-decene (99%), 10-undecynoic acid (95%), undecanal (97%), benzaldehyde (>98.0%, purum), phenylsilane (97%), dimethylphenylsilane (>98%), dimethtyloctadecylsilane (97%), CH$_2$Cl$_2$ (>99.9%, CHROMASOLV®, for HPLC), toluene (>99.9%, CHROMASOLV®, for HPLC), and o-xylene (98%, CHROMASOLV® Plus, for HPLC) were purchased from Sigma-Aldrich. Anhydrous toluene was obtained from a solvent purification system (Innovative Technologies, Inc.). Optima grade methanol and 2-propanol were purchased from Fisher. All reagents listed above were stored under a laboratory atmosphere and used as-received. 1,4-Dioxane (99%, Caledon Laboratories Ltd.), 1-octadecyne (98%, GFS Chemicals), 5-hexyn-1-ol (96%, Sigma-Aldrich), 1,7-octadiene (98%, Sigma-Aldrich), 1-

dodecene (95%, Sigma-Aldrich), octenyltrichlorosilane (96%, mixture of isomers, Sigma-Aldrich), phenylacetylene (96%, Sigma-Aldrich), 4-vinylpyridine (95%, Sigma-Aldrich), and 1-octadecanethiol (98%, Sigma-Aldrich) were purified according to the standard methods[37] and stored in a Ar-filled glove box until use.

Silicon Cleaning Procedures.

      See Chapter 2.

Preparation of H-Terminated Si(111) and Si(100).

      RCA-cleaned Si(111) or Si(100) samples were immersed in degassed 40% NH_4F (aq) for Si(111), or 1% HF (aq) for Si(100) for 5 min. The hydride-terminated surfaces were immediately dipped into water for 10 s and dried with a stream of nitrogen gas.

Patterning of H-Terminated Si Surface via Hydrosilylation.

      Several droplets of a 5 mM solution of alkene/alkyne/aldehyde in 1,4-dioxane was placed on the entire surface of a Pd or Pt catalytic stamp (typical size = 1 mm × 1 mm) for 1 min, and the solution was gently blown off with a nitrogen stream. The inked stamp was applied to a freshly prepared H-terminated Si(111) or Si(100) sample and pressed lightly (until a slight resistance was felt) for 20 min using a wrench-based homemade stamping apparatus (Figure 3.23). After the stamping, PDMS was quickly released from the Si sample, and the resulting Si

sample was rinsed 5 times with dichloromethane using a disposable pipette and immediately submitted to further experiments/analyses.
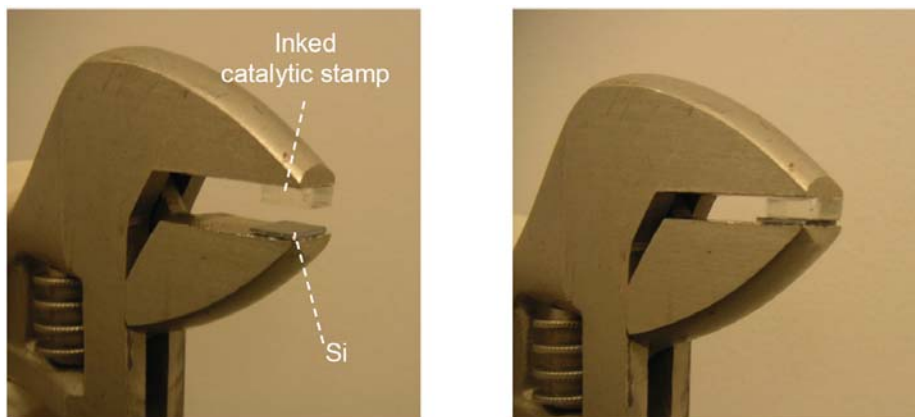
Figure 3.23. Photographs of a wrench-based homemade stamping apparatus. An inked catalytic stamp was applied on a H-terminated Si sample until a slight resistance was felt by slowly rotating the screw of the wrench.

Deactivation of Catalytic Stamps.

A Pt catalytic stamp was immersed in a 1 mM ethanolic solution of 1-octadecanethiol for 24 h to form a self-assembled monolayer on the Pt nanostructures. The resulting stamp was then rinsed thoroughly with ethanol, and the washed stamp was immediately used for the lithographic experiment described above.

Etching of Stamped Si Substrates.

Stamped Si substrates were normally rinsed with dichloromethane (a few times), and then etched by either 40% NH_4F (aq, degassed), 1% HF (aq), or 4M KOH (aq, containing 15% 2-propanol) at room temperature for a given time (30 s-5 min). After etching, the samples were dipped into water for 10 seconds and dried with a stream of nitrogen.

Synthesis Au Nanoparticles.[22]

7.5 mL of a 30 mM $HAuCl_4$ (aq) and 20 mL of a 50 mM toluene solution of TOAB were mixed under vigorous stirring. After 2 h, the color of the toluene phase turned deep orange, indicating the quantitative transfer of $HAuCl_4$ into toluene phase. Subsequently, 6.3 mL of a freshly prepared 0.5 M aqueous solution of $NaBH_4$ was added into the mixture. After 2 h of an additional stirring, the ruby-colored toluene phase was separated, washed with 0.1 M H_2SO_4 (once), 1 M Na_2CO_3 (aq) (twice), and water (3 times), and dried over anhydrous $MgSO_4$. The resulting solution could be kept in a refrigerator for a few weeks. When used, the stock solution was diluted with toluene (stock solution/toluene = 1/5) to afford a gold content ~250 mg/L.

Selective Assembly of Au nanoparticles on a Patterned Si Substrate.

An H-terminated Si(100) sample stamped with 1,7-octadiene was briefly (30 s) etched by 4 M KOH (aq, containing 15% 2-propanol) and rinsed with a

copious amount of water. The vinyl/SiH-patterned sample was stored overnight in O_2-saturated water at room temperature to oxidize and passivate the exposed H-terminated Si areas. This vinyl/SiO_x-patterned sample was then placed into a 5 mL round-bottom flask with 0.1 mL of neat 1,9-nonanedithiol in a N_2-filled glove box. The sample was illuminated by UV light (a UVP Pen Ray Lamp, Model 11SC-1, 4.1 mW/cm^2 at 2 cm) for 30 min at room temperature to facilitate the thiol-ene reaction on the vinyl groups, and then the sample was washed for 5 min in CH_2Cl_2 using a ultrasonic bath. The as-prepared thiol/SiO_x-patterned sample was then immersed overnight in a toluene solution of ~5 nm tetraoctylammonium bromide-capped Au NPs at room temperature to assemble the Au NPs selectively on the thiol groups, followed by thorough rinsing with toluene.

Preparation of Alkene-Terminated Siloxane Monolayer on SiO_x/Si(100).

An RCA-cleaned Si(100) sample was immersed in 0.5% (v/v) toluene solution of octenyltrichlorosilane for 24 h. The surface of an octenyltrichlorosilane-treated sample was gently swabbed with a toluene-soaked cotton swab to eliminate polymerized siloxane residues, and then washed in toluene using an ultasonication bath for 10 min and rinsed with ethanol and water prior to use.

Attempted Patterning on Alkene-Terminated Surfaces.

The procedure was similar to the patterning on H-terminated Si surfaces: a silane and an alkene-terminated surface were used in place of an alkene/alkyne/aldehyde and an H-terminated surface, respectively. For the stamping at an elevated temperature (65 ^{o}C), the inked Pt catalytic stamp was applied on an alkene-terminated surface at room temperature, and the whole system was immediately placed in the preheated oven for 20 min.

Surface Characterization.

The samples obtained in this study were characterized by atomic force microscopy (AFM), scanning electron microscopy (SEM), and X-ray photoelectron spectroscopy (XPS). AFM images were taken with a Digital Instruments/Vecco Nanoscope IV (tapping mode) using commercially available Si cantilevers (PPP-NCHR probe, purchased from Nanosensors, http://www.nanosensors.com/PPP-NCHR.htm) under ambient conditions. Prior to the use, AFM probes were treated with oxygen plasma (O_2 pressure: 0.2 Torr, time: 30 s) to make the surfaces hydrophilic. This treatment was important to obtain consistent results especially for phase imaging. SEM was performed with Hitachi S-4800 FE-SEM using an electron energy of 10k eV under high vacuum conditions ($<10^{-8}$ Torr). XPS was taken on a Kratos Axis 165 X-ray photoelectron spectrometer using a monochromatic Al Kα with a photon energy of 1486.6eV under high vacuum conditions ($<10^{-8}$ Torr), and ejected X-rays were

measured at 0° from the surface normal. The XPS signals were calibrated on the

basis of the C(1s) (285.0 eV).

3.6. References

1. (a) Sze, S. M. *Semiconductor Devices: Physics and Technology,* 2nd ed.; John Wiley & Sons: New York, 2002. (b) Wada, K. *Proc. SPIE* **2007**, *6782*, 678202/1-678202/8. (c) Mueller, A.; Ghosh, M.; Sonnenschein, R.; Woditsch, P. *Mater. Sci. Eng., B* **2006**, *134*, 257-262.

2. (a) Higashi, G. S.; Chabal, Y. J.; Trucks, G. W.; Raghavachari, K. *Appl. Phys. Lett.* **1990**, *56*, 656-658. (b) Higashi, G. S.; Becker, R. S.; Chabal, Y. J.; Becker, A. J. *Appl. Phys. Lett.* **1991**, *58*, 1656-1658.

3. Brook, M. A. *Silicon in Organic, Organometallic, and Polymer Chemistry*; John Wiley & Sons: New York, 2000; 401-421.

4. (a) Buriak, J. M. *Chem. Rev.* **2002**, *102*, 1271-1308. (b) Shirahata, N.; Hozumi, A.; Yonezawa, T. *Chem. Rec.* **2005**, *5*, 145-159. (c) Hamers, R. J. *Annu. Rev. Anal. Chem.* **2008**, *1*, 707-736.

5. Robert, H. *Properties of Crystalline Silicon*; Institution of Engineering and Technology: London, 1999.

6. Ubara, H.; Imura, T.; Hiraki, A. *Solid State Commun.* **1984**, *50*, 673-5.

7. Marciniec, B. *Silicon Chem.* **2002**, *1*, 155-175.

8. Hayashi, T. In *Comprehensive Asymmetric Catalysis I-III*; Jacobsen, E. N., Pfaltz, A., Yamamoto, H. Ed.; Springer: New York, 1999; 319-333.

9. Maciejewski, H.; Wawrzynczak, A.; Dutkiewicz, M.; Fiedorow, R. *J. Mol. Catal. A-Chemical* **2006**, *257*, 141-148.

10. Chalk, A. J.; Harrod, J. F. *J. Am. Chem. Soc*. **1965**, *87*, 16-21.

11. (a) Lewis, L. N.; Lewis, N. *J. Am. Chem. Soc.* **1986**, *108*, 7228-7231. (b) Lewis, L. N. *J. Am. Chem. Soc.* **1990**, *112*, 5998-6004. (c) Tamura, M.; Fujihara, H. *J. Am. Chem. Soc.* **2003**, *125*, 15742-15743.

12. Asao, N.; Sudo, T.; Yamamoto, Y. *J. Org. Chem.* **1996**, *61*, 7654-7655.

13. (a) Linford, M. R.; Chidsey, C. E. D. *J. Am. Chem. Soc.* **1993**, *115*, 12631-12632. (b) Sieval, A. B.; Demirel, A. L.; Nissink, J. W. M.; Linford, M. R.; van der Maas, J. H.; de Jeu, W. H.; Zuilhof, H.; Sudhölter, E. J. R. *Langmuir* **1998**, *14*, 1759-1768. (c) Cicero, R. L.; Linford, M. R.; Chidsey, C. E. D. *Langmuir* **2000**, *16*, 5688-5695.

14. a) Zazzera, L. A.; Evans, J. F.; Deruelle, M.; Tirrell, M.; Kessel, C. R.; Mckeown, P. *J. Electrochem. Soc.* **1997**, *144*, 2184. b) Holland, J. M.; Stewart, M. P.; Allen, M. J.; Buriak, J. M. *J. Solid State Chem.* **1999**, *147*, 251. (c) Langner, A.; Panarello, A.; Rivillon, S.; Vassylyev, O.; Khinast, J. G.; Chabal, Y. J. *J. Am. Chem. Soc.* **2005**, *127*, 12798-12799.

15. Boukherroub, R.; Morin, S.; Bensebaa, F.; Wayner, D. D. M. *Langmuir* **1999**, *15*, 3831.

16. Blackledge, C.; Engebretson, D. A.; McDonald, J. D. *Langmuir* **2000**, *16*, 8317.

17. Mizuno, H.; Buriak, J. M. *J. Am. Chem. Soc.* **2008**, *130*, 17656-17657.

18. Hurley, P. T.; Ribbe, A. E.; Buriak, J. M. *J. Am. Chem. Soc.* **2003**, *125*, 11334-11339.

19. Glasmaestar, K.; Gold, J.; Andersson, A.-S.; Sutherland, D. S.; Kasemo, B. *Langmuir* **2003**, *19*, 5475-5483.

20. Gergel-Hackett, N.; Zangmeister, C. D.; Hacker, C. A.; Richter, L. J.; Richter, C. A. *J. Am. Chem. Soc.* **2008**, *130*, 4259-4261.

21. a) Hoyle, C. E.; Lee, T. Y.; Roper, T. *J. Polym. Sci. Part A: Polym. Chem.* **2004**, *42*, 5301-5338. b) Besson, E.; Gue, A.-M.; Sudor, J.; Korri-Youssoufi, H.; Jaffrezic, N.; Tardy, J. *Langmuir* **2006**, 22, 8346-8352.

22. Brust, M.; Bethell, D.; Kiely, C. J.; Schiffrin, D. J. *Langmuir* **1998**, *14*, 5425-5429.

23. Mizuno, H.; Buriak, J. M. *ACS Appl. Mater. Interfaces* **2009**, *1*, 2711-2720.

24. Lewis, L. N.; Uriarte, R. J. *Organometallics* **1990**, *9*, 621-625.

25. (a) Effenberger, F.; Gotz, G.; Bidlingmaier, B.; Wezstein, M. *Angew. Chem., Int. Ed.* **1998**, *37*, 2462-2464. (b) Boukherroub, R.; Morin, S.; Sharpe, P.; Wayner, D. D. M.; Allongue, P. *Langmuir* **2000**, *16*, 7429-7434. (c) Kong, Y. K.; Kim, J.; Choi, S.; Choi, S.-B. *Tetrahedron Lett.* **2007**, *48*, 2033-2036.

26. (a) Li, Z.; Chang, S.-C.; Williams, R. S. *Langmuir* **2003**, *19*, 6744-6749. (b) Petrovykh, D. Y.; Kimura-Suda, H.; Opdahl, A.; Richter, L. J.; Tarlov, M. J.; Whitman, L. J. *Langmuir* **2006**, *22*, 2578-2587.

27. *Practical Surface Analysis, Volume 1, Auger and X-ray Photoelectron Spectroscopy*, 2nd ed.; Briggs, D.; Seah, M. P. Eds.; John Wiley and Sons: Chichester, U.K., 1990.

28. Cai, W.; Lin, Z.; Strother, T.; Smith, L. M.; Hamers, R. J. *J. Phys. Chem. B* **2002**, *106*, 2656-2664.

29. Wagner, C. D.; Naumkin, A. V.; Kraut-Vass, A.; Allison, J. W.; Powell, C. J.; Rumble, J. R., NIST X-ray Photoelectron Spectroscopy Database. In *NIST Standard Reference Database 20, Version 3.5*, National Institute of Standards and Technology, Gaithersburg: 2007. http://srdata.nist.gov/xps/

30. Louette, P.; Bodino, F.; Pireaux, J.-J. *Surf. Sci. Spectra* **2006**, *12*, 38-43.

31. Lee, J. N.; Park, C.; Whitesides, G. M. *Anal. Chem.* **2003**, *75*, 6544-6554.

32. (a) Lukevics, E.; Dzintara, M. *J. Organomet. Chem.* **1985**, *295*, 265-315. (b) Caseri, W.; Pregosin, P. S. *Organometallics* **1988**, *7*, 1373-1380. (c) Hilal, H. S.; Rabah, A.; Khatib, I. S.; Schreiner, A. F. *J. Mol. Catal.* **1990**, *61*, 1-17.

33. Finnie, K. R.; Haasch, R.; Nuzzo, R. G. *Langmuir* **2000**, *16*, 6968-6976.

34. Tanaka, M.; Kobayashi, T.; Hayashi, T.; Sakakura, T. *Appl. Organomet. Chem.* **1988**, *2*, 91-92.

35. Hulteen, J. C.; Treichel, D. A.; Smith, M. T.; Duval, M. L.; Jensen, T. R.; Van Duyne, R. P. *J. Phys. Chem. B* **1999**, *103*, 3854-3863.

36. Hamers, R. J. *Annu. Rev. Anal. Chem.* **2008**, *1*, 707-736.

37.   *Purification of Laboratory Chemicals*, 5th ed., Armarego, W. L. F.; Chai,

C. L. L. Eds.; Elsevier: Amsterdam, 2003.

Chapter 4
Catalytic Stamp Lithography 2: Hydrogenation and the Heck Reaction

4.1. Introduction

In order to generalize the concept of catalytic stamp lithography, reactions other than hydrosilylation needed to be demonstrated. This chapter deals with two additional reactions, hydrogenation and the Heck reaction.

In the first part of this chapter, hydrogenation-based catalytic stamp lithography, performed on azide-terminated surfaces, is described. Using a Pd catalytic stamp shown in Chapter 2, surface azide groups were reduced to amino groups in a site-selective manner in the presence of a reducing agent (mainly hydrogen). Two stamping procedures (printing and imprinting) were examined to obtain successful patterning conditions. Although the reaction here is a simple monofunctional group transformation (azide to amine) and limited in terms of resulting surface properties compared to the aforementioned hydrosilylation (Chapter 3), the concept of catalytic stamp lithography would be further supported through this part.

The latter part of this chapter focuses on the Heck reaction-based catalytic stamp lithography. Two types of surface precursors, alkene- and bromophenyl-terminated surfaces, were prepared, and nanoscale patterning through Pd-catalyzed carbon-carbon bond formations was carried out on both surfaces. A

variety of inks were utilized to achieve spectroscopic and chemical evidence to elucidate Heck reaction-mediated pattern formation. A limitation in stamp reusability is also addressed in this part.

4.2. Review of Related Topics

Siloxane Monolayers on Silicon Oxide

Oxide surfaces, including the native oxide layer on single crystalline silicon substrates, spontaneously form well-defined self-assembled monolayers (SAMs) with silanes (RSiX$_3$, where X = Cl, OMe, OEt, etc.).[1,2] The driving force for the assembly is the *in situ* formation of the polysiloxane (-Si-O-Si-) network, connected to surface silanol (Si-OH) groups.[2a] Figure 4.1 outlines the mechanism of the SAM formation. In general, the SiO$_x$ surface is first activated by cleaning with a strong acid/peroxide[3] or UV-ozone treatment[4] to maximize the number of silanol groups on the surface (~10^{15} OH groups/cm^2).[2b] The activated surface is then treated with silane molecules either in solution or vapor phase. Because of the absorbed water on the hydrophilic silanol-terminated interface, silane groups (RSiX$_3$) are first hydrolyzed to yield hydroxysilyl groups [RSi(OH)$_3$].[4] Condensation between surface silanols and hydrolyzed silanes results in the formation of an organosiloxane monolayer.
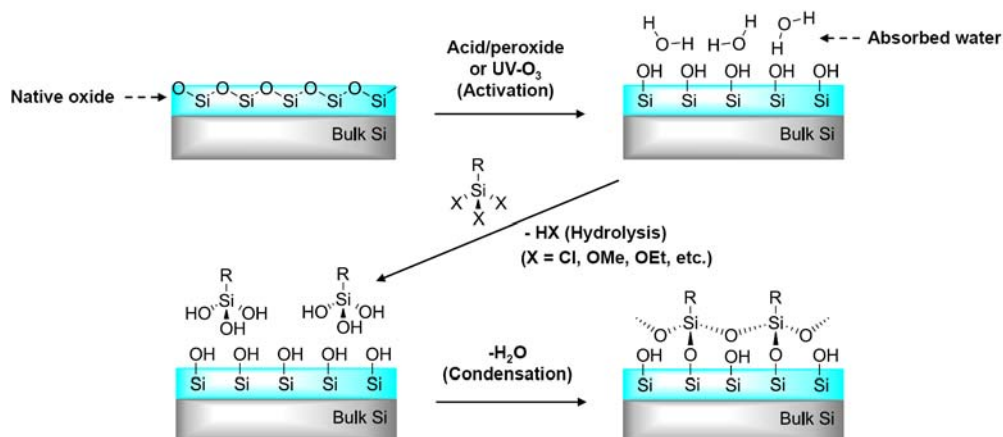
Figure 4.1. Schematic outline for the silane SAM formation on SiO$_x$/Si. The native oxide layer on bulk Si is usually hydroxyl-terminated either by acid/peroxide or UV-ozone treatment. When this activated surface is treated with a silane, the silane is first hydrolyzed by the surface-absorbed water molecules. The hydrolyzed silanes can form siloxane bonds with surface silanol groups and neighboring silanes, yielding an organosiloxane monolayer.

Desired surface properties can usually be achieved by using ω–functionalized alkylsilanes. For instance, an alkene-terminated surface, used for the surface Heck reaction, is directly generated via the solution phase assembly of ω–alkene silanes, such as 7-octenyltrichlorosilane.[5] Because some of the useful functional groups are not compatible with the reactive SiX$_3$ groups, post-modification routes have also been developed. For example, bromine-terminated SAMs can be transformed into a number of unique functional groups through nucleophilic substitution.[6] The azide-terminated surface, used for hydrogenation-

based catalytic stamp lithography in this chapter, is prepared through this approach.[6]

Reduction of Azides

Reduction of azides to afford amines is a synthetically well-established process in the molecular system.[7] Because azides can be readily prepared from halides and alcohols with excellent regio- and stereoselectivity,[7b] subsequent reduction leads to the controlled formation of amine compounds. A number of reducing systems (agents) have been reported for this reaction, such as $LiAlH_4$,[8] $NaBH_4$,[9] and catalytic hydrogenation.[10] Although the system of choice often depends on the other groups present in the target molecule, catalytic hydrogenation is most commonly used if simple reduction of azide groups is required. Transition metals, such as Pt, Pd, and Ni, are the standard catalysts used for a heterogeneous approach (which facilitates the easy work-up) (Figure 4.2).[7]

$$R-\overset{\oplus}{N}=N=\overset{\ominus}{N} \quad + \quad H-H \quad \xrightarrow{\text{Transition metal catalyst (Pt, Pd, Ni, etc.)}} \quad R-N\overset{H}{\underset{H}{\diagdown}} \quad + \quad N\equiv N$$
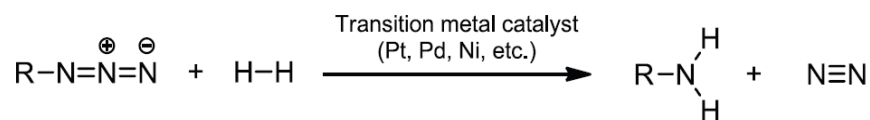
Figure 4.2. Chemical equation for transition metal-catalyzed hydrogenation of azide.

Surface azide groups can be reduced in similar ways to molecular systems,[6,11] which results in the generation of useful amine-terminated surfaces. In order to achieve complete reduction of all the surface azide groups, use of

homogeneous systems provides a convenient route. Balachander *et al.* have performed LiAlH$_4$-based reduction of an azide-terminated siloxane SAM formed on a glass substrate.[6] In contrast, heterogeneous systems are suitable to induce site-selective reactions (i.e., patterning). Catalytic hydrogenation has been utilized to create patterned amine/azide surfaces as described below.[11]

Patterning of Azide-Terminated Surfaces

Using catalytically activated AFM probes, hydrogenation-mediated patterning of azide-terminated surfaces has been demonstrated. One example has been already described in Chapter 1, where a Pt-coated AFM probe induced site-specific hydrogenation over surface azide groups in hydrogen-saturated 2-propanol (see Figure 1.12).[11a] Another example has demonstrated catalytic transfer hydrogenation using a Pd-coated AFM tip as a catalytic probe, and sodium formate as a hydrogen source (Figure 4.3a). The resulting amine pattern (micron scale) was labeled with a fluorescent dye (TAMRA) and visualized by confocal microscopy (Figure 4.3b).[11b]
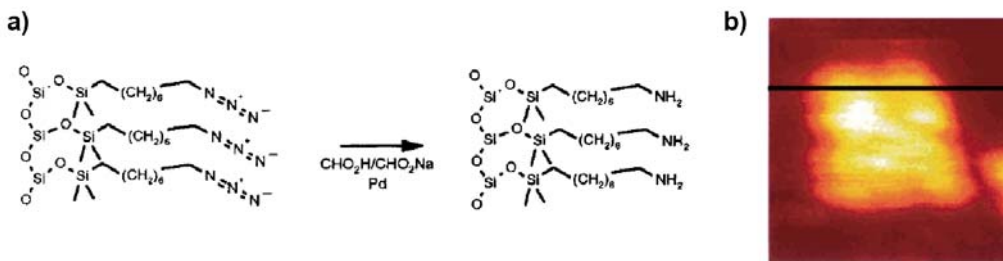
Figure 4.3. (a) Pd-catalyzed transfer hydrogenation of azide groups on a surface. (b) Confocal microscopy image (3 μm × 3 μm) of a TAMRA labeled-amine/azide patterned surface created via the reaction (a). Reprinted with permission from ref. 11b. Copyright © 2000 American Chemical Society.

The Heck Reaction

The palladium-catalyzed carbon-carbon bond formation between an aryl halide and an alkene in the presence of base is referred to as the Heck reaction (Figure 4.4a).[12] It is industrially used as a key reaction to synthesize natural products and pharmaceuticals.[12d] Figure 4.4b shows the typical catalytic mechanism for the Heck reaction.[12c] As usually seen in other palladium-catalyzed reactions, the cycle starts with the oxidative addition of an aryl halide to Pd^0 (1). The next step is the formation of Pd π-complex with an alkene (2), followed by *syn* insertion of the coordinated double bond into the Pd-C bond (3,4). After bond rotation to place the β-hydride *syn* to the Pd (5,6), reductive elimination proceeds to yield a coupling product with excellent *trans* selectivity (7,8). Finally, Pd^0 is regenerated through the reaction with base (9). A variety of conditions, including

homogeneous/heterogeneous,[13] and ligand-[14], base-[15], and solvent-free[16] systems, have been developed for the Heck reaction.
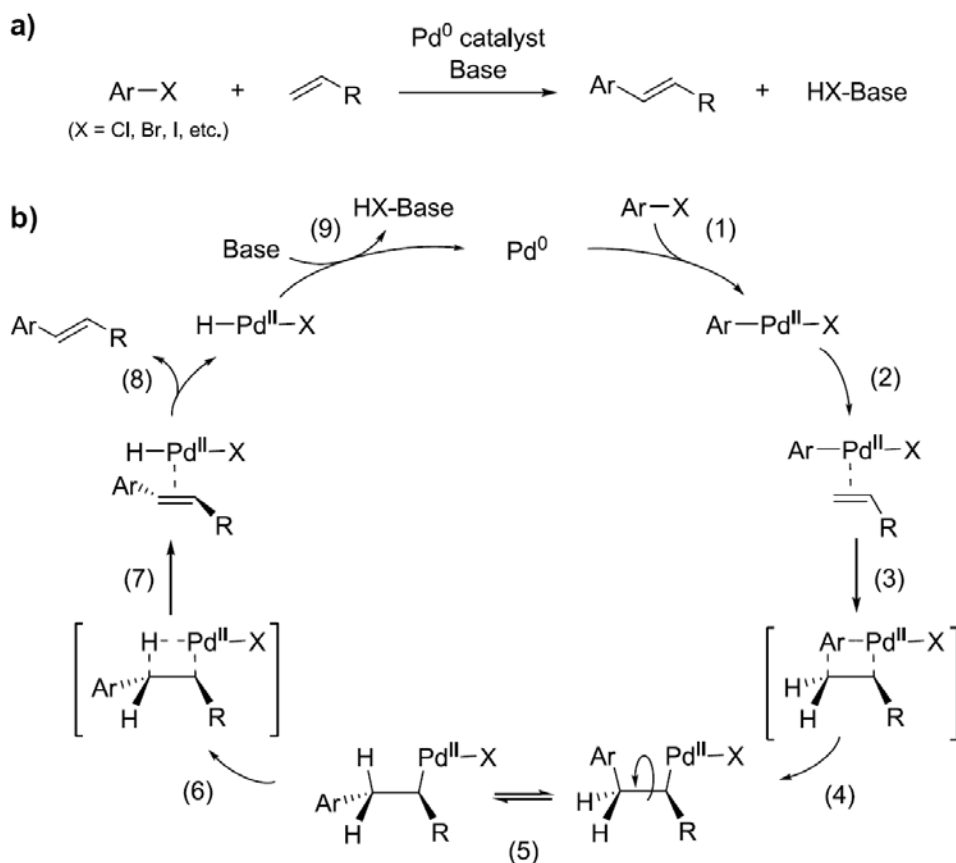
Figure 4.4. (a) Chemical equation for the Heck reaction. (b) Reaction mechanism for the Heck reaction. (1) Oxidative addition. (2) Alkene coordination. (3,4) *Syn*-insertion. (5) Bond rotation. (6,7,8) Reductive (β-hydride) elimination. (9) Pd^0 regeneration.

Surface Heck reactions have been reported by several groups.[17] For example, Cai and co-workers performed the reaction between 4-fluorostyrene and a bromophenyl-terminated thiolate SAM on gold using a Pd-dibenzylideneacetone

(dba) complex as a homogeneous catalyst, and a yield of 60-70% was estimated by XPS.[17b] Lewis and co-workers also demonstrated the Heck reaction on an oxide-free silicon surface, terminated with alkene groups.[17c] Using the same Pd(dba)$_2$ catalyst, 1-iodo-4-trifluoromethylbenzene was linked on the surface in this case.

Heck Reaction-Mediated Patterning of Organic Monolayers

Alkene-terminated SAMs on gold substrates have been utilized as a platform for Heck reaction-based patterning.[18] A silicon nitride AFM cantilever was modified with polyvinylpyrrolidone (PVP)-stabilized palladium nanoparticles and utilized as a catalytic probe. 4-Iodobenzoic acid was site-selectively grafted with features down to 15 nm, as confirmed by AFM friction imaging (Figure 4.5).
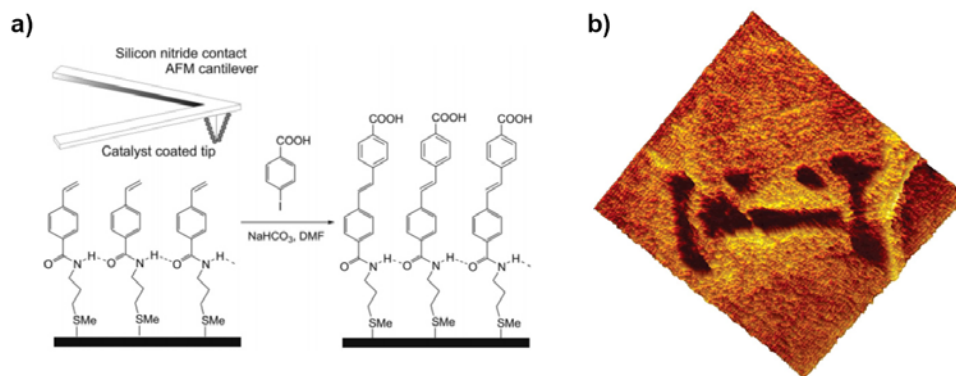
Figure 4.5. (a) Schematic of a PVP-stabilized Pd nanoparticle-coated AFM probe and the use of it for the Heck reaction between alkene (styrene)-terminated surface and 4-iodobenzoic acid. (b) AFM friction image of a patterned surface via the process (a). Each line is ~25 nm wide. Reprinted with permission from ref. 18. Copyright © 2006 American Chemical Society.

4.3. Results and Discussion 1: Hydrogenation of Azide

Azide-Terminated Surface Fabrication

In order to demonstrate nanopatterned hydrogenation with a Pd catalytic stamp, azide-terminated surfaces were required. An azide-terminated surface on a SiO_x substrate is generally fabricated in two steps: a bromine-terminated siloxane monolayer was first produced on a native oxide-capped silicon substrate, and then the terminal bromines were replaced by azide groups via nucleophilic substitution.[6]
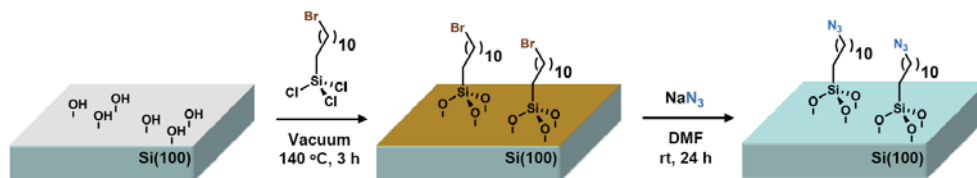
Figure 4.6. Outline for the fabrication of an azide-terminated siloxane monolayer on a native oxide-capped Si(100) surface. An activated oxide surface was treated with vaporized 11-bromoundecyltrichlorosilane under vacuum and high temperature (140 °C). After the formation of a corresponding bromine-terminated siloxane monolayer, nucleophilic substitution reaction was carried out with sodium azide to afford azide terminations.

Figure 4.6 shows a schematic outline of our approach. Vapor phase deposition of 11-bromoundecyltrichlorosilane on freshly activated SiO_x/Si(100) samples was carried out at 140 °C under vacuum. The incorporation of bromine was monitored by XPS (Figure 4.7a, brown line), and the spin doublet peak from Br(3d) was observed at 70.5 ($3d_{5/2}$) and 71.6 ($3d_{3/2}$) eV.[19] The contact angle of

the resulting bromine-teminated surface was $82 \pm 1°$, which was in agreement with previous reports.[6] Subsequently, the sample was immersed in a saturated DMF solution of sodium azide for 24 h to convert bromine to azide.[6] XPS analysis of the resulting sample showed the complete disappearance of the Br(3d) peak (Figure 4.7a, cyan line) and the emergence of two nitrogen peaks at 401 and 405 eV (Figure 4.7b, cyan line).[20] After the sodium azide-treatment, a slight decrease in contact angle was confirmed ($77 \pm 1°$), a similar value found in previous reports.[6]
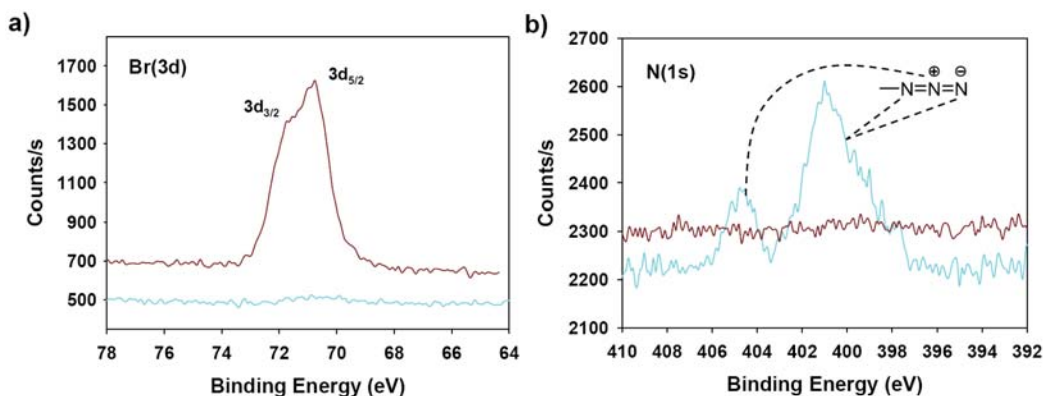
Figure 4.7. XPS spectrum of bromine- (brown) and azide- (cyan) terminated surfaces. (a) Br(3d) region. (b) N(1s) region.

Attempted Catalytic Stamp Lithography

As-prepared azide-terminated surfaces were subjected to catalytic stamp lithography. In the previous hydrosilylation-based patterning chapter (Chapter 3), a catalytic stamp was first inked with molecules to be patterned, and then the inked stamp was applied to a target surface (the "printing" procedure). Despite

the thorough screening of lithographic conditions (time and temperature), including a source of hydrogen (hydrogen,[10] triethylsilane,[21] ammonium formate,[22] or hydrazine[23]), however, our attempts with the printing procedure turned out unsuccessful (Figure 4.8a). Only when hydrazine (5 mM, dissolved in 2-propanol) was used as a hydrogen source, the pseudohexagonal pattern of a parent Pd catalytic stamp was slightly confirmed in the tapping mode AFM phase image (Figure 4.8b).
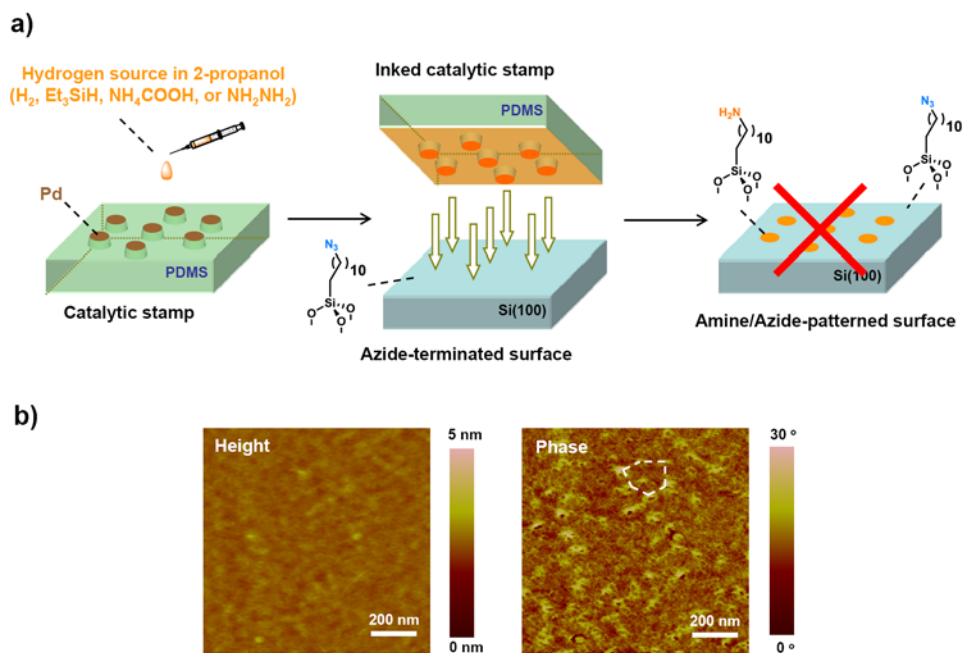
Figure 4.8. (a) Schematic of attempted catalytic stamp lithography on an azide-terminated surface with the printing procedure. Ink was first applied on a catalytic stamp, and then the inked stamp was brought into contact with an azide-terminated surface. Very poor patterns were confirmed in this case. (b) AFM height and phase images of an azide-terminated surface stamped with hydrazine (5 mM in 2-propanol). The expected hexagonal patterns were partially confirmed (shown by white dashed line).

Evolution of Catalytic Stamp Lithography: Imprinting-Style

It was speculated from the above observation that the generation of palladium hydride species, which is considered to be a key for the expected reduction of azide groups, might be problematic with the printing procedure. Because hydrogen sources were removed by a stream of nitrogen after the inking step, the population of prerequisite palladium hydrides on the catalytic stamp would be fundamentally limited with this procedure.

In order to allow more efficient generation of palladium hydride species before and during stamping, the inking of a hydrogen source was performed on the precursor azide surface, and a catalytic stamp was pressed on the *wet* surface (the "imprinting" procedure). Under these conditions, the desired palladium hydrides would be produced *in situ*, permitting effective formation and rapid consumption of reducing species. In addition, nitrogen gas, formed as a byproduct of the reaction, might be more effectively eliminated from the reaction system because of the existence of a liquid medium (used to dissolve a hydrogen source). Thus, the imprinting procedure was newly developed as an alternative method for the original printing-style catalytic stamp lithography.

Figure 4.9 outlines the general procedure for the imprinting-style catalytic stamp lithography. An azide-terminated surface was first covered with a saturated 2-propanol solution of gaseous hydrogen, and then a Pd catalytic stamp was applied onto the wet surface under ambient conditions. The imprinting was continued for 5 min under continuous pressure. During this process, highly

localized catalytic hydrogenation proceeded underneath the nanopatterned Pd catalysts exclusively; therefore, the subsequent release of the Pd catalytic stamp resulted in the translation of the original Pd nanostructures into the array of amine groups. After washing with dichloromethane, ethanol, and H$_2$O, the sample was submitted to a series of analyses.

Figure 4.9. Schematic outline for catalytic stamp lithography with an azide-terminated surface by an imprinting-style procedure. Compared to Figure 4.8a, the first inking was carried out on the azide-terminated surface. A Pd catalytic stamp was then applied on the wet precursor surface to induce localized catalytic hydrogenation.

Figure 4.10 shows tapping mode AFM images of a Pd catalytic stamp and an imprinted azide-terminated surface. The domain size and center-to-center spacing of the parent hexagonally patterned Pd nanostructure were 33 and 116 nm, respectively (Figure 4.10a). Because of the subtle difference in heights (<0.2 nm) between original azide and newly formed amine groups, no topographic features were detected in the height-mode AFM image (Figure 4.10b). In the phase image,

however, a hexagonally pattern dot array, with nearly identical domain size and center-to-center spacing of the parent catalytic stamp, was confirmed (Figure 4.10c). Since the positive (brighter) features should result from the attractive interaction between the functionalized domains and the oxide-capped silicon cantilever,[24] the successful formation of hydrophilic amine functionality by imprinting-style catalytic stamping was implied. It should be noted that the catalytic stamp could be reused multiple times (at least 6 times) (Figure 4.10d-h).
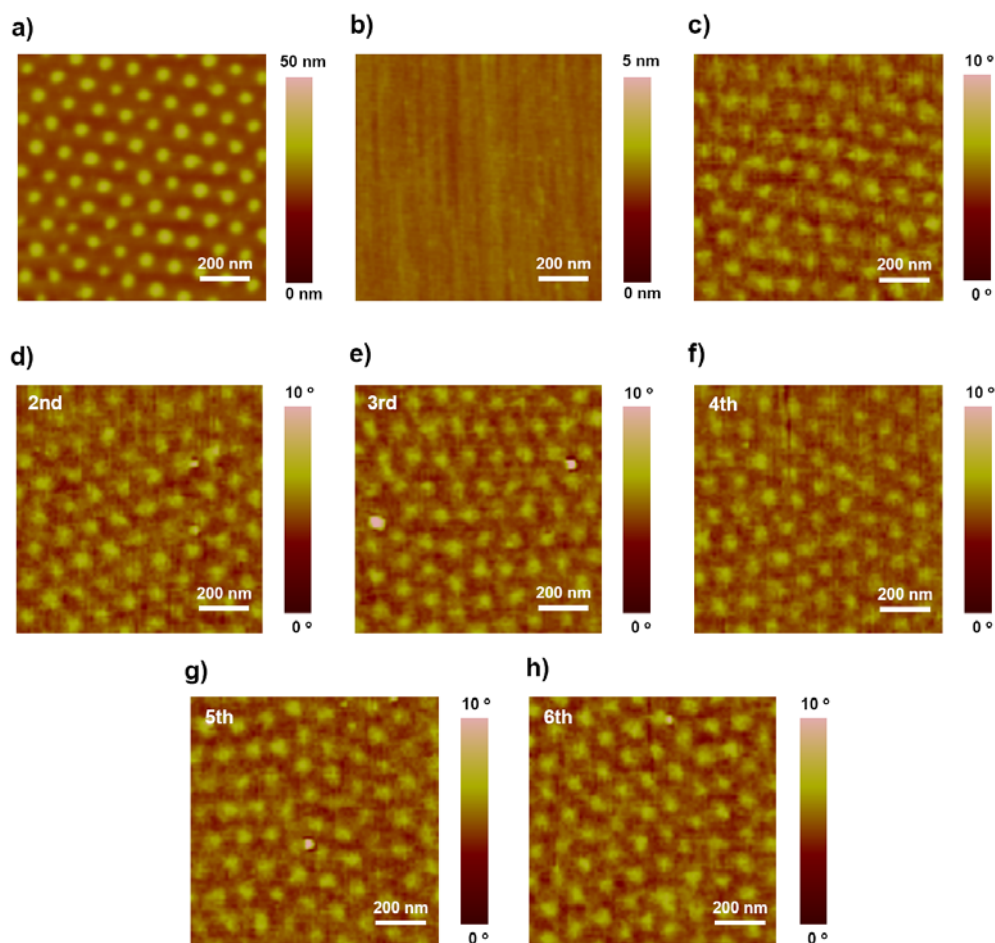
Figure 4.10. AFM images of a Pd catalytic stamp and patterned surfaces. (a) A height image of a Pd catalytic stamp, whose Pd size is 33 nm and center-to-center spacing is 116 nm. (b,c) Height and phase images of a patterned surface using the stamp in shown (a). (d-h) Phase images of patterned surfaces, obtained upon reuse of the catalytic stamp shown in (a).

To investigate the details of the resulting imprinted surface, XPS was performed. No contamination of the sample by Pd leaching was detected in the Pd(3d) region (Figure 4.11a).[25] However, high resolution XPS spectra of N(1s)

region was not able to elucidate the formation of amine groups, due to the dominant coverage of azide groups on the surface (Figure 4.11b).
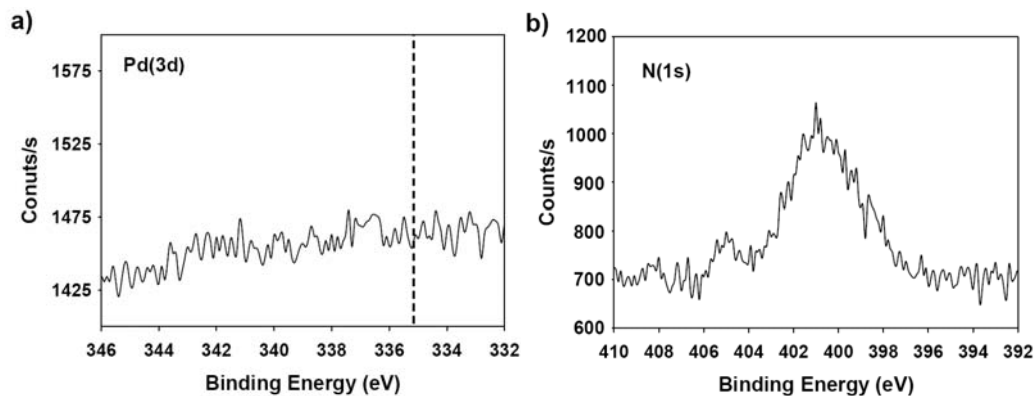
Figure 4.11. High resolution XPS spectra of Pd(3d) (a) and N(1s) (b) regions recorded with an amine/azide patterned surface. The dashed line in (a) corresponds to Pd^0 (~335.4 eV).

The generation of an expected amine/azide patterned surface by imprinting-style catalytic stamp lithography was confirmed by demonstrating specific chemical modifications on amine or azide groups (Figure 4.12). First, a selective reaction on azide-terminated moieties, Cu^I-catalyzed azide-alkyne 1,3-dipolar cycloaddition (CuAAC, click chemistry[26]), was carried out (Figure 4.12a-b). When the imprinted sample was treated with an ethanol/water (2/1, v/v) solution of 1-octadecyne (1 mM) containing a catalytic amount of CuSO$_4$ (10 μM) and sodium ascorbate (15 μM) for 24 h, 1,3-dipolar cycloaddition between surface azide groups and 1-octadecyne proceeded.[27] While the original amine/azide patterned surface has no topographic features as mentioned previously (Figure 4.12a), the AFM height image of the resulting surface showed a pseudohexagonal

array of nanoholes (Figure 4.12b), suggesting the successful attachment of 1-octadecyne molecules only on the azide-terminated region. Alternatively, the amine groups were selectively reacted with an aldehyde molecule (Figure 4.12a-c). The patterned sample was immersed into an ethanol solution of undecanal (1 mM) for 3 h to link it on the amine-terminated moiety via imine formation.[28] Due to the attachment of long alkyl (undecanyl) chain, height growth was observed only on the hexagonally patterned amine moiety (Figure 4.12c).
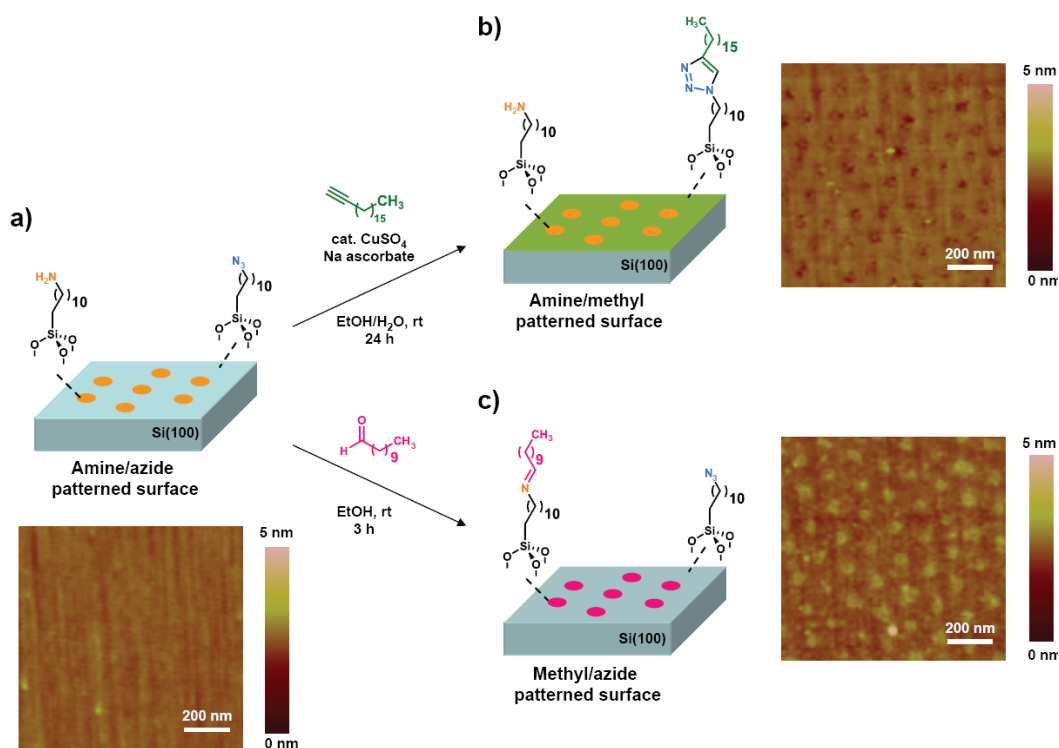
Figure 4.12. Outline for the chemical modification of an amine/azide-patterned surface. (a) AFM height images of (a) a featureless (flat) amine/azide-patterned surface, (b) an amine/methyl-patterned surface obtained through Cu^{I}-catalyzed azide-alkyne cycloaddition, and (c) a methyl/azide-patterned surface obtained through imine formation.

The section analyses of resulting AFM images showed that each nanohole (formed via click chemistry) or nanodomain (formed via imine formation) is approximately 1.3 nm deep or 0.7 nm tall, respectively (Figure 4.13a,b), which are significantly less than the theoretically calculated numbers. For example, the expected depth (or height) of the nanoholes (or nanodomains) is ~2.3 nm (or ~1.2 nm), if the reacted molecules are in all *trans* conformations (Figure 4.13c). This observation is due to two factors. First, the AFM tip pressure will result in some compression, and secondly, the created features are most likely poorly packed (i.e., low yield), probably due to the heterogeneous nature of surface reactions.
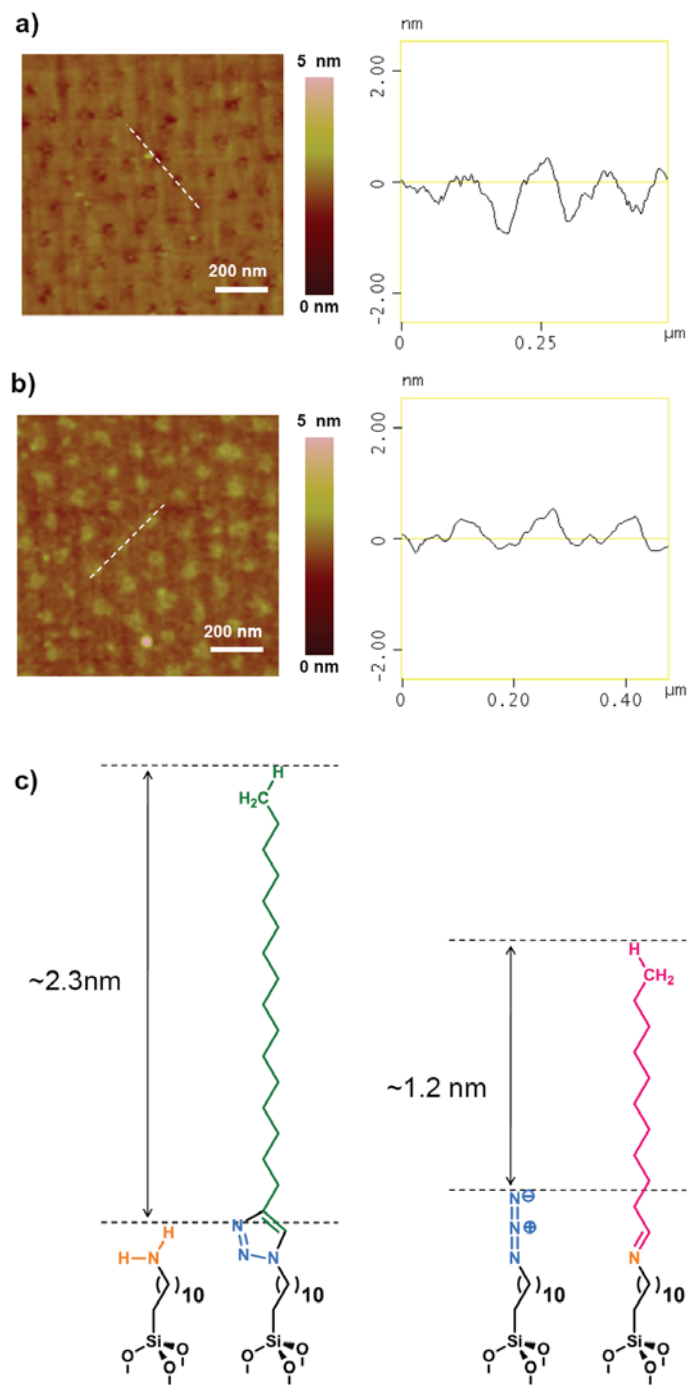
Figure 4.13. AFM height images and corresponding section analyses of (a) an amine/methyl-terminated surface and (b) an azide/methyl-terminated surface. (c) Comparisons of original and modified features, assuming the alkyl chains have all *trans* conformations.

4.4. Results and Discussion 2: The Heck Reaction

The successful patterning with hydrogenation-based, imprinting-style catalytic stamp lithography was followed by the investigation with a carbon-carbon bond forming reaction. Here, the Pd-catalyzed surface Heck reactions with two possible schemes (alkene-terminated surface/aryl halide ink and aryl halide-terminated surface/alkene ink) are discussed.

Fabrication of Precursor Surfaces

In order to fabricate an alkene-terminated surface, vapor phase deposition of 7-octenyltrichlorosilane on a native-oxide capped Si(100) surface was first investigated. However, the contact angle measurement of the resulting surface showed a significantly lower value (~60°) compared to the reported value (~92°),[5,29] suggesting the poor quality of the SAM formed with this method. We therefore utilized a solution-phase approach to prepare the required surface (Figure 4.14).[5] An activated native-oxide capped Si(100) was immersed in a freshly prepared anhydrous toluene solution of 7-octenyltrichlorosilane (0.5 v/v%) for 24 h. Polymeric siloxane residues were also formed on the surface, but they could be removed by gentle swabbing with toluene-soaked cotton. The contact angle measurement of as-prepared surface agreed with the expected value for alkene-terminated surfaces (92 ± 2°).[5,29]
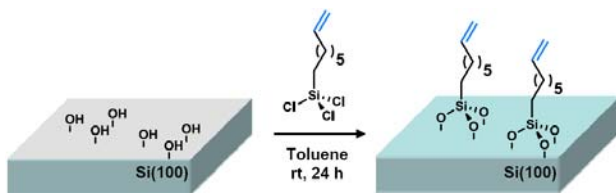
Figure 4.14. Outline for the solution phase synthesis of an alkene-terminated surface. An activated oxide-capped Si(100) surface was immersed in a 0.5 v/v% solution of 7-octenyltrichlorosilane for 24 h.

The bromophenyl-terminated surface was also generated from the similar solution-phase approach, using 4-(4-bromophenyl)-1-butyltrichlorosilane as a SAM precursor (Figure 4.15a). The contact angle of the resulting surface was 82 ± 2°, which was in good agreement with bromine-terminated surfaces.[6] In addition, XPS measurements were carried out to confirm the incorporation of bromine on the surface (Figure 4.15b). The high resolution XPS spectra of Br(3d) region revealed a spin doublet peak at 70.8 (3d$_{5/2}$) and 71.2 (3d$_{3/2}$) eV, which was attributed to carbon-bound bromine.[30]
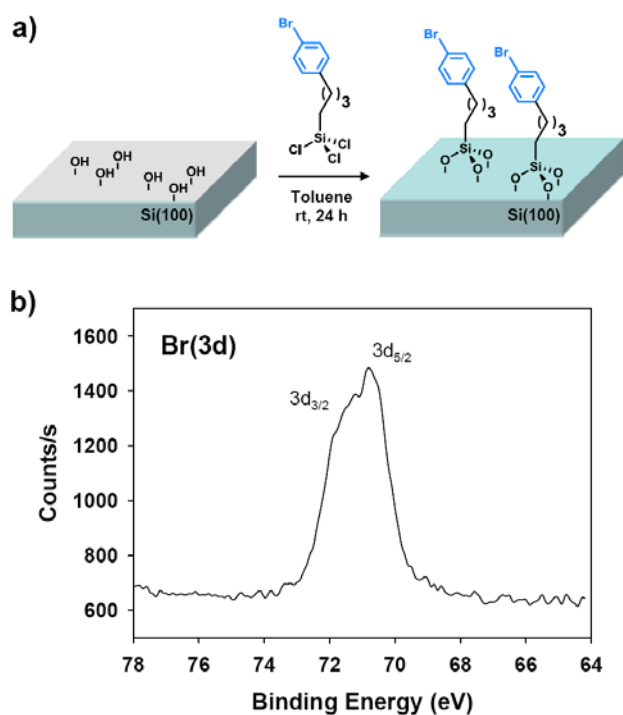
Figure 4.15. (a) Outline for the solution phase synthesis of a bromophenyl-terminated surface. (b) Br(3d) region of high resolution XPS spectrum of a bromophenyl-terminated surfaces.

Imprinting-Style Catalytic Stamp Lithography on Alkene-Terminated Surfaces

Using alkene-terminated surfaces, Heck reaction-mediated patterning was carried out. Our initial attempt with the *printing* procedure didn't result in patterning. It was revealed, however, that successful patterning is feasible with the *imprinting* procedure. Figure 4.16 outlines typical conditions: a diluted dimethylformamide (DMF) solution of an aryl iodide (2.5 mM) containing triethylamine (2.5 mM) was first dropped onto an alkene-terminated surface. A Pd catalytic stamp was then brought into contact with the wet surface at room

temperature, and whole system was placed in an oven preheated to 130 °C. The imprinting was carried out for 30 min with static pressure. Similar to hydrosilylation and hydrogenation, nanoscale patterned Heck reaction took place underneath the immobilized Pd catalysts, and aryl groups were site-selectively attached to the alkene-terminated surface. After the removal of the catalytic stamp, the surface was extensively washed by ultrasonication treatments using toluene, ethanol, and water to eliminate any organic/inorganic residues.
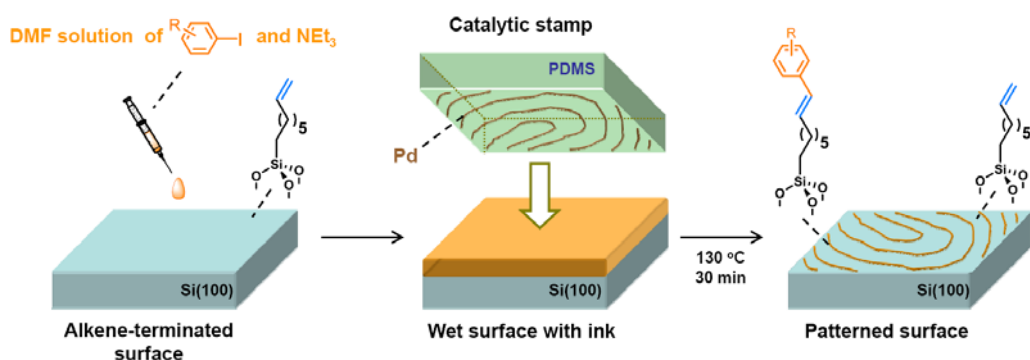
Figure 4.16. Schematic outline for the Heck reaction-mediated catalytic stamp lithography on an alkene-terminated surface (imprinting-style). A Pd catalytic stamp was applied directly onto an inked (wet) alkene-terminated surface. After 30 min of imprinting at high temperature (130 °C), a molecular nanoarray was achieved as a result of site-selective catalysis by immobilized Pd.

Figure 4.17 represents tapping-mode AFM images of a Pd catalytic stamp and an imprinted alkene-terminated surface. The Pd nanostructure of the employed catalytic stamp was 15 nm in line width and 59 nm in interline distance

(Figure 4.17a). When iodopentafluorobenzene[31] was imprinted on an alkene-terminated surface with this stamp, the formation of a similar linear pattern was observed as positive (brighter) features in the AFM height image (Figure 4.17b). The incorporation of utilized pentafluorophenyl groups was suggested by the AFM phase image (Figure 4.17c), since the more hydrophobic nature of the pentafluorophenyl groups compared to the surrounding alkene groups could be confirmed from the negative (darker) features recorded.[24]
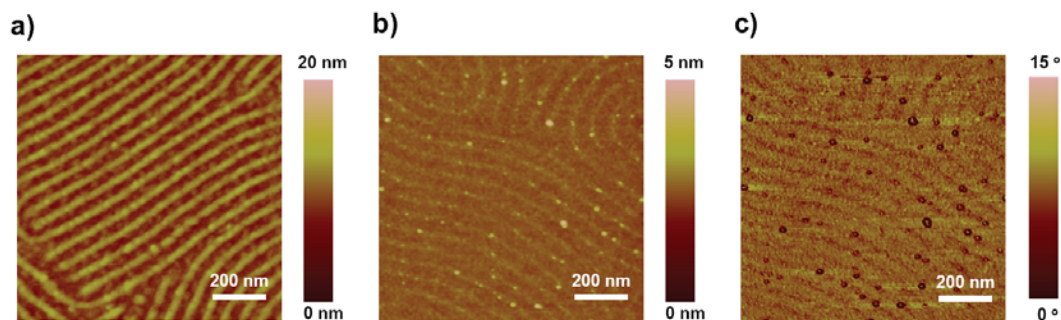
Figure 4.17. AFM images of a Pd catalytic stamp and an iodopentafluorobenzene-imprinted alkene-terminated surface. (a) A height image of a linearly patterned Pd catalytic stamp, with the line width of 15 nm and the interline distance of 59 nm. (b,c) Height and phase images of the patterned surface.

Figure 4.18 shows high-resolution XPS spectra obtained from the iodopentafluorobenzene-imprinted sample. In the F(1s) region, a signal was confirmed at 693 eV (Figure 4.18a), again indicating incorporation of pentafluorophenyl groups on the alkene-terminated surface.[32] Since the spectrum in the Pd(3d) region showed no peaks around 340 eV (Figure 4.18b),[25] it was

suggested that significant Pd leaching did not occur during the pattern formation. Other possible elements were also examined, and no detectable peaks were found from iodine derivatives (either iodopentafluorobenzene or byproduct HI)[25] (Figure 4.18c). Trace signals were observed, however, in the N(1s) region (Figure 4.18d),[25] indicating minor contamination by DMF and/or triethylamine in the patterning process.
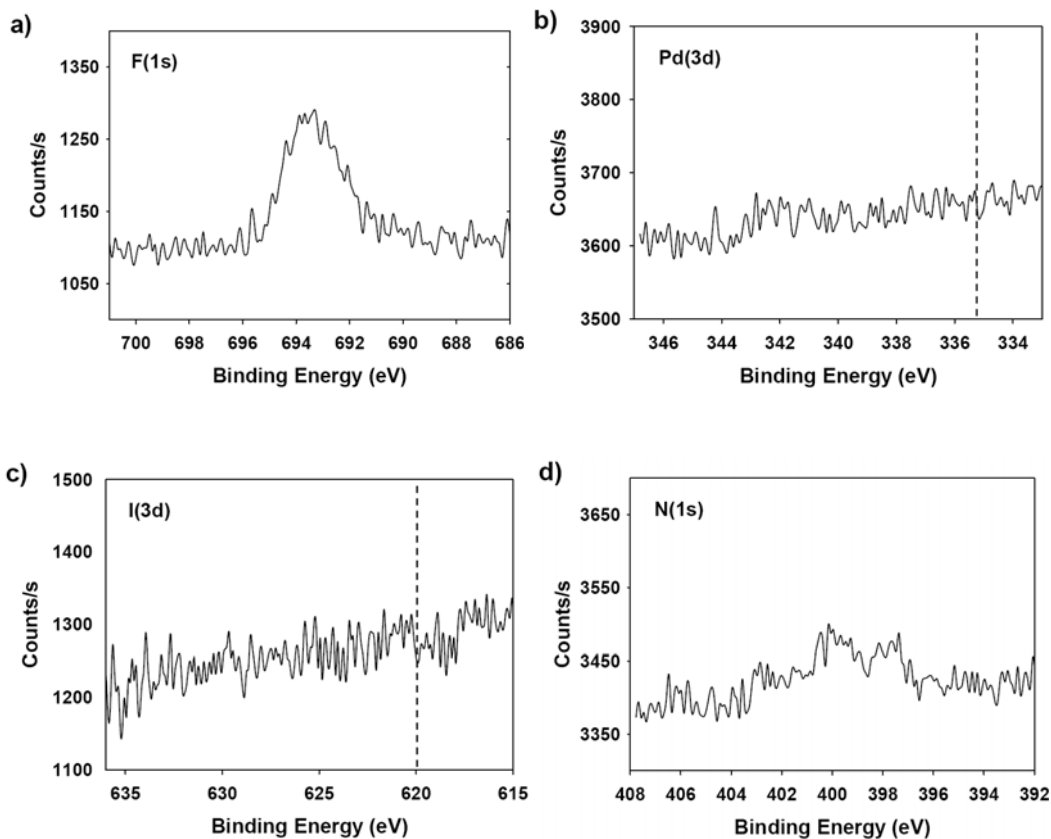
Figure 4.18. High resolution XPS spectra of (a) F(1s), (b) Pd(3d), (c) I(3d), and (d) N(1s) regions. The dashed line in (b) and (c) corresponds to elemental Pd (~335 eV) and I (~620 eV), respectively.

Another example of the Heck reaction-mediated patterning on the alkene-terminated surface is shown in Figure 4.19. A hexagonally-patterned Pd catalytic stamp (domain size = 54 nm, center-to-center spacing = 168 nm, Figure 4.19a) and 4-iodoaniline were employed in this case. The AFM images of the imprinted surface revealed the formation of the hexagonal dot array both in height and phase modes (Figure 4.19b, c, respectively). Since amine termination is less hydrophobic than the alkene groups, the pattern appeared as positive features in the phase image.[24]
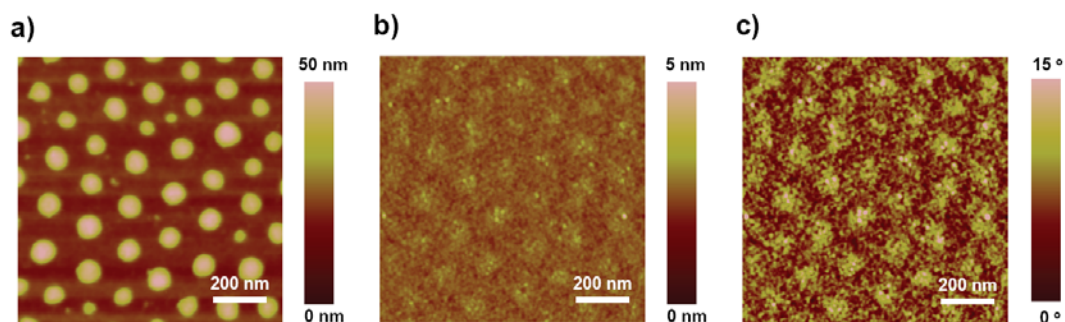
Figure 4.19. AFM images of a Pd catalytic stamp and a 4-iodoaniline-imprinted alkene-terminated surface. (a) A height-mode image of a hexagonally patterned Pd catalytic stamp with domain size of 54 nm and center-to-center spacing of 168 nm. (b,c) Height- (b) and phase-mode (c) images of the patterned surface.

The generated amine functionality was further probed by performing an amine-specific reaction. As outlined in Figure 4.20a, the 4-iodoaniline-imprinted sample was treated with a toluene solution of tetraoctylammonium bromide (TOAB)-capped Au nanoparticles (diameter: ~5 nm) for 12 h. Because of the

ligand exchange between TOAB and surface amine groups,[33] a hexagonally arranged pattern, comprising clusters of gold nanoparticles, emerged after this treatment. The pronounced height difference was clearly observed by the AFM side-view images (Figure 4.20b, c). SEM images also confirmed the selective deposition of gold nanoparticles into a hexagonal arrangement (Figure 4.20d, e).
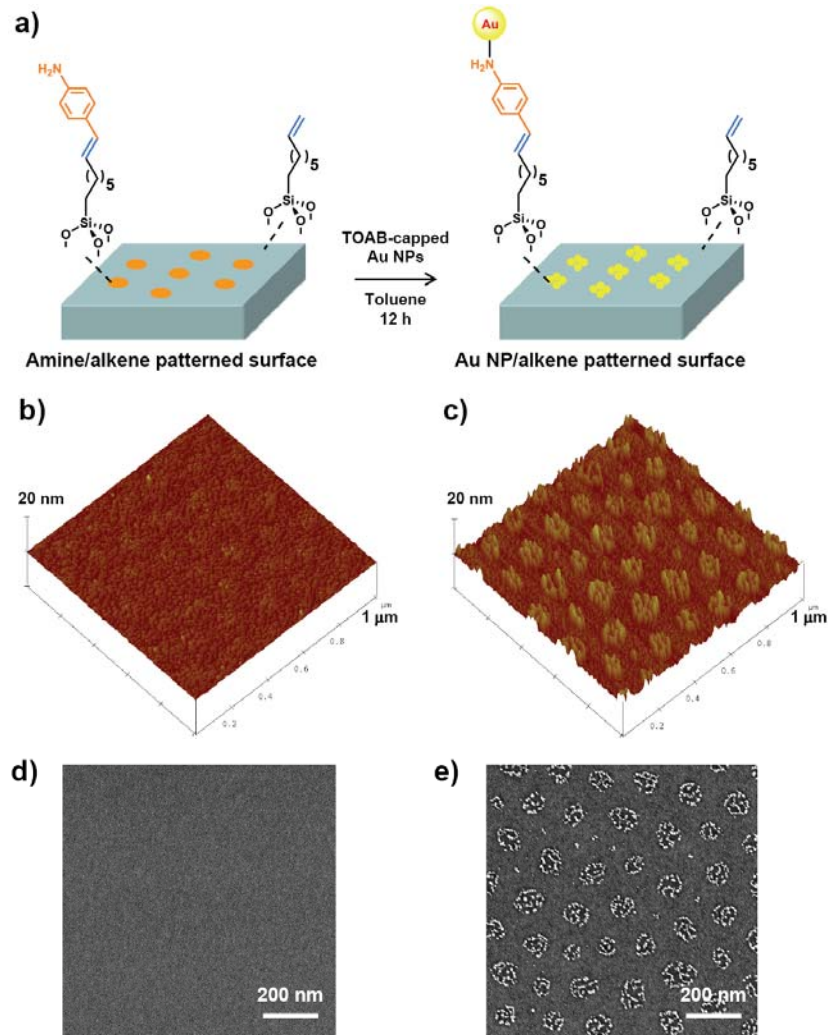
Figure 4.20. (a) Schematic outline for the assembly of TOAB-capped Au nanoparticle on the amine/alkene-patterned surface. (b,c) AFM side-view images of a featureless, amine/alkene-patterned surface (b) and a hexagonally patterned Au nanoparticle/alkene-patterned surface (c). (d,e) SEM images of an amine/alkene-patterned surface (d) and a hexagonally patterned Au nanoparticle/alkene-patterned surface (e).

Other than aryl iodides, aryl bromides (4-anisyl bromide, for example) could also be utilized to pattern an alkene-terminated surface. In contrast, when no aryl iodides or bromides were included in an ink, pattern formation was not observed. The use of an alkene-free surface, such as a native oxide-capped Si surface, also resulted in no pattern formation. These observations clearly supported the premise of pattern formation due to the reaction between aryl halides and surface alkene groups. In addition, high temperature (130 $^{\circ}$C) was necessary for successful patterning, and when imprinting was carried out at a lower temperature, the pattern resulted in poor quality. Figure 4.21 shows such a patterned surface, where 4-iodoaniline was imprinted at 110 $^{\circ}$C.
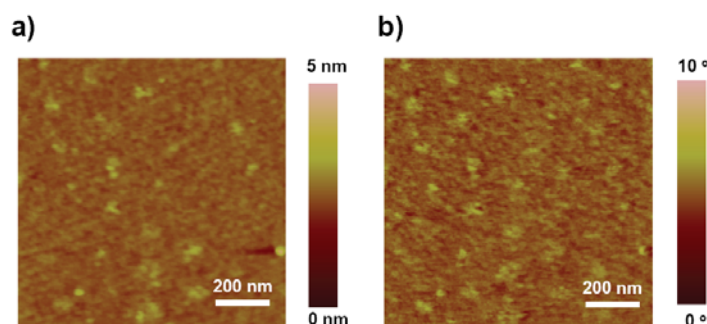
Figure 4.21. AFM height and phase images of an alkene-terminated surface imprinted with 4-iodoaniline at 110 $^{\circ}$C. Incomplete pattern formation was observed.

The reusability of catalytic stamps constitutes an important component of catalytic stamp lithography.[24] It was found, however, that no pattern could be produced once the stamps were used in this Heck reaction case. In the solution system, it is generally considered that catalytically active Pd species for the Heck

reaction originated from leaching from solid Pd supports.[34]   Although the AFM

image of a Pd catalytic stamp taken after use showed an identical appearance as

the pre-use state, a similar leaching mechanism from the Pd catalytic stamp might

occur during the imprinting.   Indeed, the high resolution XPS spectrum of the

patterned surface, taken immediately after the imprinting (no washing), revealed a

small quantity of Pd species on the surface (Figure 4.22).   Although the exact

reason is unclear, the newly exposed Pd surface did not catalyze the Heck reaction,

suggesting inactive Pd species, such as palladium black.[13,34]   Post-treatment with

NaBH$_4$ (aq) or Ar/H$_2$ plasma, however, could not retrieve any catalytic activity.

When catalytic stamp lithography is performed with a reaction which emits

byproducts, the reusability of the stamps might be limited.
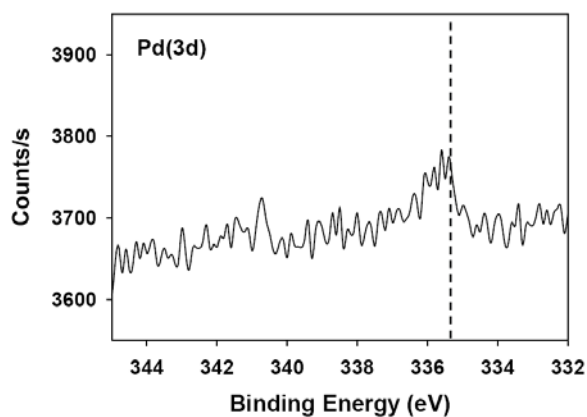
Figure 4.22. High resolution XPS spectrum [Pd(3d) region] of an imprinted surface (ink =

iodopentafluorobenzene). The dashed line corresponds to elemental Pd (~335.4 eV). A small

amount of leached Pd from a catalytic stamp was confirmed.

Patterning of Bromophenyl-Terminated Surface

It was confirmed that Heck reaction-mediated patterning was also applicable on a bromophenyl-terminated surface.[17a,b] When styrene was included in an ink, pattern formation was confirmed by AFM (Figure 4.23). While hydrosilylation-based catalytic stamp lithography could be carried out only with one scheme (alkene/alkyne/aldehyde inks and H-Si terminated surface), the Heck reaction-based catalytic stamp lithography allows more flexibility in terms of the choice of inks and surfaces, extending the scope and opportunity of catalytic stamp lithography.
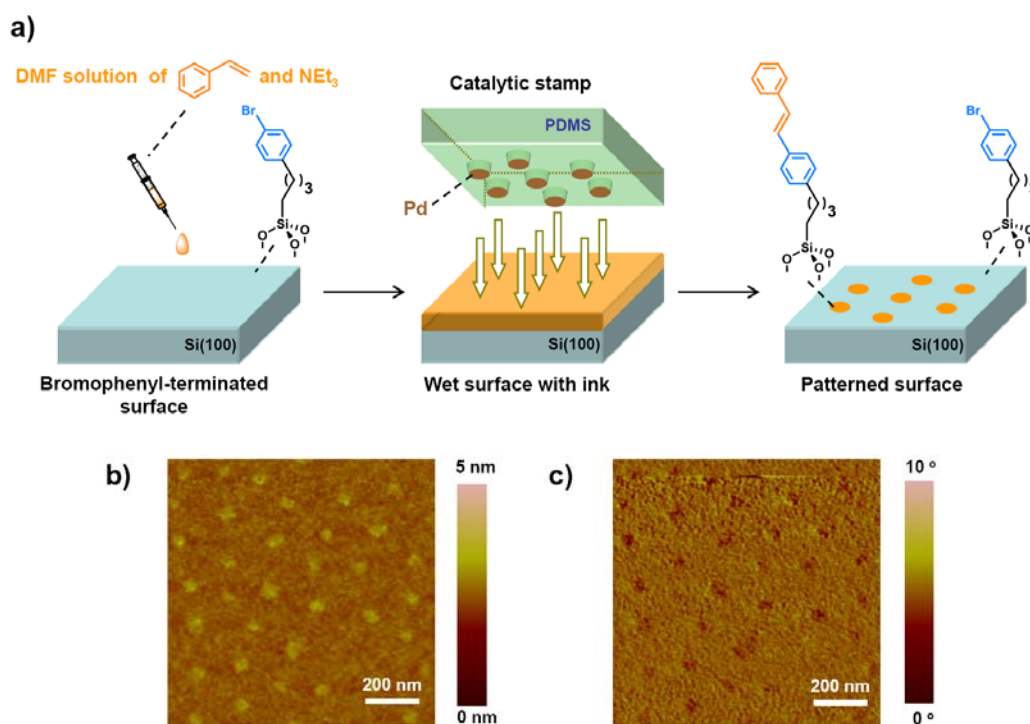
Figure 4.23. (a) Schematic outline for the Heck reaction-based catalytic stamp lithography using a styrene-containing ink and a bromophenyl-terminated surface. (b,c) AFM height and phase images of a styrene-imprinted bromophenyl-terminated surface.

4.5. Conclusion

This chapter discussed surface patterning with hydrogenation and the Heck reaction to generalize the concept of catalytic stamp lithogrphy. Azide-, alkene-, or bromophenyl-terminated siloxane monolayers were prepared on oxide-capped Si surfaces and used as platforms for each reaction. To achieve successful patterning, a new imprinting-style procedure was established.

An azide-terminated surface could be site-selectively hydrogenated via the imprinting of a Pd catalytic stamp through a hydrogen-containing ink layer, yielding a patterned amine/azide-terminated surface. By performing surface reactions selectively on amine (imine formation) or azide moieties (alkyne-azide cycloaddition), the generation of a patterned surface was confirmed. While hydrogenation here only allows simple transformation of azide to amine, the reusability of a catalytic stamp was achieved.

The Heck reaction-based catalytic stamp lithography could be performed both on alkene- and bromophenyl-terminated surfaces with the imprinting-style procedure. Elevated temperature was required for high quality patterning. Different from hydrogenation, varieties of molecular inks were utilized to create functional surfaces, and the premise of the Heck reaction-mediated pattern formations were supported by XPS analysis and the selective chemical modifications using Au nanoparticles. Although the reusability of catalytic stamps was not achieved, this observation provided an important insight on the selection of reactions for catalytic stamp lithography.

4.6. Experimental Section

Generalities.

Unless otherwise noted, all the experiments were performed under ambient conditions. Teflon beakers and tweezers were used exclusively during the cleaning of the Si wafers. Si(100) (p-type, B-doped, ρ = 0.01-0.02 Ω-cm, thickness = 600-650 μm) and Si(111) (p-type, B-doped, ρ = 1-10 Ω-cm, thickness = 600-650 μm) wafers were purchased from MEMC Electronic Materials, Inc. Water was obtained from a Millipore system (resistivity = 18.2 MΩ). Sulfuric acid (BAKER ANALYZED ACS Reagent) and H_2O_2 (30%, CMOS) were purchased from J. T. Baker. $HAuCl_4 \cdot xH_2O$ (99.999%), tetraoctylammonium bromide (98%), sodium azide (>99.5%, *ReagentPlus*®), hydrazine hydrate (N_2H_4 50-60%, regent grade), sodium ascorbate (>99%), undecanal (97%), iodo-pentafluorobenzene (99%), 4-iodoaniline (98%), 4-bromobenzyl bromide (98%), allylmagnesium bromide (1.0 M in diethyl ether), chloroplatinic acid hydrate (>99.9%) and toluene (>99.9%, CHROMASOLV®, for HPLC) were purchased from Sigma-Aldrich. Copper sulfate pentahydrate (99.999%) was purchased from Strem Chemicals. Dimethylformamide (99%) was obtained from Caledon Laboratories Ltd. 11-Bromoundecyltrichlorosilane was obtained from Gelest Corp. Optima grade methanol and 2-propanol were purchased from Fisher. Anhydrous toluene, diethyl ether, and THF were obtained from a solvent purification system (Innovative Technologies, Inc.). All reagents listed above were used as-received. Octenyltrichlorosilane (96%, mixture of isomers, Sigma-

Aldrich), and styrene (99%, Reagent Plus, Sigma-Aldrich) were purified according to the standard methods[35] before use. ^{1}H and ^{13}C NMR chemical shifts are reported in parts per million relative to residual non-deuterated solvent as an internal standard.

Activation of Oxide-Capped Silicon Substrates.

Pieces of Si(100) and Si(111) (~1 cm^2) were degreased in methanol using a ultrasonic bath for 15 min. The wafers were then immersed in a hot piranha acid bath [H_2SO_4/30 % H_2O_2 = 3/1 (v/v), *Note: Piranha solution reacts violently with organics. Special precaution should be made when working with this mixture*] and heated (80 ^{o}C) for 30 min. The wafers were rinsed with an excess amount of water and dried with a stream of nitrogen gas.

Preparation of Azide-Terminated Siloxane Monolayer on SiO$_x$/Si.

A piranha-cleaned Si(100) or Si(111) sample was immediately placed into a desiccator containing an open vial of 11-bromoundecyltrichlorosilane (15 μL). The desiccator was closed, pumped to ~1 Torr, and heated to 140 ^{o}C. After 3 h with static vacuum, the desiccators was cooled to room temperature, and the sample was exposed to ambient atmosphere and briefly rinsed with toluene. The resulting sample was gently swabbed with toluene-soaked cotton to eliminate polymerized siloxane residue, and then washed in toluene using an ultrasonication bath for 10 min. The bromine-terminated sample was then immersed into 5 mL

of DMF solution of sodium azide (8 mg/mL, saturated) for >24 h at room temperature in the dark. The azide-terminated sample was finally rinsed with ethanol and water and used immediately.

Patterning of Azide-Terminated SiO$_x$/Si(100) Surface via Hydrogenation.

Several droplets of 2-propanol saturated with H$_2$ (gas) were placed on an azide-terminated SiO$_x$/Si(100) surface. A Pd catalytic stamp was applied to the wet sample and pressed lightly for 5 min using a homemade stamping apparatus. After the stamping, PDMS was released from the substrate, and the resulting sample was washed with dichloromethane (ultrasonic bath, 5 min), ethanol (rinse), and water (rinse).

Click Chemistry on the Amine/Azide-Patterned Surface.

An amine/azide-patterned sample was immersed for 24 h in 6 mL of a mixed EtOH/H$_2$O (2/1) solution containing 1-octadecyne (1 mM), copper sulfate (10 μM), and sodium ascorbate (15 μM) at room temperature to promote the Cu-catalyzed 1,3-dipolar cycloaddition of 1-octadecyne selectively on the azide groups. The resulting sample was thoroughly washed with dichloromethane (ultrasonic bath, 5 min), ethanol (rinse) and water (rinse).

Imine Formation on the Amine/Azide-Patterned Surfaces.

An amine/azide-patterned sample was immersed into 5 mL of a ethanol solution of undecanal (1 mM) for 3 h at room temperature. The resulting sample was washed with dichloromethane (ultrasonic bath, 5 min), ethanol (rinse) and water (rinse).

Synthesis of 4-(4-Bromophenyl)-1-butene.[36]

A 250 mL three-necked round-bottom flask equipped with reflux condenser and dropping funnel was evacuated, heated, cooled, filled with Ar, and charged with 4-bromobenzyl bromide (5.0 g, 20 mmol) in 15 mL of anhydrous diethyl ether. Allylmagnesium bromide (21 mmol, 21 mL of a 1 M solution in ether) was then added via the dropping funnel over a period of 30 min, and the reaction mixture was allowed to stir for 2 h at room temperature. The mixture was then refluxed in an oil bath until the starting material (4-bromoallyl bromide) was disappeared (~3 h, checked by thin layer chromatography). After the reaction was completed, the flask was cooled to room temperature, and water was added to quench the reaction. The mixture was transferred to a separatory funnel, and organic layer was washed with water and brine, dried over anhydrous magnesium sulfate, and concentrated with a rotatory evaporator. The crude product was then purified by column chromatography to yield 4-(4-bromophenyl)-1-butene as a colorless liquid (3.2 g, 74%): $R_f = 0.80$ (hexane): ^{1}H NMR (400 MHz, CDCl$_3$) δ 7.36 (d, J = 8.2 Hz, 2H), 7.05 (d, J = 8.2 Hz, 2H), 5.60 (m, 1H), 5.05 (m, 2H),

2.66 (t, J = 8.2 Hz, 2H), 2.34 (m, 2H): ^{13}C NMR (100 MHz, CDCl$_3$) δ 140.7, 137.5, 131.3, 130.1, 119.5, 115.2, 35.2, 34.7.

Synthesis of 4-(4-Bromophenyl)-1-butyltrichlorosilane.[37]

A 100 mL three-necked round-bottom flask equipped with reflux condenser was evacuated, heated, cooled, filled with Ar, and placed with 4-(4-bromophenyl)-1-butene (3.2 g, 15.2 mmol) and dried chloroplatinic acid (1.4 mg, 0.0031 mmol) in 20 mL of anhydrous THF. Trichlorosilane (3.1 g, 22.8 mmol, 2.3 mL) was then added via a syringe, and the reaction mixture was allowed to stir for 1 day at room temperature. The mixture was then refluxed in an oil bath for additional 3 h to complete the reaction. After THF was removed under reduced pressure, vacuum distillation was carried out to yield 4-(4-Bromophenyl)-1-butyltrichlorosilane as a colorless liquid (2.8g, 53%): b.p. 120 ^{o}C (0.25 torr): ^{1}H NMR (400 MHz, CDCl$_3$) δ 7.31 (d, J = 8.2 Hz, 2H), 6.97 (d, J = 8.2 Hz, 2H), 2.52 (t, J = 6.9 Hz, 2H), 1.57 (m, 4H), 1.35 (m, 2H): ^{13}C NMR (100 MHz, CDCl$_3$) δ 141.1, 131.8, 130.5, 120.0, 35.1, 33.8, 24.5, 22.3.

Preparation of Alkene- and Bromophenyl-Terminated Siloxane Monolayer on SiO$_x$/Si(100).

A piranha-cleaned Si(100) sample was immersed in 0.5% (v/v) anhydrous toluene solution of octenyltrichlorosilane for 24 h in a Ar-filled glove box at room temperature. The surface of the resulting sample was gently swabbed with

toluene-soaked cotton to eliminate polymerized siloxane residue, and then washed in toluene using ultasonication bath for 10 min. Finally, the sample was rinsed with ethanol and water prior to use. A similar approach was used to prepare bromophenyl-terminated $SiO_x/Si(100)$ samples by using 4-(4-bromophenyl)-1-butyltrichlorosilane instead of octenyltrichlorosilane.

Patterning of Alkene-Terminated SiO$_x$/Si(100) Surface via the Heck Reaction.

Several droplets of a DMF solution of an aryl iodide (2.5 mM) and triethylamine (2.5 mM) were placed on an alkene-terminated $SiO_x/Si(100)$ surface. A Pd catalytic stamp was applied onto the wet surface and pressed lightly at room temperature. Subsequently, the whole system was placed in an oven preheated at 130 ^{o}C. After 30 min, PDMS was released from the Si sample, and the resulting Si sample was washed with toluene (ultrasonic bath, 10 min), ethanol (rinse), and water (rinse).

Selective Assembly of Au NPs on the Amine/Alkene-Patterned Surface.

An amine/alkene-patterned sample was immersed for 12 h in a toluene solution of ~5 nm (in diameter) tetraoctylammonium bromide (TOAB)-capped Au NPs at room temperature. The resulting sample was thoroughly rinsed with toluene and dried with a stream of N_2.

Patterning of Bromophenyl-Terminated SiO~x~/Si(100) Surface via the Heck Reaction.

Several droplets of a DMF solution of styrene (2.5 mM) and triethylamine (2.5 mM) were placed on an bromophenyl-terminated SiO_x/Si(100) surface. A Pd catalytic stamp was applied onto the wet surface and pressed lightly at room temperature. Subsequently, the whole system was placed in an oven preheated at 130 ^{o}C. After 30 min, PDMS was released from the Si sample, and the resulting Si sample was washed with toluene (ultrasonic bath, 10 min), ethanol (rinse), and water (rinse).

Surface Characterization.

The samples obtained in this study were characterized by atomic force microscopy (AFM), scanning electron microscopy (SEM), and X-ray photoelectron spectroscopy (XPS). AFM images were taken with a Digital Instruments/Vecco Nanoscope IV (tapping mode) using commercially available Si cantilevers (PPP-NCHR probe, purchased from Nanosensors, http://www.nanosensors.com/PPP-NCHR.htm) under ambient conditions. Prior to the use, AFM probes were treated with oxygen plasma (O_2 pressure: 0.2 Torr, time: 30 s) to make the surfaces hydrophilic. This treatment was important to obtain consistent results especially for phase imaging. SEM was performed with Hitachi S-4800 FE-SEM using an electron energy of 10k eV under high vacuum conditions ($<10^{-8}$ Torr). XPS was taken on a Kratos Axis 165 X-ray

photoelectron spectrometer using a monochromatic Al Kα with a photon energy of 1486.6eV under high vacuum conditions (<10^{-8} Torr), and ejected X-rays were measured at 0° from the surface normal. The XPS signals were calibrated on the basis of the C(1s) (285.0 eV).

4.7. References

1.   Sagiv, J. *J. Am. Chem. Soc.* **1980**, *102*, 92-98.

2.   (a) Ulman, A. *Chem. Rev.* **1996**, *96*, 1533-1554.   (b) Aswal, D. K.; Lenfant, S.; Guerin, D.; Yakhmi, J. V.; Vuillaume, D. *Anal. Chim. Acta* **2006**, *568*, 84-108. (c) Onclin, S.; Ravoo, B. J.; Reinhoudt, D. N. *Angew. Chem., Int. Ed.* **2005**, *44*, 6282-6304.

3.   Wasserman, S. R.; Tao, Y. T.; Whitesides, G. M. *Langmuir* **1989**, *5*, 1074-1087.

4.   Brzoska, J. B.; Azouz, I. B.; Rondelez, F. *Langmuir* **1994**, *10*, 4367-4373.

5.   Kim, T. K.; Yang, X. M.; Peters, R. D.; Sohn, B. H.; Nealey, P. F. *J. Phys. Chem. B* **2000**, *104*, 7403-7410.

6.   Balachander, N.; Sukenik, C. N. *Langmuir* **1990**, *6,* 1621-1627.

7.   (a) Sheradsky, T. In The Chemistry of the Azido Group; Patai, S., Ed.; Interscience: New York, 1971; 331. (b) Scriven, E. F. V.; Turnbull, K. *Chem. Rev.* **1988**, *88*, 297-368.

8.   Boyer, J. H. *J. Am. Chem. Soc.* **1951**, *73*, 5865-5866.

9.   Boyer, J. H.; Ellzey, S. E., Jr. *J. Org. Chem.* **1958**, *23*, 127-129.

10.   Corey, E. J.; Nicolaou, K. C.; Balanson, R. D.; Machida, Y. *Synthesis* **1975**, 590-591.

11.   (a) Muller, W. T.; Klein, D. L.; Lee, T.; Clarke, J.; McEuen, P. L.; Schultz, P. G. *Science* **1995**, *268*, 272-273. (b) Blackledge, C.; Engebretson, D. A.; McDonald, J. D. *Langmuir* **2000**, *16*, 8317-8323.

12. (a) Heck, R. F.; Nolley, J. P. *J. Org. Chem.* **1972**, *37*, 2320-2322. (b) Mizoroki, T.; Mori, K.; Ozaki, A. *Bull. Chem. Soc. Jpn.* **1971**, *44*, 581. (c) Beletskaya, I. P.; Cheprakov, A. V. *Chem. Rev.* **2000**, *100,* 3009-3066. (d) de Vries, J. G. *Can. J. Chem.* **2001**, *79*, 1086-1092.

13. Phan, N. T. S.; Van Der Sluys, M.; Jones, C. W. *Adv. Synth. Catal.* **2006**, *348*, 609-679.

14. Yao, Q.; Kinney, E. P.; Yang, Z. *J. Org. Chem.* **2003**, *68*, 7528-7531.

15. Portnoy, M.; Ben-David, Y.; Milstein, D. *Organometallics* **1993**, *12*, 4734-4735.

16. Diaz-Ortiz, A.; Prieto, P.; Vazquez, E. *Synlett* **1997**, 269-270.

17. (a) Yam, C. M.; Cho, J.; Cai, C. *Langmuir* **2003**, *19*, 6862-6868. (b) Deluge, M.; Cai, C. *Langmuir* **2005**, *21*, 1917-1922. (c) Plass, K. E.; Liu, X.; Brunschwig, B. S.; Lewis, N. S. *Chem. Mater.* **2008**, *20*, 2228-2233.

18. Davis, J. J.; Bagshaw, C. B.; Busuttil, K. L.; Hanyu, Y.; Coleman, K. S. *J. Am. Chem. Soc.* **2006**, *128*, 14135-14141.

19. Jin, H.; Kinser, C. R.; Bertin, P. A.; Kramer, D. E.; Libera, J. A.; Hersam, M. C.; Nguyen, S. T.; Bedzyk, M. J. *Langmuir* **2004**, *20*, 6252-6258.

20. Prakash, S.; Long, T. M.; Selby, J. C.; Moore, J. S.; Shannon, M. A. *Anal. Chem.* **2007**, *79*, 1661-1667.

21. Mandal, P. K.; McMurray, J. S. *J. Org. Chem.* **2007**, *72*, 6599-6601.

22. Gartiser, T.; Selve, C.; Delpuech, J. J. *Tetrahedron Lett.* **1983**, *24*, 1609-1610.

23. Furst, A.; Berlo, R. C.; Hooton, S. *Chem. Rev.* **1965**, *65*, 51-68.

24. (a) Mizuno, H.; Buriak, J. M. *J. Am. Chem. Soc.* **2008**, *130*, 17656-17657. (b) Mizuno, H.; Buriak, J. M. *ACS Appl. Mater. Interfaces* **2009**, *1*, 2711-2720.

25. Wagner, C. D.; Naumkin, A. V.; Kraut-Vass, A.; Allison, J. W.; Powell, C. J.; Rumble, J. R., NIST X-ray Photoelectron Spectroscopy Database. In *NIST Standard Reference Database 20, Version 3.5*, National Institute of Standards and Technology, Gaithersburg: 2007. http://srdata.nist.gov/xps/

26. Kolb, H. C.; Finn, M. G.; Sharpless, K. B. *Angew. Chem., Int. Ed.* **2001**, *40*, 2004-2021.

27. Lummerstorfer, T.; Hoffmann, H. *J. Phys. Chem. B* **2004**, *108*, 3963-3966.

28. Rozkiewicz, D. I.; Ravoo, B. J.; Reinhoudt, D. N. *Langmuir* **2005**, *21*, 6337-6343.

29. Janssen, D.; De Palma, R.; Verlaak, S.; Heremans, P.; Dehaen, W. *Thin Solid Films* **2006**, *515*, 1433-1438.

30. Basu, R.; Lin, J.-C.; Kim, C.-Y.; Schmitz, M. J.; Yoder, N. L.; Kellar, J. A.; Bedzyk, M. J.; Hersam, M. C. *Langmuir* **2007**, *23*, 1905-1911.

31. Albeniz, A. C.; Espinet, P.; Martin-Ruiz, B.; Milstein, D. *Organometallics* **2005**, *24*, 3679-3684.

32. (a) Davis, D. W.; Shirley, D. A.; Thomas, T. D. *J. Am. Chem. Soc.* **1972**, *94*, 6565-6575. (b) Trudell, B. C.; Price, S. J. *Can. J. Chem.* **1977**, *55*, 1279-1284.

33.   (a) Thomas, K. G.; Zajicek, J.; Kamat, P. V. *Langmuir* **2002**, *18*, 3722-3727. (b) Prasad, B. L. V.; Stoeva, S. I.; Sorensen, C. M.; Klabunde, K. J. *Chem. Mater.* **2003**, *15*, 935-942.

34.   (a) Koehler, K.; Kleist, W.; Proeckl, S. S. *Inorg. Chem.* **2007**, *46*, 1876-1883. (b) Huang, L.; Wong, P. K.; Tan, J.; Ang, T. P.; Wang, Z. *J. Phys. Chem. C* **2009**, *113*, 10120-10130.

35.   *Purification of Laboratory Chemicals*, 5th ed., Armarego, W. L. F.; Chai, C. L. L. Eds.; Elsevier: Amsterdam, 2003.

36.   Srivastava, R. R.; Singhaus, R. R.; Kabalka, G. W. *J. Org. Chem.* **1999**, *64*, 8495-8500.

37.   Lindner, E.; Salesch, T. *J. Organomet. Chem.* **2001**, *628*, 151-154.

Chapter 5
Conclusion

This thesis has discussed the development of stamp-based nanoscale patterning of organic monolayers, catalytic stamp lithography. To conclude the entire story, this chapter highlights the results of each chapter and addresses potential research directions of catalytic stamp lithography.

5.1. *Summaries of Chapters*

Chapter 1

Chapter 1 discussed the background and motivation of this thesis work. As an introduction, the current situation regarding nanoscale patterning of organic monolayers was described showing four representative patterning techniques (photolithography, scanning beam lithography, scanning probe lithography, and soft lithography). Because of the simplicity and efficiency, in particular, a stamp-based technique of microcontact printing (μCP) was emphasized. In addition, it was proposed that the integration of localized catalytic reactions could be promising to downsize the resolution limit of conventional μCP by avoiding challenging problems of ink diffusion and stamp deformation. In order to accomplish such a unique stamping scheme, hybrid nanostructured metal/PDMS architectures were proposed and termed as catalytic stamps.

Chapter 2

Chapter 2 described the detailed procedures for the fabrication of catalytic stamps. In order to construct nanopatterned transition metal catalyst arrays on flexible PDMS supports, metallic nanostructures were first synthesized on rigid SiO_x/Si substrates, and then they were transferred onto PDMS surfaces by a simple peel-off approach. Since the metallic nanostructures were produced via the use of self-assembled block copolymer templates, expensive patterning tools such as photolithography and electron-beam lithography were avoided. Catalytic stamps with various morphologies (hexagonally-arranged dot or linear arrays), metals (Pd, Pt, and Au), sizes (15-54 nm), and spacings (59-124 nm), were produced in this chapter.

Chapter 3

In Chapter 3, hydrosilylation-based patterning was presented as a proof-of-concept demonstration of catalytic stamp lithography. When terminal alkenes, alkynes, or aldehydes with different chemical functionalities were used as molecular inks, the Pd or Pt nanopatterns on catalytic stamps were translated into corresponding molecular arrays on hydrogen-terminated Si(111) and Si(100) surfaces, since catalytic hydrosilylation took place exclusively underneath patterned metallic nanostructures. With this straightforward approach, the resolution limit of conventional μCP (~100 nm) could be downsized to a sub-20 nm scale, while maintaining the advantages of stamp-based patterning (i.e., large-

area, high-throughput capabilities, and low cost). Characterization of the as-obtained molecular arrays were obtained via AFM imaging, XPS analysis, the stability tests under organic and aqueous solutions, and the chemical modification of patterned surfaces. Although unsuccessful, pattern creation was also attempted on alkene-terminated Si substrates using silanes as molecular inks, to determine the scope and limitations of hydrosilylation-based catalytic stamp lithography.

Chapter 4

To generalize the concept of catalytic stamp lithography, Chapter 4 dealt with hydrogenation- and the Heck reaction-mediated surface patterning. An azide-terminated surface was utilized for hydrogenation, and vinyl- and bromophenyl-terminated surfaces were utilized for the Heck reaction. A different procedure from catalytic stamp lithography with hydrosilylation was invented, where molecular inks were placed on the precursor surfaces (instead of catalytic stamps), followed by the application of catalytic stamps onto the wet surfaces. It was found that this imprinting-style stamping was necessary for the successful patterning with both hydrogenation and the Heck reaction. Because patterned surfaces could be further modified through appropriate chemical reactions, it was suggested that this simple approach can be potentially useful for the construction of a higher degree of nanoarchitectures.

5.2. Proposed Research Directions

Development of New Fabrication Methods for Catalytic Stamps

While the block copolymer-templated synthesis of catalytic stamps has been shown to be viable for catalytic stamp lithography, this method is fundamentally limited in terms of the patterns available. In fact, this thesis showed only two patterns, hexagonally-arranged dot and linear arrays, although the control of size/spacing of the patterns was possible by modulating the molecular weights of block copolymers. In order to pattern organic monolayers with more complex structures, which will be required for a number of potential applications, methods to fabricate catalytic stamps with arbitrary geometries need to be developed.

One possible route to produce catalytic stamps with more complex patterns of catalysts is *nanoskiving*,[1] a new technique developed by the Whitesides group to create arrays of metallic structures with nanoscale dimensions. Figure 5.1 illustrates its general procedure. The first step is the replication of a patterned epoxy substrate from a PDMS master. A thin metallic film is deposited on the surface of the topographically patterned epoxy surface by electron-beam evaporation or sputtering, which is then covered by more epoxy to embed a metallic film in an epoxy matrix. An ultramicrotome with a diamond knife is applied to section the epoxy block. The sliced epoxy pieces containing the metal are transferred onto a silicon substrate, followed by the removal of epoxy by oxygen plasma to generate freestanding metallic structures on the

silicon. The dimensions of resulting structures depend upon the size of the original epoxy (x), the thickness of the metallic film (y), and the thickness of the epoxy slice (z). Since all parameters is tunable on the nanometer scale (~20 nm), a variety of metallic nanostructures can be produced via this method.
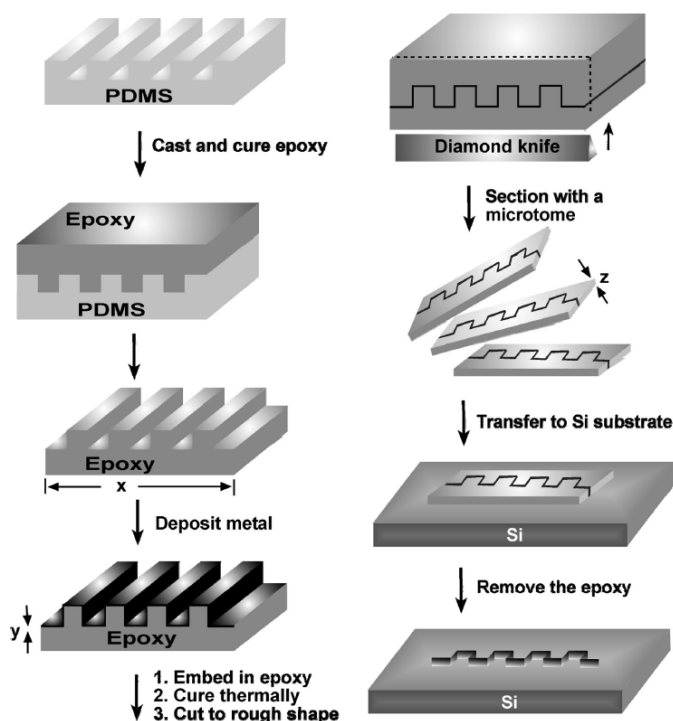
Figure 5.1. Outline for nanoskiving. A topographically patterned epoxy is produced by the replication from a PDMS master. A thin metal film is deposited on the epoxy substrate and embedded in epoxy. A ultramicrotome sectioning produces slices of metal/epoxy materials, which are transferred onto a Si surface. A oxygen plasma treatment is carried out to remove epoxy matrix, generating a free-standing metallic nanostructure on the Si surface. Reprinted with permission from ref. 1b. Copyright © 2007 American Chemical Society.

Figure 5.2 represents some of the fascinating examples of gold nanostructures on SiO_2/Si produced by nanoskiving.[1a]
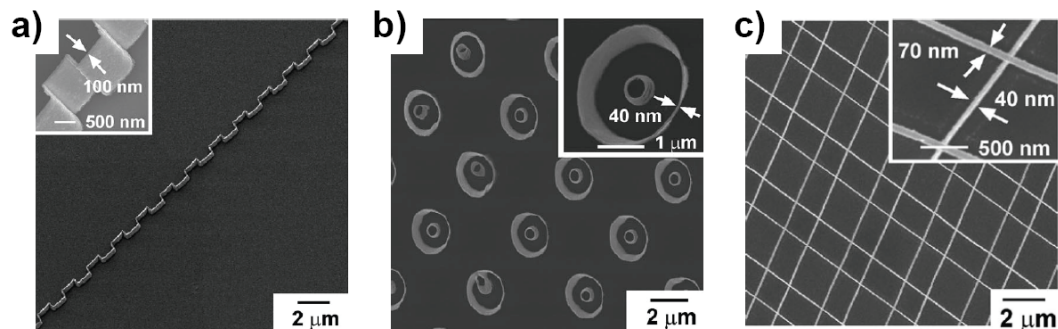
Figure 5.2. SEM images of gold nanostructures formed via nanoskiving. Reprinted with permission from ref. 1a. Copyright © 2008 American Chemical Society.

In order to exploit nanoskiving for the fabrication of catalytic stamps, three pathways would have to be considered. First, the resulting metallic nanostructures formed on Si would be transferred onto PDMS through the peel-off approach, as described in Chapter 2 (Figure 5.3). Secondly, the sliced epoxy pieces might be incorporated on PDMS to produce metal/epoxy/PDMS hybrid stamps yet the rigidity of the epoxy resin may be unsuitable for the stamp application. Thirdly, the PDMS might be utilized as a substrate in place of epoxy to create metal/PDMS structures directly. In this case, however, the feasibility of ultramicrotome with flexible PDMS can be challenging.
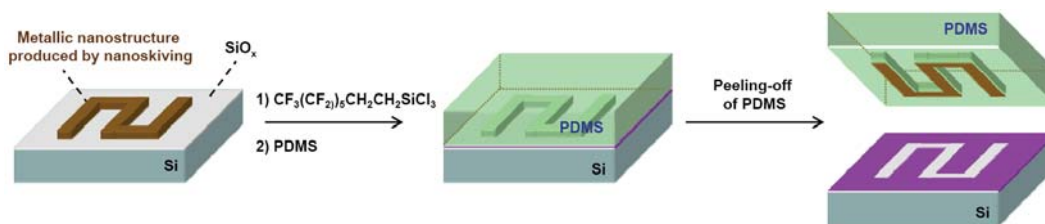
Figure 5.3. Nanoskiving-based fabrication of catalytic stamps. Metallic nanostructures produced by nanoskiving is transferred onto the surface of PDMS via a peel-off approach.

Although nanoskiving is an attractive candidate to provide arbitrary metallic nanostructures useful for designing catalytic stamps, the development of block copolymer-based nanofabrication is also ongoing.[2] Nealey *et al.* have shown a large variety of nanostructures made by the directed assembly of block copolymers on chemically nanopatterned substrates.[2b,c] With these progressing techniques, the fabrication of catalytic stamps with desired metallic geometries would be eventually feasible to pattern organic monolayers with complex structures.

Investigation of the Quality of Patterned Organic Monolayers

In this thesis, the primary analysis tool for the patterned organic monolayers was AFM. XPS measurements and chemical modifications of patterned surfaces were also conducted to provide additional evidence to prove that a corresponding surface reaction (hydrosilylation, hydrogenation, or the Heck reaction) is the only possible reaction that could occur under these conditions.

Because one of the foci of this thesis was to show the versatility of catalytic reactions, a systematic study to achieve a perfect monolayer with a selected system was not performed. Further investigation would be necessary, however, to assess the quality of patterned organic monolayers, since high quality monolayers are necessary for the sophisticated technological application.

Organic monolayers are usually characterized in terms of thickness (by ellipsometry), ordering and orientation (by FTIR), uniformity and coverage (by goniometry, AFM, and STM), chemical composition (by XPS), and physical and chemical stability (by thermal treatment and etching, etc.).[3] Unfortunately, some of these techniques (ellipsometry, FTIR, goniometry, and XPS) are not suitable to evaluate *patterned* organic monolayers because the resulting information is an average of the entire surface. In fact, it is known that the peak intensities of FTIR strongly depend on the packing density of organic monolayers.[3b] Because the net surface coverage of typical patterned samples is low (<15% of a 2-D surface for hexagonal patterns), these techniques are, indeed, close to uninformative. Further improvement in the detection limit (sensitivity) of these techniques is anticipated.

The density of the patterned organic monolayers is highly important. In the case of hydrosilylation, the degree of the packing might be explained by the stability tests of patterned monolayers toward etchants. As discussed in Chapter 3 (Figure 3.19), when a phenylacetylene-patterned $Si(100)$-H_x was treated with 4 M KOH (aq) for 30 s, the resulting surface showed discontinuous patterns, although the original linear structure could be still confirmed. This result indicates that the

quality of the patterned monolayer is not uniform: some parts are densely packed, others seem to not be so densely packed. However, understanding the detailed nature of organic monolayers probably requires other protocols and analytical tools. In this respect, STM may provide useful information regarding the defects present in the organic monolayers, as often seen in the study of thiolate SAMs on Au.[4]

Once methods to evaluate the quality of patterned organic monolayers are established, the optimization of stamping conditions (time, pressure, concentration of molecular inks, etc.) to create "perfect" monolayers should be explored. In addition, since the formation of organic monolayers is influenced by the nature of underlying substrate,[5] the comparative studies by changing the doping type and level of Si substrates would be very intriguing research.

The Mechanism of Pattern Formations: Catalyzed or Mediated?

There is a huge ongoing debate as to whether heterogeneous catalysis by transition metals is indeed heterogeneous or not. In the case of the Heck reaction, it is generally considered that leached Pd species from the heterogeneous support is responsible for the actual catalysis.[6] The fact that the catalytic stamp lost the patterning ability after a single use in the Heck reaction indicated that the pattern formation is based on the leached Pd from the stamp; in this case, therefore, the Pd-*mediated* pattern formation is definitively correct. This thesis also showed, however, some circumstantial evidence suggesting *catalysis* for hydrosilylation

and hydrogenation, since, in these reactions, catalytic stamps could be reused multiple times and XPS of patterned surfaces showed no significant transfer of metals (Pt or Pd). In order to further clarify whether the surface chemistry outlined here is metal-mediated, or indeed metal-catalyzed, a detailed study needs to be carried out. As pointed out previously, surface analysis techniques, especially XPS, with improved sensitivity will play critical roles in this respect.

If the reactions take place in a heterogeneous catalytic fashion upon stamping, the interfacial contact between the surface of catalysts (embedded in PDMS) and reactive surface species (on bulk substrates) is critical, because both surfaces are not "flat" from an atomic/molecular perspective. In this case, how do the reactions occur?

In the hydrosilylation of H-terminated Si surfaces, it has been proposed that the generation of surface radical species is the key to initiate the reaction. Once the surface silyl radicals are formed thermally or photochemically, the attachement of alkene/alkyne molecules propagates on the surface via the chain mechanism, as described in Chapter 3 (see Figure 3.5). In the case of Pt-catalyzed hydrosilylation, the formation of surface silyl radicals is not likely; however, the formation of surface silyl *cation* species[7] might be possible via the hydrogen absorption by Pt.[8] Once such surface silyl cations are produced, a similar chain mechanism should be possible as shown in Figure 5.4. This cation-mediated mechanism can explain the pattern formation by catalytic stamp lithography, because even a partial contact between catalysts and surface Si-H

groups can induce the required reactions diffusively. If the diffusion of the silyl cation-mediated surface hydrosilylation happens in a similar manner as the radical-mediated hydrosilylation, the pattern formation would be still limited to the areas directly below the catalysts (localized catalysis), since the lateral diffusion of the radical-mediated surface hydrosilylation has been estimated within a few nm.[9]
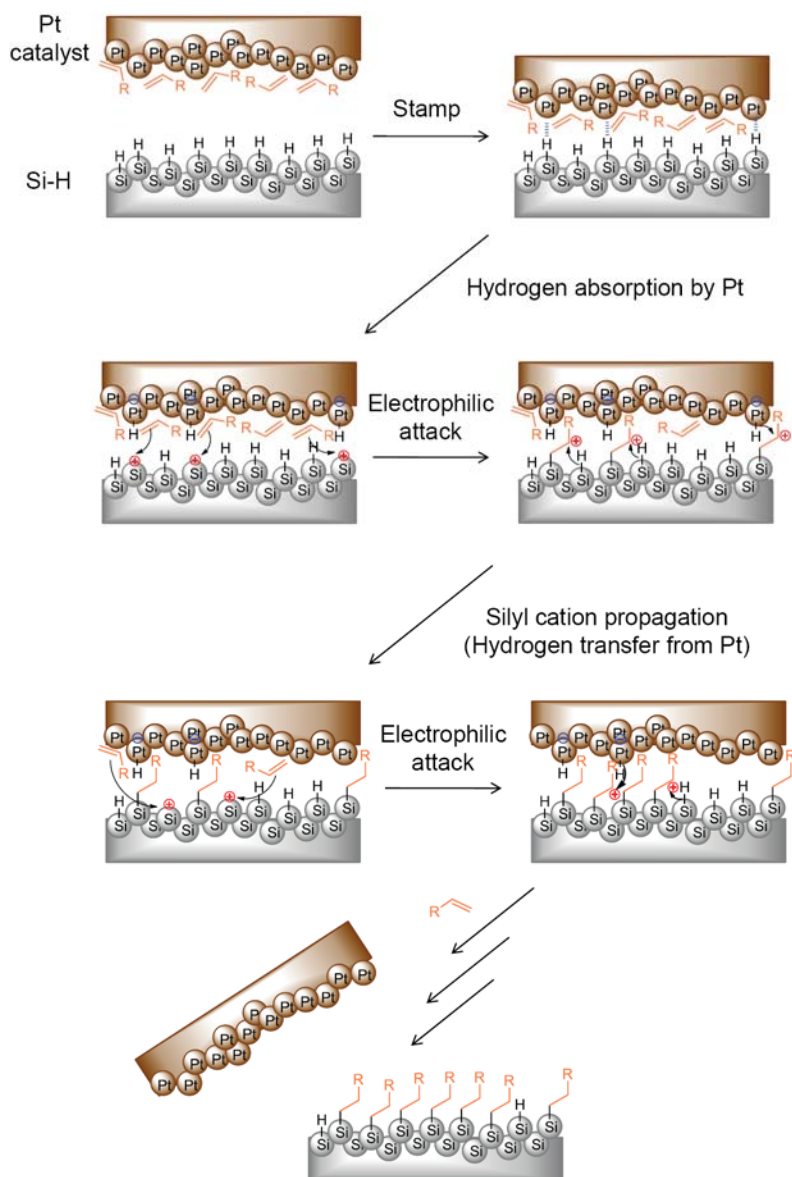
Figure 5.4. A plausible mechanism for the cation-mediated surface hydrosilylation during catalytic stamp lithography. Surface silyl cations are first formed via the hydrogen absorption of Pt catalyst. Alkenes (as molecular inks) attack the silyl cations and generate surface carbocation species. The carbocations can absorb neighboring hydrogen from Si-H to produce new surface silyl cations (Pt-H can also be a hydrogen source). This cation propagation continues until a monolayer is formed underneath the catalyst.

Potential Applications

The ultimate goal of catalytic stamp lithography is to offer technologically useful nanopatterned surfaces with organic monolayers. Organic molecules have extremely large variations compared to current metal-depend structures, suggesting the possibility of more precise control to construct a system suited for specific applications. Because catalytic stamp lithography is, in fact, a bottom-up approach and requires little in the way of (i.e., diluted solution of) molecular inks, direct patterning of expensive materials is possible. In addition, secondary (or higher) modifications are feasible on the patterned surfaces. Here, two potential uses of nanopatterned surfaces produced by catalytic stamp lithography are discussed.

1. Catalytic Stamp Lithography for Biomolecular Nanoarrays

Fabrication of arrays of biomolecules on planar substrates is an ongoing technology for studying fundamental ligand-receptor interactions and enzymatic functions, and for screening drug candidates in a combinatorial approach.[10] The common dimensions of patterned spots are on the micron scale (i.e., microarrays), and better efficiency (smaller samples required) should be achievable by making them on the nanoscale (nanoarrays). Catalytic stamp lithography has potential to create biomolecular nanoarrays in direct/indirect fashions.

For example, relatively small biomolecules, such as carbohydrates (with alkene terminations), would be directly patterned on H-terminated Si substrates

via hydrosilylation-based catalytic stamp lithography. The blank space can be filled with poly(ethylene glycol) (PEG)-terminated molecules as protein-resistant[11] (Figure 5.5). Such surface might be useful to mimic the biological environment (membranes, etc.) for cell culture, tissue engineering, and biosensors.[12] Other biomacromolecules, such as DNA,[13] proteins,[14] or antibodies,[15] would be incorporated via indirect approaches, where post-modifications on patterned surfaces are used.
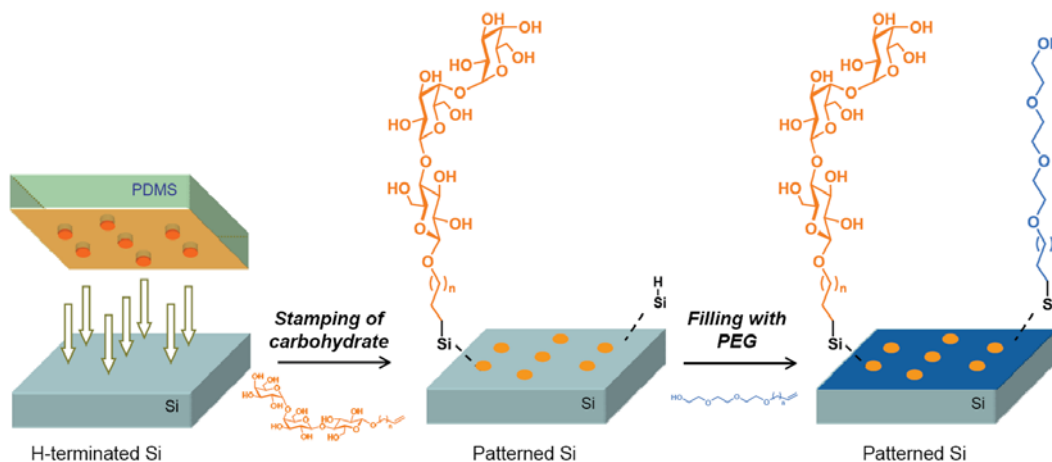

Figure 5.5. Catalytic stamp lithography-based fabrication of biomolecular nanoarrays. Relatively small biomolecules, such as carbohydrates, might be attached to H-terminated Si surface via hydrosilylation. The remaining space can be filled with other functional terminations, such as PEG.

2. Catalytic Stamp Lithography for Molecular Electronics

One actively ongoing area of research in nanoscience is molecular electronics, where the active components of traditional inorganic-based structures are replaced by organic molecules. Current status of molecular electronics is still in the early stage, and both experimental and theoretical studies are rapidly growing with interesting results.[3,4,16] Organic monolayers have played important roles in research on molecular electronics. The straightforward fabrication of large-area, uniform surfaces is an ideal starting point to study the fundamental mechanisms of electron transport (tunneling, hopping, or thermionic conduction) through molecules.[3,4] Much of the early research and device performance was studied based on the thiolate SAMs on Au surfaces.[4]

Organic monolayers covalently attached to Si have, however, several advantages over thiolate-Au systems because of the stable Si-C bonds that can withstand acid/base, organic/aqueous, and high temperature environments.[17] While obtaining reproducible results are still often challenging due to the case-by-case quality of organic monolayers on Si (impurities, defects, oxide formation), it would eventually be necessary to fabricate integrated circuits with organic components in view of future device applications.[18] In other words, together with the basic investigation of properties of molecules bound to Si surfaces, the development of methods to pattern them would be equally significant.

Catalytic stamp lithography may offer a convenient and flexible opportunity for this purpose. The nanopattern capability with high-throughput,

large-area, and low-cost scheme is remarkably unique over other patterning techniques. Accordingly, continuing progress of catalytic stamp lithography is highly anticipated.

5.3. References

1. (a) Xu, Q.; Rioux, R. M.; Dickey, M. D.; Whitesides, G. M. *Acc. Chem. Res.* **2008**, *41*, 1566-1577. (b) Xu, Q.; Rioux, R. M.; Whitesides, G. M. *ACS Nano* **2007**, *1*, 215-227. (c) Xu, Q.; Bao, J.; Rioux, R. M.; Perez-Castillejos, R.; Capasso, F.; Whitesides, G. M. *Nano Lett.* **2007**, *7*, 2800-2805.

2. (a) Hawker, C. J.; Russell, T. P. *MRS Bull.* **2005**, *30*, 952-966. (b) Kim, S. O.; Solak, H. H.; Stoykovich, M. P.; Ferrier, N. J.; de Pablo, J. J.; Nealey, P. F. *Nature* **2003**, *424*, 411-414. (c) Stoykovich, M. P.; Mueller, M.; Kim, S. O.; Solak, H. H.; Edwards, E. W.; de Pablo, J. J.; Nealey, P. F. *Science* **2005**, *308*, 1442-1446. (d) Tang, C.; Lennon, E. M.; Fredrickson, G. H.; Kramer, E. J.; Hawker, C. J. *Science* **2008**, *322*, 429-432.

3. (a) Aswal, D. K.; Lenfant, S.; Guerin, D.; Yakhmi, J. V.; Vuillaume, D. *Analytica Chimica Acta* **2006**, *568*, 84-108. (b) Ishizaki, T.; Saito, N.; Lee, S.; Takai, O. *Nanotechnology* **2008**, *19*, 055601/1-055601/6.

4. Love, J. C.; Estroff, L. A.; Kriebel, J. K.; Nuzzo, R. G.; Whitesides, G. M. *Chem. Rev.* **2005**, *105*, 1103-1169.

5. Miramond, C.; Vuillaume, D. *J. Appl. Phys.* **2004**, *96*, 1529-1536

6. (a) Koehler, K.; Kleist, W.; Proeckl, S. S. *Inorg. Chem.* **2007**, *46*, 1876-1883. (b) Huang, L.; Wong, P. K.; Tan, J.; Ang, T. P.; Wang, Z. *J. Phys. Chem. C* **2009**, *113*, 10120-10130.

7. Stewart, M. P.; Buriak, J. M. *J. Am. Chem. Soc.* **2001**, *123*, 7821-7830.

8.   Lewis, L. N. *J. Am. Chem. Soc.* **1990**, *112*, 5998-6004.

9.   Cicero, R. L.; Linford, M. R.; Chidsey, C. E. D. *Langmuir* **2000**, *16*, 5688-5695.

10.   (a) Weinrich, D.; Jonkheijm, P.; Niemeyer, C. M.; Waldmann, H. *Angew. Chem., Int. Ed.* **2009**, *48*, 7744-7751. (b) Liu, Y.; Palma, A. S.; Feizi, T. *Biol. Chem.* **2009**, *390*, 647-656.   (c) Muyal, J. P.; Singh, S. K.; Fehrenbach, H. *Crit. Rev. Biotechnol.* **2008**, *28*, 239-251.

11.   Mrksich, M. *Curr. Opin. Colloid Interface Sci.* **1997**, *2*, 83-88.

12.   Chaki, N. K.; Vijayamohanan, K. *Biosens. Bioelectron.* **2002**, *17*, 1-12.

13.   (a) Chrisey, L. A.; Lee, G. U.; O'Ferrall, C. E. *Nucl. Acids Res.* **1996**, *24*, 3031-3039.   (b) Lin, Z.; Strother, T.; Cai, W.; Cao, X.; Smith, L. M.; Hamers, R. J. *Langmuir* **2002**, *18*, 788-796.   (c) Zhang, X.; Kumar, S.; Chen, J.; Teplyakov, A. V. *Surf. Sci.* **2009**, *603*, 2445-2457.

14.   Jun, Y.; Cha, T.; Guo, A.; Zhu, X. Y. *Biomaterials* **2004**, *25*, 3503-3509.

15.   (a) Herrwerth, S.; Rosendahl, T.; Feng, C.; Fick, J.; Eck, W.; Himmelhaus, M.; Dahint, R.; Grunze, M. *Langmuir* **2003**, *19*, 1880-1887.   (b) Yakovleva, J.; Davidsson, R.; Lobanova, A.; Bengtsson, M.; Eremin, S.; Laurell, T.; Emneus, J. *Anal. Chem.* **2002**, *74*, 2994-3004.

16.   (a) Barth, J. V.; Costantini, G.; Kern, K. *Nature* **2005**, *437*, 671-679. (b) Heath, J. R. *Annu. Rev. Mater. Res.* **2009**, *39*, 1-23.

17.   Buriak, J. M. *Chem. Rev.* **2002**, *102*, 1271-1308.

18. Smits, E. C. P.; Mathijssen, S. G. J.; van Hal, P. A.; Setayesh, S.; Geuns, T. C. T.; Mutsaers, K. A. H. A.; Cantatore, E.; Wondergem, H. J.; Werzer, O.; Resel, R.; Kemerink, M.; Kirchmeyer, S.; Muzafarov, A. M.; Ponomarenko, S. A.; de Boer, B.; Blom, P. W. M.; de Leeuw, D. M. *Nature* **2008**, *455*, 956-959.